Performance Analysis of Photovoltaic Fed Distributed Static Compensator for Power Quality Improvement

Dissertation submitted to the

National Institute of Technology Rourkela

in partial fulfillment of the requirements

of the degree of

Doctor of Philosophy

in

Electrical Engineering

by

Soumya Mishra
(Roll Number: 512EE1013)

under the supervision of

Prof. Pravat Kumar Ray

November, 2016

Department of Electrical Engineering

National Institute of Technology Rourkela

Electrical Engineering
National Institute of Technology Rourkela

Dr. Pravat Kumar Ray
Assistant Professor
Department of Electrical Engineering,
National Institute of Technology,
Rourkela, India, 769008.
Email: rayp@nitrkl.ac.in

November, 2016

Supervisor's Certificate

This is to certify that the work presented in this dissertation entitled “Performance Analysis of Photovoltaic Fed Distributed Static Compensator for Power Quality Improvement" by Soumya Mishra, Roll Number: 512EE1013, is a record of original research carried out by him under my supervision and guidance in partial fulfillment of the requirements of the degree of Doctor of Philosophy in Electrical Engineering. Neither this dissertation nor any part of it has been submitted for any degree or diploma to any institute or university in India or abroad.

Place: Rourkela
Date:

Pravat Kumar Ray

Dedicated
To
My Family

…Soumya Mishra

Declaration of Originality

I, Soumya Mishra, Roll Number 512EE1013 hereby declare that this dissertation entitled as “Performance Analysis of Photovoltaic Fed Distributed Static Compensator for Power Quality Improvement” represents my original work carried out as a doctoral student of NIT Rourkela and, to the best of my knowledge, it contains no material previously published or written by another person, nor any material presented for the award of any other degree or diploma of NIT Rourkela or any other institution. Any contribution made to this research by others, with whom I have worked at NIT Rourkela or elsewhere, is explicitly acknowledged in the dissertation. Works of other authors cited in this dissertation have been duly acknowledged under the section "Bibliography". I have also submitted my original research records to the scrutiny committee for evaluation of my dissertation.

I am fully aware that in case of any non-compliance detected in future, the Senate of NIT Rourkela may withdraw the degree awarded to me on the basis of the present dissertation.

November 2016

NIT Rourkela Soumya Mishra

Acknowledgement

I would like to express my sincere gratitude and appreciation to my supervisor, **Prof. Pravat Kumar Ray**, Department of Electrical Engineering, National Institute of Technology, Rourkela, for his criticisms, valuable guidance and constant encouragement throughout the course of this research work and I consider myself extremely lucky to get the opportunity to work under the guidance of such a dynamic personality.

My special thanks are due to **Prof. A. Biswas** (Director) and Prof. J.K. Satapathy, Head of Electrical Engineering Department, NIT Rourkela National Institute of Technology, Rourkela for his encouragement, valuable suggestion and providing all the facilities to successfully complete this dissertation work.

I would like to extend special thanks to all the members of my doctoral scrutiny committee – **Prof. Anup Kumar Panda** (Chairman), **Prof. S. Karmakar**, **Prof. K. B. Mohanty** and **Prof. S. K. Behera,** for their thoughtful advice, inspiration and encouragement throughout the research work. I take this opportunity to thank the other faculty members and the supporting staff members of the Electrical Engineering department for their timely cooperation and support at various phases of my work.

I am really indebted to Mr. Bhanu Pratap Behera for his very generous help whenever it was needed during the period of research work.

I express my heartfelt thanks to the **International Journal Reviewers** for giving their valuable comments on the published papers in different international journals, which helps to carry the research work in a right direction. I also thank the **International Conference Organizers** for intensely reviewing the published papers.

I would like to extend special thanks to my friends **Mr. S. Mohanty, Mr. S. K. Dash, Miss S. Swain, Mrs. S. D. Swain, Mr. A. Kumar, Mr. J. K. Jain** and **Mr. R. K. Khadenga** for their valuable suggestions and encouragement. I would also like to extend special thanks to all my elders, friends and well-wishers for their constant help, motivations and encouragement.

I would like to acknowledge Ministry of **Human Resource Development (MHRD)**, Govt. of India for providing financial assistance throughout my research.

And it goes without saying, that I am indebted to my parents **Mr. Amarendra Mishra**, **Mrs. Surama Tripathy**, Sister **Miss. Stuti Mishra**, and Wife **Mrs. Priyanka Kumari** whose patience, support and endurance made completion of my thesis.

Above all, I would like to thank **The Almighty God** for the wisdom and perseverance that he has been bestowed upon me during this research work, and indeed, throughout my life.

Abstract

Owing to rising demand for electricity, shortage of fossil fuels, reliability issues, high transmission and distribution losses, presently many countries are looking forward to integrate the renewable energy sources into existing electricity grid. This kind of distributed generation provides power at a location close to the residential or commercial consumers with low transmission and distribution costs. Among other micro sources, solar photovoltaic (PV) systems are penetrating rapidly due to its ability to provide necessary dc voltage and decreasing capital cost. On the other hand, the distribution systems are confronting serious power quality issues because of various nonlinear loads and impromptu expansion. The power quality issues incorporate harmonic currents, high reactive power burden, and load unbalance and so on. The custom power device widely used to improve these power quality issues is the distributed static compensator (DSTATCOM). For continuous and effective compensation of power quality issues in a grid connected solar photovoltaic distribution system, the solar inverters are designed to operate as a DSTATCOM thus by increasing the efficiency and reducing the cost of the system.

The solar inverters are interfaced with grid through an L-type or LCL-type ac passive filters. Due to the voltage drop across these passive filters a high amount of voltage is maintained across the dc-link of the solar inverter so that the power can flow from PV source to grid and an effective compensation can be achieved. So in the thesis a new topology has been proposed for PV-DSTATCOM to reduce the dc-link voltage which inherently reduces the cost and rating of the solar inverter. The new LCLC-type PV-DSTATCOM is implemented both in simulation and hardware for extensive study. From the obtained results, the LCLC-type PV-DSTATCOM found to be more effective than L-type and LCL-type PV-DSTATCOM.

Selection of proper reference compensation current extraction scheme plays the most crucial role in DSTATCOM performance. This thesis describes three time-domain schemes viz. Instantaneous active and reactive power (p-q), modified p-q, and IcosΦ schemes. The objective is to bring down the source current THD below 5%, to satisfy the IEEE-519 Standard recommendations on harmonic limits. Comparative evaluation shows that, IcosΦ scheme is the best PV-DSTATCOM control scheme irrespective of supply and load conditions.

In the view of the fact that the filtering parameters of the PV-DSTATCOM and gains of the PI controller are designed using a linearized mathematical model of the system. Such a design may not yield satisfactory results under changing operating conditions due to the complex, nonlinear and time-varying nature of power system networks. To overcome this,

evolutionary algorithms have been adopted and an algorithm-specific control parameter independent optimization tool (JAYA) is proposed. The JAYA optimization algorithm overcomes the drawbacks of both grenade explosion method (GEM) and teaching learning based optimization (TLBO), and accelerate the convergence of optimization problem. Extensive simulation studies and real-time investigations are performed for comparative assessment of proposed implementation of GEM, TLBO and JAYA optimization on PV-DSTATCOM. This validates that, the PV-DSTATCOM employing JAYA offers superior harmonic compensation compared to other alternatives, by lowering down the source current THD to drastically small values.

Another indispensable aspect of PV-DSTATCOM is that due to parameter variation and nonlinearity present in the system, the reference current generated by the reference compensation current extraction scheme get altered for a changing operating conditions. So a sliding mode controller (SMC) based p-q theory is proposed in the dissertation to reduce these effects. To validate the efficacy of the implemented sliding mode controller for the power quality improvement, the performance of the proposed system with both linear and non-linear controller are observed and compared by taking total harmonic distortion as performance index. From the obtained simulation and experimentation results it is concluded that the SMC based LCLC-type PV-DSTATCOM performs better in all critical operating conditions.

Table of Contents

List of Figures

List of Tables

List of Abbreviations

PQ	Power Quality
PV	Photovoltaic
PCC	Point of Common Coupling
DG	Distributed Generation
DSP	Digital Signal Processing
SVM	Space Vector Modulation
CSI	Current Source Inverter
THD	Total Harmonic Distortion
MPPT	Maximum Power Point Tracking
PID	Proportional Integral and Derivative
TLBO	Teaching-Learning Based Optimization
PSO	Particle Swarm Optimization
PWM	Pulse Width Modulation
IVA	Imaginary Volt Ampere
IGBT	Insulated Gate Bipolar Transistor
GEM	Grenade Explosion Method
DSTATCOM	Distribution Static Synchronous Compensators
FFT	Fast Fourier Transform
SMC	Sliding Mode Controller
UPFC	Unified Power Flow Controllers
VSC	Voltage Source Converter

1 Chapter 1

Introduction

- To develop the background for carrying research on PV-DSTATCOM.
- To provide an extensive review on PV-DSTATCOM.
- To provide the information about motivations and objectives of the thesis.
- To provide a brief idea about thesis organizations.

1.1 Background

Owing to rising demand for electricity, shortage of fossil fuels, reliability issues, high transmission and distribution losses, presently many countries are looking forward to integrate the renewable energy sources (such as solar energy, wing energy, tidal energy and geothermal energy etc.) into existing electricity grid. This kind of distributed generation provides power at a location close to the residential or commercial consumers with low transmission and distribution costs. Among other micro sources, solar photovoltaic (PV) systems are penetrating rapidly due to its ability to provide necessary dc voltage, low running cost, need of less maintenance and decreasing capital cost [1] [2]. The PV systems have several applications, out of which grid integration of photovoltaic system is one of the important applications.

1.1.1 Grid Integration of PV system

The power obtained from the PV system is in the form of dc quantity. So to integrate the solar energy into the conventional grid an inverter is needed to convert the dc voltage to ac. For integration, it is important to match the frequency and phase of output ac voltage with the grid voltage. Also it is necessary that the voltage obtained across the inverter should be of higher magnitude than the grid so that the power can flow from PV source to grid [3] [4] [5] [6] [7] [8]. A schematic diagram of grid integrated PV system is shown in Fig. 1.1. Though the integration of solar energy into the conventional grid system increases the reliability of the distribution system, unfortunately it adds to the power quality issues present in the system due to power electronic based loads.

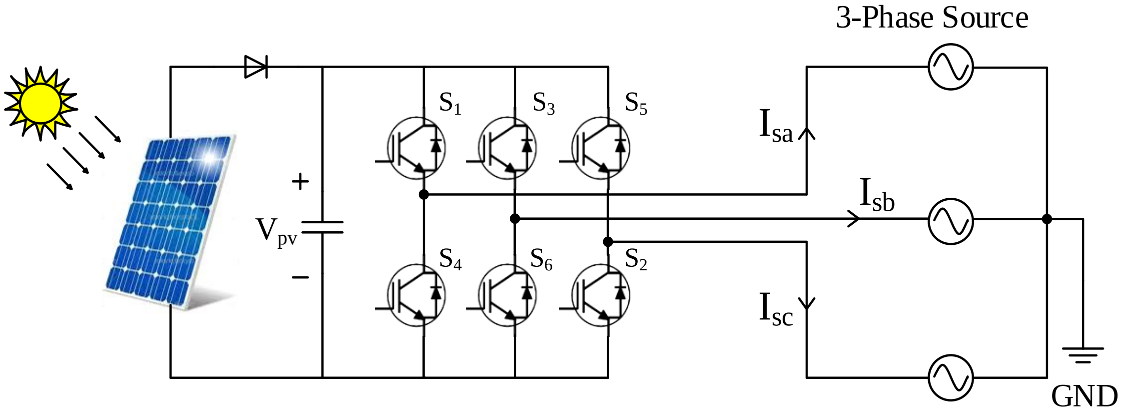

Fig. 1.1 Schematic diagram of grid integrated solar system

1.1.2 Power Quality

The distribution systems are confronting serious power quality issues because of various nonlinear loads and unplanned expansion [9] [10] [11] [12] [13] [14] [15]. The power quality issues incorporate voltage quality, current quality and frequency quality. But in distribution system, it is observed that the deviations in the voltage and frequency are much less than 1.0 percent. However, the current waveform barely resembles to the sine wave. Due to advancement in power electronics, the usage of power electronic devices has been increased in recent years. These devices can chop the current into seemingly arbitrary waveforms. Mostly these distortions are periodic and integer multiple of power system fundamental frequency. This has been termed as ‘Harmonics’. In present power system, the term Harmonics is rigorously utilized to define the distortion in voltage and current.

The power converters are when used as current source type nonlinear loads they inject a non-sinusoidal current (i.e. harmonic) into the utility grid. Due to this, the line voltage at the point of common coupling get distorted where other linear and nonlinear loads are connected. As a consequence, the harmonic distortion can have influences on the entire distribution systems. Therefore, it is necessary to identify the sources and impacts of harmonics as well as the methods to decrease the harmonic so that the overall efficiency of the distribution system can be increased.

1.1.2.1 Sources of Harmonics

There are different sources of harmonics in power distribution system. Some of the major sources are listed below:

- Fluorescent Lamps
- Adjustable speed drives
- Switching power supplies
- Electric furnace
- High voltage DC systems
- Modern electronic equipment
- Electric rotating machines and Transformers

1.1.2.2 Effects of harmonics

Except heat producing loads, most of the other electrical loads are sensitive to harmonics. In fact, harmonics may lead to their improper operation such as:

- Interference with communication line when flows through transmission line
- Higher transmission losses
- Extra neutral current
- Improper working of metering devices
- Resonance problem
- Overheating of transformers, motors etc.
- Poor power factor and efficiency
- Malfunctioning of protective relays

1.1.2.3 Harmonic reduction techniques

In order to solve the problem of harmonic pollution effectively, many harmonic limitation standards such as IEEE 519-2014, IEC 1000-3-2 and IEC 1000-3-4 have been established [16] [17] [18] [19] [20]. However, IEEE Recommended Practice and Requirement for Harmonic Control in Electric Power Systems (IEEE 519-2014 Standard) provides an excellent basis for limiting harmonics. IEEE 519-2014 Standard for harmonic current limits for general distribution systems (120V-69KV) is presented in Table 1.1. A lot of research has been done to find out a tool that would be able to compensate the disturbances caused due to nonlinear loads so that the IEEE 519 Standards can be met even under sudden load changes, irrespective of the supply voltage conditions.

Table 1.1 Current distortion limits at PCC

Maximum Harmonic Current Distortion in Percent of I_{load}	Individual Harmonic Order (Odd Harmonics)					
$\frac{I_{source}}{I_{load}}$	< 11	$11 \leq n < 17$	$17 \leq n < 23$	$23 \leq n < 35$	$35 \leq n$	TDD
<20*	4.0	2.0	1.5	0.6	0.3	5.0
20-50	7.0	3.5	2.5	1.0	0.5	8.0
50-100	10.0	4.5	4.0	1.5	0.7	12.0
100-1000	12.0	5.5	5.0	2.0	1.0	15.0
>1000	15.0	7.0	6.0	2.5	1.4	20.0

Where

$$TDD = \frac{\sqrt{\sum_{h=2}^{\infty}(I^{(h)})^2}}{I_{rated}} \tag{1.1}$$

The traditional techniques of eliminating harmonics in current was to use passive filters in parallel with grid system. But they have the following disadvantages:

- Fixed compensation, large size, heavy weight
- Resonance problem with system impedance
- Being not able to compensate when harmonic orders are varying
- Compensation is limited to a fewer order of harmonics

Due to these disadvantages, power electronics is applied to power system for compensating the power quality issues [21]. The technology of the application of power electronics to power distribution system for the benefit of a customer or group of customer is called 'Custom Power'. The custom power devices are of two types: network reconfiguring type and compensating type. In the thesis, only compensating type of custom power device is discussed. Compensating type devices are used for active filtering, load unbalancing, power factor correction and voltage regulation. The family of compensating devices includes:

- Distributed Static Compensator (DSTATCOM) [Shunt connected device]
- Dynamic Voltage Restorer (DVR) [Series connected device]
- Unified Power Quality Conditioner (UPQC) [Both series and shunt connected device]

However, the shunt compensators are more popular than the series compensators because of greater ease of protection [22] [23] [24] [25] [26] [27] [28]. The schematic diagram of a DSTATCOM applied to distribution system is shown in Fig. 1.2.

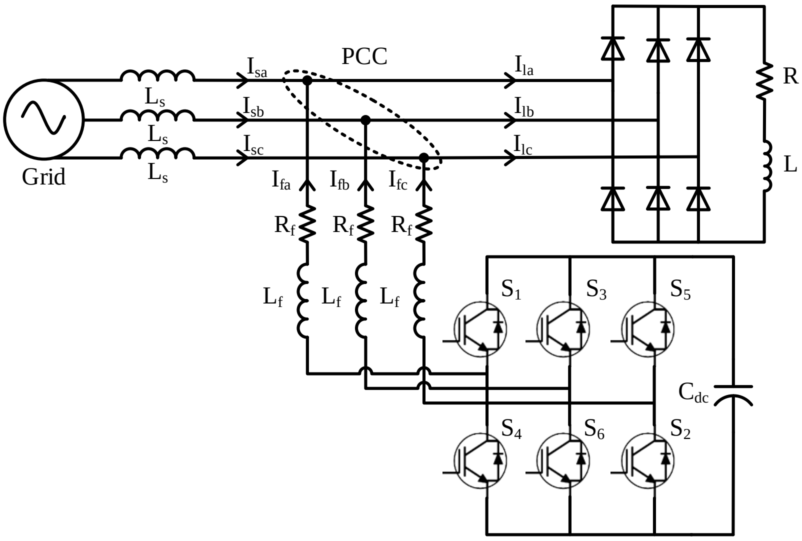

Fig. 1.2 Schematic diagram of DSTATCOM applied to distribution system

As discussed in Section 1.1.1, the new trend is to integrate solar energy into distribution system. For taking care of the power quality issues of a grid integrated PV system, two voltage source inverters are required. Out of which one will be solely responsible for integration and the other will take care of power quality. This configuration will make the system more unstable, costly and inefficient as inverter technology is not so developed as rectifier technology. So a conscious effort has been made to reduce the number of inverter in the system. Hence, the system topology is restructured with a single inverter through which the photovoltaic source is integrated to distribution system and simultaneously with a proper inverter control technology the same inverter is used as DSTATCOM to monitor the power quality issues. These devices are popularly named as PV-DSTATCOM.

1.1.2.4 Photovoltaic Fed Distributed Static Compensator

The schematic diagram of a photovoltaic fed DSTATCOM (PV-DSTATCOM) is shown in Fig. 1.3. The PV-DSTATCOM comprises of solar array, dc/dc boost converter, a voltage source solar inverter and grid interfacing passive ac filter. The solar PV systems are integrated to gird through the VSI and passive ac interfacing filter [29] [30] [31] [32] [33] [34]. The dc voltage generated by a PV array varies widely and low in magnitude. So the dc/dc boost converter is used to generate a regulated higher dc voltage for desired converter input voltage.

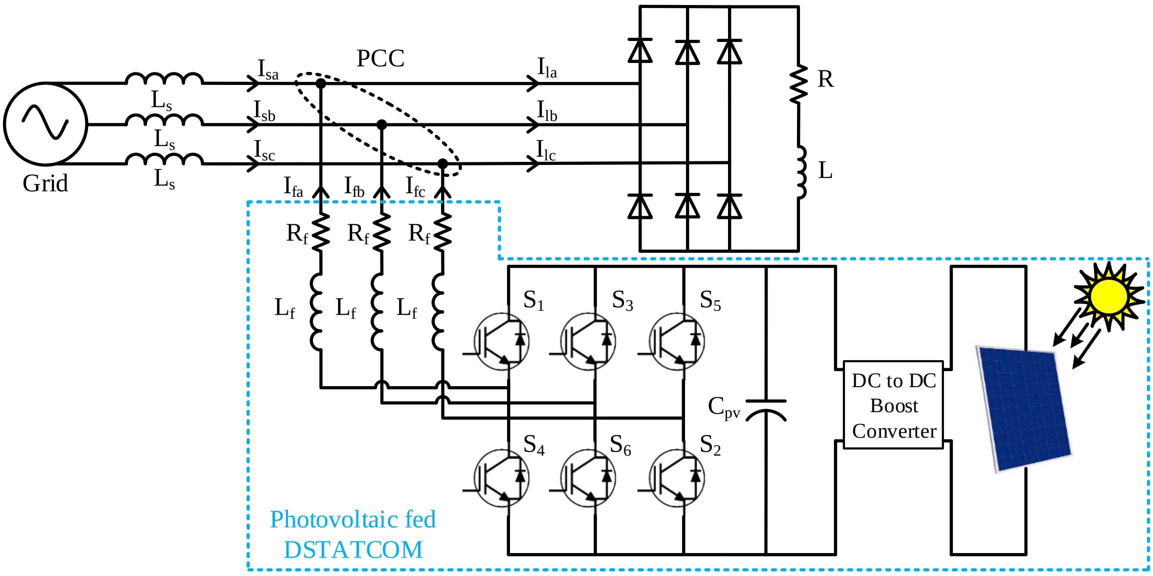

Fig. 1.3 Schematic diagram of a dual stage PV-DSTATCOM

In a conventional grid connected system, the solar inverter takes care of the power injection from PV source to grid. When solar insolation is available, the solar power is generated and feed to load or grid as per requirement. But when solar insolation is not available or not sufficient for generation of solar power the solar inverter remains idle. Hence the solar inverter operates during day time and remains idle for the rest of period thereby reducing the efficiency of the system. Therefore, the active filtering operations are added to the solar inverter through proper inverter control. The grid connected PV systems [35] [36] [37] [38] [39] capable of power quality improvement of the system with paralleled solar inverter known as PV-DSTATCOM. The PV-DSTATCOM can provide load harmonics compensation, power factor correction, reactive power compensation, load balancing and simultaneously inject active power from the PV source to grid or/and load.

1.2 Literature review on PV-DSTATCOM

To improve the current quality in the grid integrated PV distribution sector, the PV-DSTATCOMs are introduced. A grid connected PV system comprises of two stages (i.e. two loops) are presented in 1996 [40]. The outer loop takes care of power quality issues (i.e. current harmonics and reactive power) whereas the inner loop is a dc/dc conversion process with MPPT algorithm. But two stage power conversion process causes more power loss for the system. In 2002, Nak-gueon et.al. [41] proposed a control algorithm for PV power generation system which also acts as shunt active filter. They have implemented dq transformation to compensate negative component and harmonics component. For generation of reference dc-link voltage, Incremental Conductance (IC) MPPT algorithm is used. A control algorithm is proposed by Mostafa et.al. in 2004 for the DG interface to mitigate power quality problems [42]. In the paper an Adaptive Linear (ADALINE) neuron structure has been implemented to multi output system for symmetrical component estimation. The ADALINE structure deals with unbalance, harmonics and reactive power compensation. The advantage of the proposed system is its insensitivity to parameter variation. However, no experimental validation is given for the system.

In [43] [44], the authors have presented a grid connected PV system which is also utilized as active filter. The system successfully reduced the effects of harmonics in load current due to nonlinear load and improves the power factor of the grid. Both the PV fed active filter (PV-AF) operate at higher dc-link voltage and no experimental validation has been carried out. Tsai-Fu [45] in 2005 proposed a single phase inverter system for PV power injection and active power filtering. To increase the accuracy of the estimated current the authors have proposed a self-learning algorithm. In [46] [47], they have proposed a single stage three phase grid connected PV system with a modified MPPT method. The PV system is integrated with grid through an Incremental conductance algorithm and L-type passive interface filter. The results presented show the reactive power compensation capability of the compensator but harmonics compensation ability has not been analyzed. A three phase four wire PV based DG [48] is proposed which also compensates harmonics and reactive power under unbalanced and nonlinear load conditions. It eliminates the negative and zero sequence components in the load current and reduces the neutral current to zero. A dc/dc boost converter and an L-type passive filter is used to integrate PV system into grid. However, with proposed system power loss is more and rating of solar inverter is very high.

An amplitude-clamping and amplitude scaling algorithm is presented for PV power generation and active power filtering in [49]. Here a single phase system is presented which needs only two active switches, thus by reducing the cost significantly. For experimental validation DSP platform is used. In [50] a multifunctional four leg grid connected compensator is presented. The system is implemented in real time under DSP-FPGA platform. For increasing the dc bus utilization, a three dimensional space vector modulation (3D-SVM) is implemented. The dc-link voltage is maintained around 800V. Grid connected PV system with additional active power conditioning capability are presented in [51] [52]. In [51], a single phase system is proposed whereas in [52] a three phase three wire system is presented. Both the system performs satisfactorily but the controller implemented are not intended to perform under non-ideal mains conditions.

Another study is presented in [53], to analyze the performance of the photovoltaic based active filter under uniform and non-uniform radiation. Different PV-AF configurations and their control strategies are considered. Under partial shading condition the compensating performance of all the PV-AF configurations are monitored. From the study, it is concluded that under uniform radiation all the PV-AF configuration are being able to extract similar amount of power but under non-uniform radiation with different shading patterns the power extractions changes. The centralized inverter topology was the only topology which brought the grid current THD to less than 5% as required by IEEE 519 standard. However, this topology also considers only L-type passive filter as ac interface. In 2009, many authors have presented grid connected PV system which has also active filter functionality [54] [55] [56]. The authors have presented a single phase system and all use the MPPT algorithm to generate the reference dc voltage. Though the systems are presented in literature achieve the objectives but they are limited to single phase system. Also the performances are only shown for ideal supply voltage conditions.

Fabio et. al. [57] reported a solar system connected to grid operating as an active power filter. For generation of reference current instantaneous reactive power theory is implemented. For different isolation, the active and reactive power flow between grid and PV system is shown. However, there is no evidence for the harmonic compensation ability of the system. Again in [58], a solar inverter is developed showing the harmonic and reactive power compensation ability under dSPACE 1104 platform in real time domain. But the results produced are not so much convincing as they only operated under ideal conditions.

A three phase grid connected PV system is presented and controlled to control the active and reactive power by Tsengenes and Adamidis in [59]. IC MPPT method is used for the extraction of reference dc voltage which is further used for dc-link voltage control. The p-q theory is used for generation of reference current and reactive power control. The system is simulated under MATLAB/Simulink platform and the results are shown for active power and reactive power compensation of load. Though the paper produces good simulation results for reactive power compensation, the harmonic compensation is not considered. Again no experimentation has been carried out in order to verify the performance of the system in real time domain.

A dynamic modeling for grid connected current source inverter based PV system is derived in [60]. Also the control, steady state and transient performance of the PV system based on CSI are considered. The system is operated with both CSI and VSI for comparing the compensating ability of the system. It is proved that CSI based PV system performs better than the other in all conditions. However, no results are produced to show the reactive power compensation ability of the system. In [61], the authors have presented grid connected DG system for the mitigation of unbalanced and harmonic voltage disturbances.

The solar inverter is interfaced with grid through LCL filter. A dynamic model is desired for LCL-type grid connected PV system. Though both simulation and experimental results are presented in paper for load voltage, but they are not sufficient. The results are only produced for ideal supply conditions and also the harmonic compensation ability of system is not verified.

Zamre et.al. [62] reported a three phase grid connected inverter for photovoltaic application. The authors have utilized the Park's transformation and sinusoidal PWM method to generate the pulses for solar inverter. The inverter is controlled to stabilize output voltage and current and the excess power is delivered to the grid. The system is simulated in MATLAB/Simulink and the results are produced for inverter voltage and current. The THD of the current is measured to be 4.64% after compensation. The solar inverter is interfaced with utility grid through LC-type ac interface filter. The presented result confirms that the inverter control algorithm is successfully converting PV dc power to ac power with acceptable THD range but system is only simulated under ideal supply conditions.

Kamatchi and Rengarajan [63] proposed a three phase four wire PV based DSTATCOM for power quality improvement. In the paper they have considered two stage grid integration process. The system includes, a battery storage system, dc/dc boost converter and a three leg VSC with star/delta transformer. For generation of reference current synchronous reference frame theory has been used. The proposed system provides harmonic reduction, reactive power compensation and neutral current compensation at PCC. The PV-DSTATCOM is simulated under MATLAB/Simulink environment and the simulation results are presented for source current before and after compensation for ideal as well as load fault conditions. From the spectral analysis of source current, it is observed that the THD has been reduced from 27.59% to 5.38%. However, the THD after compensation is not meeting IEEE 519 standard (i.e. above 5%). The experimentation also has not been carried out for the system.

The modeling and control of dual stage multifunctional PV system is given in [64]. The system includes a boost converter for dc/dc conversion and a parallel four leg inverter for dc/ac conversion. The presented system performs both as grid connected PV system and active filter. For allowing a wide range of input voltage from PV system to grid and to compensate the nonlinear unbalance load current, an LCL-type passive ac interface filter is used. From the presented both simulation and experimentation results, it is verified that with the proposed system the solar power can be supplied to grid as well as load and the harmonic compensation can be done. It is observed that the THD of grid current reduces from 20.01% to 4.59% with the proposed system. Though a very good understanding of

PV-AF system has been provided in the paper still the inverter operated with a very high dc link voltage.

In [65], a system is proposed which can combinedly operated as grid connected PV system and an active filter. The proposed system is also a dual stage grid connected PV system which is providing the power factor correction, load balancing, harmonic elimination and reactive power compensation. The system is simulated under the platform of PSCAD/EMTDC. The results are presented for different insolation levels and different load conditions. A considerable amount of results are produced for PV-AF confirming the compensation ability of the system. However, again the dc link voltage is maintained at higher level. Also due to dual stage integration more power loss occurs in the system.

In [66], the authors have proposed a PV interfacing inverter for residential distribution system which can compensate harmonics. A system model including the residential load and photovoltaic array is developed. The system is a dual stage system and interfaced with grid through LC-type passive interface filter. The harmonics of distribution current are reduced by harmonic-damping virtual resistance. Also the system performance is verified by introducing PFC capacitors in different locations. For system stability check, bode plot analysis has been carried out. However, a detailed harmonic and reactive power compensation analysis is not provided.

Muhammad et. al. proposed a grid connected photovoltaic plant which takes care of generator side output current harmonics [67]. The solar inverter is interfaced with grid through a LCL passive filter. For synchronization a synchronous reference frame based PLL is implemented. The system controller is developed in DSP TMS320F28335 and used as interfacing with hardware prototype. But in the paper not much simulation as well as experimental results are produced. Also the THD achieved after compensation is above 5% precisely it is 7.90%.

Kamatchi and Rengarajan [68] has proposed an IcosΦ algorithm for reference current generation in order to compensate harmonics and reactive power using a photovoltaic fed DSTATCOM. The PV-DSTATCOM consist of a 35V battery for storage, dc/dc boost converter, three leg voltage source inverter and a L-type passive interface filter. The battery system presented is charged through an uncontrolled rectifier from the grid. The dc link voltage control performance is controlled with conventional PI controller and with a fuzzy logic controller. With PI and fuzzy controller, the THD of source current reduces from 23.98% to 2.28% and 0.82% respectively. The system is presented with convincing simulation results however no experimentation has been carried out. Being a dual stage power conversion integration more losses occurs in the system. Also insertion of another rectifier module make the system costlier and lossy.

In [69], Bhim Singh et. al. proposed an improved linear sinusoidal tracer (ILST) control algorithm for single stage dual purpose grid connected solar system. The solar inverter is interfaced with grid through a LCL-type passive filter. The incremental conductance MPPT algorithm is used for generation of reference voltage. The system performance is checked under linear load, unbalanced nonlinear load and for sudden change solar insolation level. The experimentation also has been carried out successfully. However, the dc-link voltage is maintained at a higher level of around 700V.

1.3 Motivations of the Thesis

Several encouraging factors are responsible for selecting this topic for the dissertation. Still, the primary sources of motivations for the dissertation are as follows.

- The grid connected PV distribution system with additional active power filtering ability usually operates in dual stage power conversion mode. But due to this more power loss occurs and the system efficiency decreases. Besides that most of the reference current generation techniques, responsible for active filtering ability of the PV-DSTATCOM existing in the literature are incompetent under non-ideal supply voltage condition. This has motivated to develop a PV-DSTATCOM which operates in single stage power conversion mode and to generate a reference current generation technique that can perform satisfactorily under ideal as well as non-ideal supply voltage conditions.
- The PV-DSTATCOMs are interfaced with grid through passive ac interface filter. These filters may be L-type or LCL-type. In L-type PV-DSTATCOM the occurrence of voltage drop across L, is an issue in maintaining high voltage across dc link. Due to high dc-link voltage the rating of the solar inverter increases. In LCL-type PV_DSTATCOM the value of passive filters is reduced but still the voltage across the dc-link voltage is maintained at high value. These problems have propelled to develop a new topology which can operate at reduced dc-link voltage thus by reducing the rating of solar inverter.
- The conventional PI controller tuning method and linearized approach of calculating value for the passive interface filter has some major drawbacks. The modeling of PV-DSTATCOM network using conventional mathematical based linearized approaches is very difficult as it represents a highly complex, nonlinear and time varying system. Therefore, for a wide range of operating conditions these linearly modeled PV-DSTATCOMs do not perform satisfactorily. Hence

optimization of PV-DSTATCOM is necessary. Different optimization techniques are applied to power system but they are algorithm-specific control parameter dependent. When these parameters are not chosen optimally the performance of the optimization tools deteriorate. So there is an urge to develop and implement an optimization technique for improving the performance of PV-DSTATCOM which is independent of algorithm-specific control parameters.

- The dynamic performance of the PV-DSTATCOM mainly depends upon the current controller technique. From the literature survey, it is found that most of the predictive and nonlinear controls are applied to dc-link control not to current controller. So when operating conditions or system parameters are changed, the compensating ability of the PV-DSTATCOM gets affected or in other words the current controller does not perform satisfactorily. This has motivated to develop an average nonlinear model for PV-DSTATCOM and a current controller considering the nonlinearity of the system so that the controller performance will be robust towards any change in supply voltage conditions or system parameters.

1.4 Objectives of the Thesis

- To implement a simple yet an effective reference current generation scheme for ideal as well as non-ideal supply voltage condition and verify its superiority over other most frequently implemented reference current generation scheme such as p-q theory and modified p-q theory.
- To propose a new topology for PV-DSTATCOM, which will operate at a reduced dc-link voltage as compared to L-type or LCL-type PV-DSTATCOM and evaluate their performance ability through both simulated and experimental results.
- To propose a new optimization technique for the performance enhancement of PV-DSTATCOM which is independent of algorithm-specific control parameter in view of achieving accuracy and fast convergence.
- To evaluate the efficacy of the proposed optimized PV-DSTATCOM through both simulated and experimental results.
- To implement a nonlinear controller to current control scheme of PV-DSTATCOM and verify its robustness by operating the system in both simulation and hardware prototype.

1.5 Thesis Organization

The thesis consists of six chapters. The organization of the dissertation and a brief chapter-wise description of the work presented are as follows.

Chapter 1 provides an extensive review on PV-DSTATCOM topologies, control techniques and reference generation schemes. Remarks on the review are presented along with the discussion of merits and demerits. At the end, the motivations behind the presented work, objectives of the dissertation and the chapter-wise organization of the thesis are outlined.

Chapter 2 discusses the design of L-type PV-DSTATCOM to inject solar power to grid, eliminate harmonics and compensate reactive power simultaneously. Different L-type PV-DSTATCOM control schemes for reference compensation filter current extraction are discussed and a comparison between $p - q$, modified $p - q$ and $Icos\Phi$ control schemes are presented. Evaluations are carried out for the compensator performance under different load conditions and supply voltage conditions.

Chapter 3 proposed a LCLC-type passive ac interface filter for PV-DSTATCOM to inject solar power to grid and to improve the power quality. Also the design of LCL-type PV-DSTATCOM is presented. The performance of proposed PV-DSTATCOM is observed and analyzed with reduced dc-link voltage and reduced power rating of solar inverter. The effectiveness of the LCLC-type PV-DSTATCOM is assessed with different load conditions using simulation results obtained from MATLAB/Simulink and real-time results obtained from experimentation. The experimentation has been carried out under the platform of dSPACE 1103.

Chapter 4 proposed a JAYA optimized LCLC-type PV-DSTATCOM. In order to overcome the shortcomings of optimization techniques like GEM and TLBO, JAYA optimization tool is proposed which is free from algorithm specific control algorithm. To observe the effectiveness of the optimized PV-DSTATCOM, different load conditions and sudden change in load conditions are considered for simulation in Simulink. An experimental set up is developed to notice the execution of JAYA optimized PV-DSTATCOM in real-time environment. From the both simulation and experimentation results it is found that the proposed optimized system handle the adverse conditions more effective than GEM or TLBO optimized PV-DSTATCOM.

Chapter 5 deals with the application of a nonlinear control to current controller scheme of PV-DSTATCOM. In this chapter, sliding mode control is applied to reference current generation scheme to make it robust towards any external disturbances or to any parameter variation. Here an average model for the LCLC-type PV-DSTATCOM is developed keeping PV system under consideration. The state space model of the system is also presented for better understanding of the dynamics during transient conditions. From the simulation as well as experimentation results, it is depicted that the SMC based PV-

DSTATCOM compensates harmonics and reactive power better than all other presented linear controller in adverse operating conditions.

Chapter 6 presents the concluding explanations and some scopes for future research on the presented work.

2 Chapter 2

L-type PV-DSTATCOM: Realization and Control

- Design an L-type PV-DSTATCOM to inject solar power to grid, eliminate harmonics and compensate reactive power simultaneously.
- Develop different control schemes and to find out the most suited control algorithm for PV-DSTATCOM.
- To generate and track reference current most accurately for different load conditions under consideration of grid perturbation.
- To simulate the developed control schemes in MATLAB/Simulink for all load conditions under grid perturbation

Photovoltaic fed distributed static compensator (PV-DSTATCOM) is an effective approach for integrating solar energy into the grid with additional power quality improvement features like harmonic mitigation, reactive power compensation and load balancing. The power quality conditioning performance in terms of total harmonic distortion and superior power factor of supply current is appreciably influenced by the passive components associated with the solar voltage source inverter. That means an AC passive interface filter is used to interconnect the inverter and photovoltaic (PV) panels to the grid. The PV panels and solar inverter with power quality conditioning capabilities are when interfaced to the grid through a first order L-type passive filter is labeled as L-type PV-DSTATCOM. The primary objective of the interface filter is to reduce the switching harmonic distortion of the injected current as much as possible to prevent the switching harmonics from propagating into power supply without affecting the flow of harmonics to be compensated.

In this chapter, the focus has been given for the design and switching control of L-type PV-DSTATCOM. In actual systems the load is connected at the end of feeder. If the load is unbalanced, then the point of common coupling (PCC) voltage will be unbalanced. In addition, the PCC voltage will be distorted by both the harmonics generated by a non-linearity in the load and by the switching frequency harmonics generated by the PV-DSTATCOM. Furthermore, there will be reactive power, switching and resistive losses in the PV-DSTATCOM circuit. Taking these factors into consideration, we must choose the switching control algorithm such that irrespective of any disturbance the algorithm shall perform satisfactorily.

This chapter is organized as follows: Section 2.1 presents the concept and an overview of the L-type PV-DSTATCOM, Section 2.2 elucidates the mathematical realization of the circuit, Section 2.3 describes about different switching control techniques, Section 2.4 presents the simulation results and discussions and finally Section 2.5 conclude the work done in this chapter.

2.1 L-type PV-DSTATCOM Structure

To illustrate the functioning of L-type PV-DSTATCOM, a three phase, three wire (3p3w) photovoltaic fed distribution system is shown in Fig. 2.1. Here a three phase balanced supply (V_{sa}, V_{sb}, V_{sc}) is connected across a three phase diode bridge rectifier with ohmic-inductive load. The load is such that the load currents (I_{la}, I_{lb}, I_{lc}) may not be balanced and contain harmonics and dc offset.

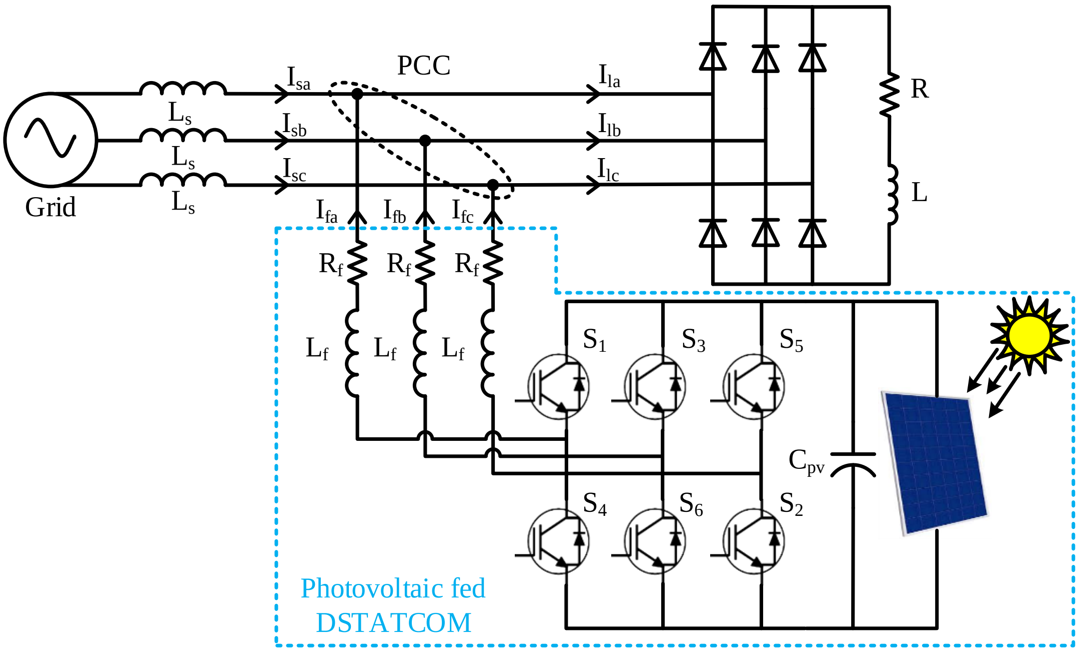

Fig. 2.1: Schematics of L-type PV-DSTATCOM

In addition, the power factor of the load may be poor. The photovoltaic system is integrated to the three phase grid through a voltage source inverter and an L-type (L_f) passive filter whose internal resistance is R_f. The injected compensator current is represented by I_{fa}, I_{fb}, I_{fc}. All the voltages and currents that are indicated in this figure are instantaneous quantities. The point of common coupling is encircled in Fig. 2.1. The purpose of the PV-DSTATCOM is to inject currents in such a way that the source currents (I_{sa}, I_{sb}, I_{sc}) are harmonic free balanced sinusoids and their phase angle with respect to the source voltages has a desired value. Along with this, during the availability of solar radiation, the photovoltaic system will inject active power to the load. The mathematical modeling of L-type PV-DSTATCOM is explained in next section.

2.2 Design of L-type PV-DSTATCOM

For the realization of any system, it is very essential to develop the model analogous to its ideal characteristics. So under this section the modeling of photovoltaic (PV) system and the DSTATCOM is described elaborately.

2.2.1 Modeling of PV system

As the incident of solar radiation produces a current, the PV cells are considered as current source. To understand the electronic behavior of a solar cell it is useful to create a model which is electrically equivalent. An ideal solar cell may be modeled by a current source in parallel with a diode. The basic equation that mathematically describes the I-V characteristics of the ideal photovoltaic cell is

$$I = I_{ph,cell} - I_{0,cell}\left[exp\left(\frac{qV_d}{aKT}\right) - 1\right] \tag{2.1}$$

where $I_{ph,cell}$ is the current generated by the incident light (directly proportional to the solar irradiation), I_d is the current flowing through Shockley diode ($I_d = I_{0,cell}\left(e^{qV_d/aKT} - 1\right)$), K is the Boltzmann constant [1.3806503*10^{-23}J/K], q is the electron charge [1.60217646*10^{-19}C], T [K] is the temperature of the p-n junction, a is the diode ideality constant.

In practice no solar cell is ideal, so a shunt resistance and a series resistance component are added to the model. After adding the resistances, the equivalent circuit diagram of a practical photovoltaic cell is shown in Fig. 2.2.

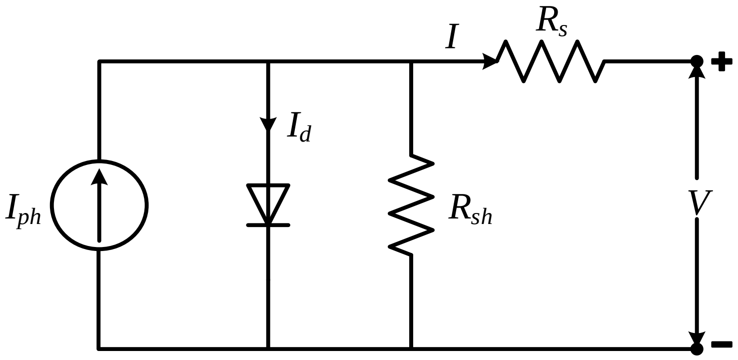

Fig. 2.2 Equivalent circuit of a practical photovoltaic device.

From the above equivalent circuit diagram, the current produced by a solar cell is expressed as

$$I = I_{ph} - I_d - I_{sh} \tag{2.2}$$

The current flowing through the elements are governed by the voltage across them

$$V_d = V + IR_s \tag{2.3}$$

where V is the voltage across the output terminal, I is the output current and R_s is the series resistance.

By Ohms law, the current diverted through the shunt resistor is

$$I_{sh} = \frac{V_d}{R_{sh}} \tag{2.4}$$

Now substituting(2.1), (2.3) and (2.4) in(2.2),

$$I = I_{ph,cell} - I_{0,cell}\left(e^{q(V+R_sI)/aKT} - 1\right) - \frac{V + R_sI}{R_{sh}} \tag{2.5}$$

The above equation is applicable for single cell. But in practical a PV array consist of several cells. By considering the array consist of N_s number of cells, for one module or one panel (2.5) can be written as

$$I = I_{ph} - I_0\left[exp\left(\frac{V + IR_s}{V_t a}\right) - 1\right] - \frac{V + R_sI}{R_{sh}} \tag{2.6}$$

where $V_t = N_sKT/q$ is the thermal voltage of the array

The solar cells are connected in parallel to increase current and in series to provide greater output voltage. So the equation (2.6) for one photovoltaic array can be written as

$$\boldsymbol{I = N_{pp}I_{ph} - N_{pp}I_0\left[exp\left(\frac{V + IR_s\left(\frac{N_{ss}}{N_{pp}}\right)}{V_taN_{ss}}\right) - 1\right] - \frac{V + R_sI\left(\frac{N_{ss}}{N_{pp}}\right)}{R_{sh}\left(\frac{N_{ss}}{N_{pp}}\right)}}$$

where N_{ss} is the solar module connected in series and N_{pp} is the solar module connected in parallel.

The generated current of the photovoltaic cell depends linearly on the solar irradiation and is also influenced by the temperature according to the following equation:

$$I_{ph} = \left(I_{ph,n} + K_I\Delta_T\right)\frac{G}{G_n} \tag{2.7}$$

where $I_{ph,n}$[A] is the photo-generated current at the nominal condition (generally 25^0C and 1000W/m^2), $\Delta_T = T - T_n$[K] (being T and T_n the actual and nominal temperature), G[W/m^2] is the irradiation on the device surface, and the G_n is the nominal irradiation.

The diode saturation current I_0 and its dependence on the temperature may be expressed as:

$$I_0 = I_{0,n}\left(\frac{T_n}{T}\right)^3 exp\left[\frac{qE_g}{aK}\left(\frac{1}{T_n} - \frac{1}{T}\right)\right] \tag{2.8}$$

where E_g is the bandgap energy of the semiconductor [≈1.12eV for polycrystalline Si at 25^0C] and $I_{0,n}$ is the nominal saturation current.

$$I_{0,n} = \frac{I_{sc,n}}{exp\left(\frac{V_{oc,n}}{aV_{t,n}}\right) - 1} \tag{2.9}$$

where $I_{sc,n}$ is the nominal short circuit current, $V_{oc,n}$ is the nominal open circuit voltage, $V_{t,n}$is the thermal voltage of N_s series connected cells at the nominal temperature T_n. Now the photovoltaic model can be improved by the following expression:

$$I_0 = \frac{I_{sc,n} + K_I\Delta_T}{exp\left(\frac{V_{oc,n} + K_V\Delta_T}{aV_t}\right) - 1} \tag{2.10}$$

where K_I is current temperature coefficient, K_V is the voltage temperature coefficient.

2.2.2 Design of L-type DSTATCOM

For proper functioning of DSTATCOM, the parameters such as the capacitance of dc link, the voltage across dc bus and the value of ac interfacing filter must be chosen carefully. So under this subsection the function and selection criteria of these parameters are described. The design of these components is based on the following assumptions:

- The grid voltage is sinusoidal.
- The AC side line current distortion is assumed to be 5% [70] for designing. But when distortion is more than 5%, there would be an increase of interruption in injecting compensating current.
- There is fixed capability of reactive power compensation of the active filter.
- The PWM converter is assumed to operate in the linear modulation mode (i.e. $0 \le M \le 1$), where M is the amplitude modulation factor.

2.2.2.1 Design of DC capacitor voltage

The dc bus capacitor serves two main purposes

- It maintains a dc voltage with small ripple in steady state
- Serves as an energy storage element to supply real power difference between load and source during the transient period

In steady state, the real power supplied by source should be equal to the real power demand of the load plus a small power to compensate the losses in the active filter. Thus, the dc capacitor voltage can be maintained at a reference value. However, when the load condition changes the real power balance get disturbed between source and load. This real power difference is to be compensated by the dc capacitor.

A smaller dc capacitor voltage than the reference voltage means that the real power supplied by the source is not enough to supply the load demand. Similarly, a larger dc capacitor voltage than the reference voltage means the source is suppling more real power to load than the load demand. So, the reference value of the dc bus voltage for the voltage source inverter can be defined as:

$$V_{pv} = \frac{2\sqrt{2}V_{LL}}{\sqrt{3}m} \tag{2.11}$$

where V_{LL} is the source line to line voltage, m is the modulation index (often chosen as 1).

2.2.2.2 Design of DC bus capacitor

The value of dc capacitor (C_{dc}) of VSC based DSTATCOM depend on the instantaneous energy available to the DSTATCOM during transients. The dc capacitor is calculated as follows [71]:

$$\frac{1}{2}C_{dc}\left[\left(V_{pv}\right)^2 - \left(V_{pv1}\right)^2\right] = 3V(\alpha I)t \tag{2.12}$$

where V_{pv} is the reference dc bus voltage, V_{pv1} is the minimum voltage level of dc bus voltage, V is the phase voltage of source, I is phase current of source, α is overloading factor (in general taken as 1.2), t is the time by which dc bus voltage is to be recovered.

2.2.2.3 Design of passive ac interfacing inductor

The passive L-type ac interfacing inductor acts as the link between the filter and system. A PV-DSTATCOM delivers its current through the inductor. For controllability of the DSTATCOM, this inductor should not be large. On the other hand, L_f as a first order passive filter, prevents switching frequency, which is generated by the inverter. Based on this feature, L_f should not be small. Therefore a compromise should be made to find an appropriate value of L_f. The value of the ac interfacing inductor can be determined by following expression [71]:

$$L_f = \frac{\sqrt{3}mV_{pv}}{12\alpha f_s i_{cr(p-p)}} \tag{2.13}$$

where m is the modulation index, V_{pv} is the reference dc bus voltage, f_s is the switching frequency, $i_{cr(p-p)}$ is current ripple (generally below 5% taken).

2.3 Control methods of L-type PV-DSTATCOM

The objective of PV-DSTATCOM is to improve the power quality of the system by eliminating the current harmonics, load current unbalancing and compensating the reactive power. These objectives can be achieved through a proper control scheme of PV-DSTATCOM. The controller of a PV-DSTATCOM generates a reference current in phase with source voltage and then the actual source current is compared with the reference current to calculate the error. Further, the error is used to develop the switching patterns for voltage source converter. The overall control scheme of PV-DSTATCOM is operated mainly in two control loops (a) inner current control loop [generation of reference current and switching pattern for IGBTs] (b) outer voltage control loop [dc bus voltage control]. So under this section different control methods for reference current generation and dc bus voltage control are explained.

2.3.1 Reference Current Generation

Usually, performance of the L-type PV-DSTATCOM in current control mode mainly depends upon generation of reference filter currents. In this work reference currents are generated using

- Instantaneous reactive power theory (IRPT)
- Modified Instantaneous reactive power theory (MIRPT)
- IcosΦ algorithm

2.3.1.1 Instantaneous Reactive Power Theory

The instantaneous reactive power (IRP) theory is also known as p-q theory. The instantaneous reactive power theory is **based on set of instantaneous power defined in the time domain**. As IRP theory is considered as a power theory one could expect that it does provide a clear interpretation of power phenomena in electrical system. The power properties of a three phase three wire systems with purely sinusoidal voltage and current i.e. even if without any harmonic distortions are determined by three independent features of the system:

- Permanent energy transmission and associated active power (P)
- Presence of reactive element in load and associated reactive power (Q)
- Load imbalance that causes supply current asymmetry and associated unbalanced power (D)

Moreover, according to Akagi and Nabae who developed IRP theory [72], its development was a response to “the demand to instantaneously compensate the reactive power”. So no need of worry about unbalanced power.

The IRP theory can be implemented in all reference frames but generally used in α-β coordinates due to the ease of calculation. The α-β reference frame is a static reference same as a-b-c coordinate reference frame but converted to two phase from three phase. So the calculation in this frame is easier. The control block diagram for IRPT scheme has been shown in Fig. 2.2.3.

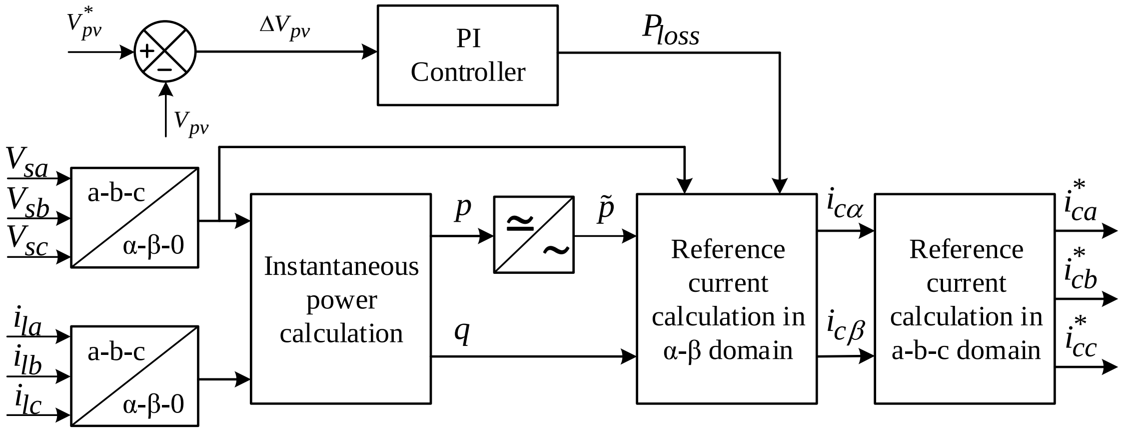

Fig. 2.2.3 Control block diagram for generation of reference current using IRPT scheme

This method uses an algebra transformation for three phase voltages and currents known as Park’s transformation which is easily converting the space vectors into the orthogonal α-β coordinates as expressed below:

$$\begin{bmatrix} V_{s\alpha} \\ V_{s\beta} \end{bmatrix} = \sqrt{\frac{2}{3}} \begin{bmatrix} 1 & -1/2 & -1/2 \\ 0 & \sqrt{3}/2 & -\sqrt{3}/2 \end{bmatrix} \begin{bmatrix} V_{sa} \\ V_{sb} \\ V_{sc} \end{bmatrix} \tag{2.14}$$

$$\begin{bmatrix} i_{l\alpha} \\ i_{l\beta} \end{bmatrix} = \sqrt{\frac{2}{3}} \begin{bmatrix} 1 & -1/2 & -1/2 \\ 0 & \sqrt{3}/2 & -\sqrt{3}/2 \end{bmatrix} \begin{bmatrix} i_{la} \\ i_{lb} \\ i_{lc} \end{bmatrix} \tag{2.15}$$

The conventional definition of apparent power (S), upon which the equipment rating is based, is related to the nominal voltage and current handled by the equipment under balanced condition. The reactive power in 3-phase system is defined to match the apparent and real power in Pythagoras triangle. However, for non-linear systems some modifications are necessary. When harmonic currents are present in the system, concept of displacement power factor and THD must be introduced. In presence of non-sinusoidal waveform, the classical & spatial vector power definition has some important differences. So, for three phase system where non-sinusoidal currents are present, the instantaneous power is calculated as follows:

$$p = V_{s\alpha} i_{l\alpha} + V_{s\beta} i_{l\beta} \tag{2.16}$$

$$q = V_{s\alpha} i_{l\beta} - V_{s\beta} i_{l\alpha} \tag{2.17}$$

For the system, which do not contain neutral connection, the zero sequence doesn't exist and the above equation can be presented in matrix form as follows

$$\begin{bmatrix} p \\ q \end{bmatrix} = \begin{bmatrix} V_{s\alpha} & V_{s\beta} \\ -V_{s\beta} & V_{s\alpha} \end{bmatrix} \begin{bmatrix} i_{l\alpha} \\ i_{l\beta} \end{bmatrix} \tag{2.18}$$

In (2.16) $V_{s\alpha} i_{l\alpha}$ and $V_{s\beta} i_{l\beta}$; means instantaneous power because they are defined by the product of the instantaneous voltage in one axis and the instantaneous current in the same axis. Therefore, p is the real power in the three-phase circuit and its dimension is (W). Conversely, $V_{s\alpha} i_{l\beta}$ and $V_{s\beta} i_{l\alpha}$ in (2.17) are not instantaneous power because they are defined by the product of the instantaneous voltage in one axis and the instantaneous current not in the same axis but in the perpendicular axis. Accordingly, q cannot be dealt with as a conventional electrical quantity. So, a new dimension must be introduced for q, because the dimension is not (W), (VA), or (VAR). Hereinafter, the authors have named the conventional instantaneous power 'p' as "instantaneous real power" and 'q' as instantaneous imaginary power and unit is imaginary volt ampere (IVA).

The instantaneous real and imaginary power calculated from (2.18) have constant values and a superposition of oscillating components. So both the instantaneous powers can be separated into two parts

- Average or DC component ($\bar{p},\ \bar{q}$)
- Oscillating or AC component ($\tilde{p},\ \tilde{q}$)

The average value '$\bar{p}$' represents the energy flowing per time unity in one direction only. The oscillating part '$\tilde{p}$' represents the oscillating energy flow per time unity, naturally produces zero value, representing an amount of additional power flow in the system without effective contribution to the energy transfer from the source to the load or from the load to the source. So, to eliminate harmonics from the source current it is necessary to compensate '$\tilde{p}$' and for compensation of reactive power both the '$\bar{q}$', '$\tilde{q}$' should be compensated. Therefore, the reference current is calculated as below:

$$\begin{bmatrix} i_{c\alpha} \\ i_{c\beta} \end{bmatrix} = \frac{1}{V_{s\alpha}^2 + V_{s\beta}^2} \begin{bmatrix} V_{s\alpha} & V_{s\beta} \\ -V_{s\beta} & V_{s\alpha} \end{bmatrix} \begin{bmatrix} -\tilde{p} + P_{loss} \\ -q \end{bmatrix} \tag{2.19}$$

The importance and calculation of P_{loss} is described in Section 2.3.2. The reference current generated in α-β domain is transformed to a-b-c reference frame through an inverse Park's transformation as mentioned below:

$$\begin{bmatrix} i_{ca}^* \\ i_{cb}^* \\ i_{cc}^* \end{bmatrix} = \begin{bmatrix} 1 & 0 \\ -\frac{1}{2} & \frac{\sqrt{3}}{2} \\ -\frac{1}{2} & -\frac{\sqrt{3}}{2} \end{bmatrix} \begin{bmatrix} i_{c\alpha} \\ i_{c\beta} \end{bmatrix} \tag{2.20}$$

2.3.1.2 Modified Instantaneous Reactive Power Theory

The conventional instantaneous reactive power theory (IRPT) is applicable to balance and sinusoidal source or grid. But in practical, the non-sinusoidal load current when flows through the system impedance the voltage at the point of common coupling gets distorted. So the source or grid voltage seen by the load is non-sinusoidal voltage rather than a sinusoidal voltage. Under non-ideal mains voltage conditions, the sum of component $(V_{s\alpha}^2 + V_{s\beta}^2)$ will not be constant and alternating values of the instantaneous real and imaginary power have current harmonics and voltage harmonics. Consequently, the PV-DSTATCOM does not generate compensation current equal to current harmonics and supplies mains more than load harmonics than required. As the conventional IRPT does not offers a convincing performance for non-sinusoidal source voltage, the authors in [73] proposed a modification to IRP theory as shown in Fig. 2.4.

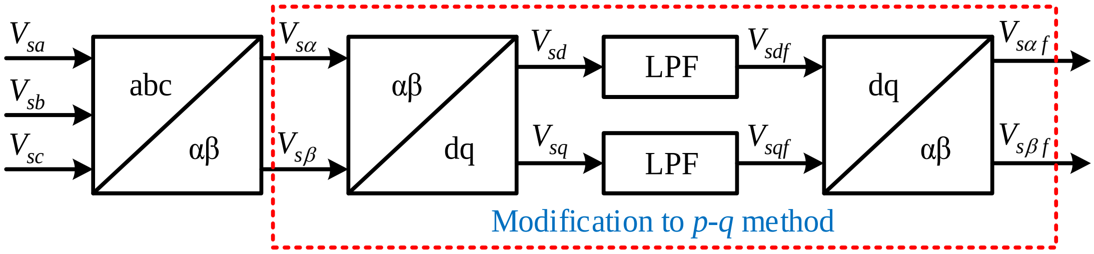

Fig. 2.4 The modified IRP theory based method for L-type PV-DSTATCOM

According to the modified instantaneous reactive power theory, the instantaneous reactive and active powers have to be calculated after filtering of mains voltages. In this method, instantaneous voltages are first converted to static α-β coordinate reference frame as expressed in (2.14) and then to synchronous d-q coordinates (Park Transformation) as Eq. (2.21):

$$\begin{bmatrix} V_{sd} \\ V_{sq} \end{bmatrix} = \begin{bmatrix} cos\phi & sin\phi \\ -sin\phi & cos\phi \end{bmatrix} \begin{bmatrix} V_{s\alpha} \\ V_{s\beta} \end{bmatrix} \tag{2.21}$$

In rotating d-q coordinate reference frame all the frequency components are shifted downward by one harmonic order. Hence in a distorted ac signal which contains harmonics, by the use of d-q transformation the fundamental frequency component appears like dc values and the frequency component appears like ripples. So the produced d-q components of the voltages are filtered by using the 5th order low-pass filter with a cut-off frequency at 50 Hz. These filtered d-q components of voltages are reverse converted to α-β coordinates as expressed in

$$\begin{bmatrix} V_{s\alpha} \\ V_{s\beta} \end{bmatrix} = \begin{bmatrix} cos\phi & -sin\phi \\ sin\phi & cos\phi \end{bmatrix} \begin{bmatrix} V_{sd} \\ V_{sq} \end{bmatrix} \tag{2.22}$$

These α-β components of voltages are used in conventional IRP theory. Hence, the non-ideal mains voltages are converted to ideal sinusoidal shape by using low pass filter (LPF) in d-q coordinate. The control block diagram for the generation of reference current using modified IRPT scheme is shown in Fig. 2.5.

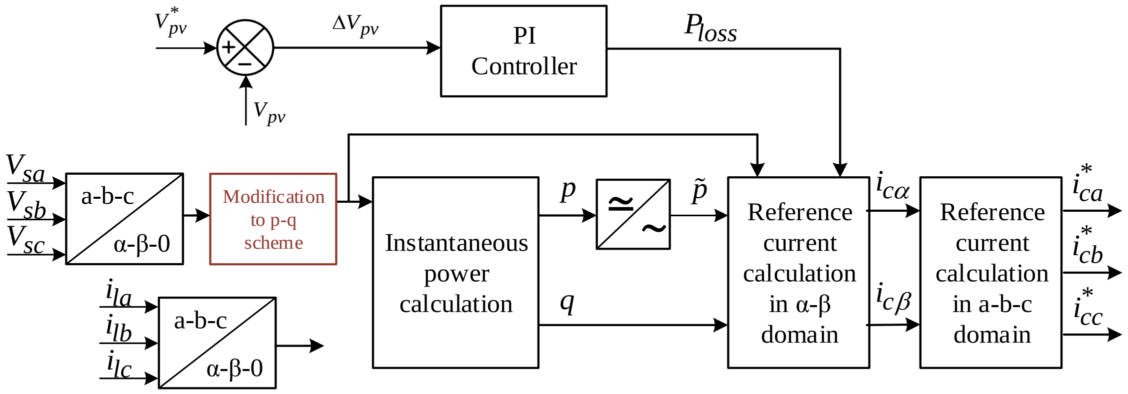

Fig. 2.5 Control block diagram for generation of reference current using modified IRPT scheme

2.3.1.3 IcosΦ Algorithm

The reference current generation algorithm for an L-type PV-DSTATCOM computes the reference compensation currents to be injected by the distributed static compensator. The choice of the control algorithm therefore decides the accuracy and response time of the filter. The calculation steps involved in the control technique have to be minimal to make the control circuit compact. The IcosΦ algorithm uses minimum computational steps and is simple to practically implement in the system conditions like distorted and asymmetrical AC source supplying non-linear unbalanced loads as compared to modified instantaneous reactive power theory. In cases where both reactive power and harmonic compensation are provided, the source is supposed to supply only the active portion of the load current (i.e., IcosΦ, where "I" is the amplitude of the fundamental load current and is the displacement power factor of the load). So the proposed algorithm is named the "IcosΦ" algorithm. It is capable of providing (a) harmonic compensation, (b) reactive power compensation, and (c) unbalance compensation in conjunction with achieving unity power factor at the source end. The algorithm is designed to work successfully for balanced as well as unbalanced and distorted source voltages feeding balanced or unbalanced nonlinear reactive loads. The entire control structure for generation of reference current using IcosΦ algorithm is shown in Fig. 2.6.

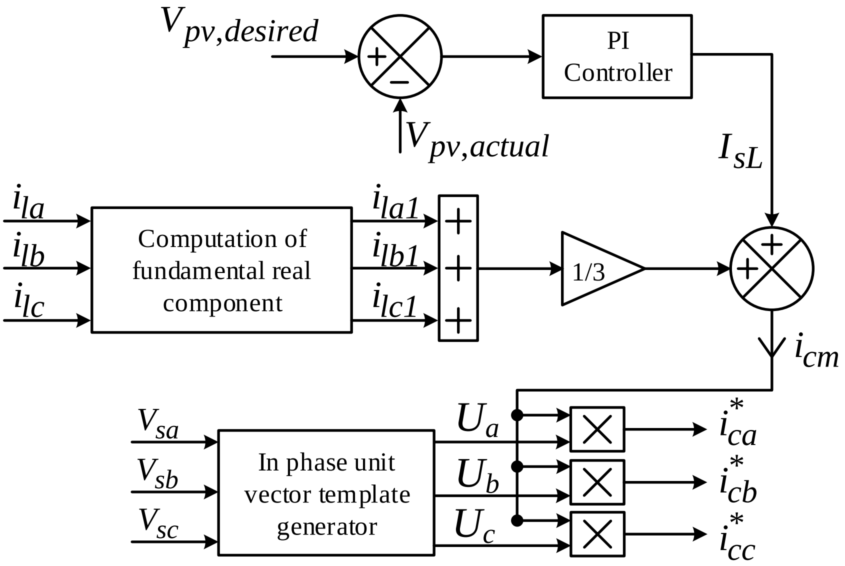

Fig. 2.6 Control structure for reference current generation using IcosΦ algorithm

Assuming a balanced source, the three-phase instantaneous voltages can be specified as:

$$V_{sa} = V_m \sin \omega t \tag{2.23}$$

$$V_{sb} = V_m \sin(\omega t - 120^0) \tag{2.24}$$

$$V_{sb} = V_m \sin(\omega t + 120^0) \tag{2.25}$$

This balanced source supply a non-linear current to the reactive non-linear load (i.e. three phase bridge rectifier with ohmic-inductive load) which can be expressed as:

$$i_{la} = I_{la1} \sin(\omega t - \varphi_{a1}) + \sum_{n=2}^{\infty} I_{lan} \sin(n\omega t - \varphi_{an}) \tag{2.26}$$

$$i_{lb} = I_{lb1} \sin(\omega t - \varphi_{b1}) + \sum_{n=2}^{\infty} I_{lbn} \sin(n\omega t - \varphi_{bn}) \tag{2.27}$$

$$i_{lc} = I_{lc1} \sin(\omega t - \varphi_{c1}) + \sum_{n=2}^{\infty} I_{lcn} \sin(n\omega t - \varphi_{cn}) \tag{2.28}$$

where φ_{a1}, φ_{b1}, φ_{c1} are the phase angles of fundamental currents in phase a, b, c; φ_{an}, φ_{bn}, φ_{cn} are the phase angles of the nth harmonic currents in a, b, and c phases; I_{la1}, I_{lb1}, I_{lc1} are three-phase fundamental current amplitudes; I_{lan}, I_{lbn}, I_{lcn} are three-phase nth harmonic current amplitudes. The magnitude of the real component of the fundamental load current in each phase is given as:

$$|Re(I_{la1})| = |i_{la1}| \cos \varphi_1 \tag{2.29}$$

$$|Re(I_{lb1})| = |i_{lb1}| \cos \varphi_1 \tag{2.30}$$

$$|Re(I_{lc1})| = |i_{lc1}| \cos \varphi_1 \tag{2.31}$$

To ensure balanced, sinusoidal currents at a unity power factor to be drawn from the source, the magnitude of the desired source current can be expressed as the average of the magnitudes of the real components of the fundamental load currents in the three phases. Hence, peak of the current supplied by the source for a balanced system can be expressed as:

$$I_{cm} = \left(\frac{|Re(I_{la1})| + |Re(I_{lb1})| + |Re(I_{lc1})|}{3}\right) + I_{sL} \tag{2.32}$$

where I_{sL} is the output of proportional plus integral (PI) controller used for maintenance of dc bus voltage. The importance and detailed calculation of I_{sL} is discussed in Section 2.3.2. For ideal compensation, it is necessary that the reference source current should be pure sinusoidal having magnitude same as i_c and also be in phase with source voltage. Therefore, the calculated peak value of the source current is multiplied with the unit templates (U_a, U_b, U_c), which are in phase with the source voltage.

$$U_a = 1 \cdot \sin \omega t \tag{2.33}$$

$$U_b = 1 \cdot \sin \omega t - 120^0 \tag{2.34}$$

$$U_c = 1 \cdot \sin \omega t + 120^0 \tag{2.35}$$

Now the reference source currents are represented as:

$$i_{ca}^{*} = I_{cm} U_a = I_{cm} \sin(\omega t) \tag{2.36}$$

$$i_{cb}^{*} = I_{cm} U_b = I_{cm} \sin(\omega t - 120^0) \tag{2.37}$$

$$i_{cc}^{*} = I_{cm} U_c = I_{cm} \sin(\omega t + 120^0) \tag{2.38}$$

2.3.2 DC bus voltage control

For continuous and effective compensation the dc bus voltage should be maintained at its reference value. The dc side capacitor serves two main purposes:

- It maintains a dc voltage with small ripple in steady state.
- Serves as an energy storage element to supply real power difference between load and source during the transient period.

In steady state, the real power supplied by the source should be equal to the real power demand of the load plus a small power to compensate the losses in the distributed static compensator. Thus, the dc capacitor voltage can be maintained at a reference value. However, when the load condition changes the real power balance gets disturbed between source and load. This real power difference is to be compensated by the dc capacitor. A lower dc capacitor voltage than the reference voltage means that the real power supplied by the source is not enough to supply the load demand and vice versa.

As in the system there is no battery storage system connected to the DC bus, the total energy delivered by the PV units may overcharge the DC capacitor. This energy should be injected into the AC source by controlling the current injected into the DC bus. Therefore to maintain the dc link voltage at its reference value a proportional plus integral (PI) controllers are used. The voltage error between the measured voltage across the DC capacitor and the reference DC bus voltage can be defined as follows:

$$V_e = V_{pv}^{ref} - V_{pv}$$

The calculated voltage error is passed through PI controller and the output is added to filter current to generate reference current. Adjusting the gains of PI compensator, a fast tracking and zero steady state error can be achieved. The voltage error has been regulated by PI controller and mathematically can be explained as:

$$P_{loss} = K_p V_e + K_i \int V_e dt$$

where K_p is $2\tau\omega_{nv}C$; K_i is $C\omega_{nv}^2$;τ represents damping factor (calculated as $\sqrt{2}/2$); ω_{nv} is natural frequency or fundamental frequency.

2.3.3 Hysteresis Band Current Controller (HBCC)

The actual L-type PV-DSTATCOM line currents are monitored instantaneously, and then compared to the reference currents generated by the control algorithm. In order to get precise instantaneous current control, the current control method must supply quick current controllability, thus quick response. For this reason, hysteresis band current control for active power filter line currents is implemented to generate the switching pattern of the inverter. There are various current control methods proposed for such active power filter configurations, but in terms of quick current controllability and easy implementation hysteresis band current control method has the highest rate among other current control methods such as sinusoidal PWM. Hysteresis band current control is the fastest control with minimum hardware and software but even switching frequency is its main drawback.

The hysteresis band current control scheme, used for the generation of switching pattern for IGBTs of voltage source inverter is shown in Fig. 2.7, composed of a hysteresis around the reference line current. The reference line current of the PV-DSTATCOM is referred to as i_c^* and actual line current of the PV-DSTATCOM is referred to as i_s. The hysteresis band current controller decides the switching pattern of active power filter. The switching logic is formulated as follows:

- If $i_s < (i_{ca}^* - HB)$ upper switch is OFF and lower switch is ON for leg "a" (SA = 1).
- If $i_s > (i_{ca}^* + HB)$ upper switch is ON and lower switch is OFF for leg "a" (SA = 0).

The switching functions SB and SC for phases "b" and "c" are determined similarly, using corresponding reference and measured currents and hysteresis bandwidth (HB).

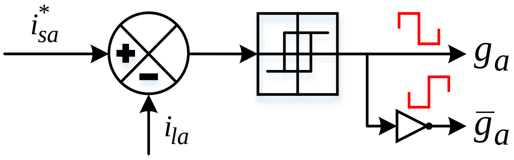

Fig. 2.7 Switching pattern generation using HBCC for leg-a

2.4 Results and Discussions

In order to verify the efficacy of the presented L-type PV-DSATCOM, a MATLAB/ SIMULINK is pursued. A balanced three phase voltage supply has been applied to a typical non-linear load comprising of a three phase diode rectifier bridge feeding a R-L load. The system simulation parameters and the specification of photovoltaic array have been summarized in Table 2.1 and

Table **2.2** respectively.

Table 2.1 L-Type PV-DSTATCOM parameters used for simulation

System Parameters	**Values**	**System Parameters**	**Values**
Source voltage (V_s)	230V/rms	Reference DC link voltage (V_{pv}^*)	650V
System frequency (f)	50Hz	Switching frequency (f_{sw})	12kHz
Source inductance (L_s)	0.18mH	PI controller gains (K_p, K_i)	0.546, 10.37
Filter impedance (R_f, L_f)	1Ω, 25mH	DC link capacitance (C_{dc})	2200μF

Table 2.2 Parameters of the KC200GT solar array at 25°C, 1.5AM, 1000 W/m^2

System Parameters	**Values**	**System Parameters**	**Values**
Rated maximum power (P_{max})	200.143W	Series resistance (R_s)	0.221Ω
Short circuit current (I_{sc})	8.21A	Shunt resistance (R_{sh})	415.405Ω
Open circuit voltage (V_{oc})	32.9V	S.C current coefficient (K_i)	0.0032A/K
Diode Ideality constant (a)	1.3	O.C voltage coefficient (K_v)	-0.1230V/K
Number of PV array in series	15	Number of PV array in parallel	5

The potential of the presented L-type PV-DSTATCOM is to compensate harmonics, reactive power and load unbalancing with ideal as well as distorted supply voltages is analyzed using the following simulation results.

2.4.1 Simulation Results

In Section 2.3 it is described that, IRP theory performs satisfactorily for ideal supply voltage conditions but not for distorted supply voltages. So, to verify the superior performance of proposed system with IcosΦ algorithm under ideal supply conditions, the results are compared with IRP theory based controller results. Under distorted supply conditions the same is compared with IRP theory and MIRP theory based controller results. The proposed L-type PV-DSTATCOM is simulated with different load conditions like nonlinear load, linear plus nonlinear load, thyristor load and unbalanced load under both ideal as well as distorted supply conditions in order to find out the effectiveness and robustness of the controllers towards load change and adverse supply conditions. The values and description for different loads are given in Table 2.3.

Table 2.3 Description of Load parameters

Load Type	**Description**	**Values**
Nonlinear Load	Three phase bridge rectifier with R-L load	R_{dc}=10Ω, L_{dc}=20mH
Linear Load	Three single phase resistors in parallel	R_1=10Ω, R_2=10Ω, R_3=10Ω

Unbalanced Load	Three phase rectifier with R load + Three single phase resistors in parallel	R_{dc}=10Ω,R_1=2Ω,R_2=5Ω, R_3= 8Ω
Thyristor Load	Three phase controlled bridge rectifier with R-L load	R_{dc}=12Ω, L_{dc}=20mH, Firing angle: 30°:- for 0.06s to 0.1s, 60°:- for 0.1s to 0.15s, 30°:- for 0.15s to 0.18s.

2.4.1.1 Performance with nonlinear load under ideal supply voltage

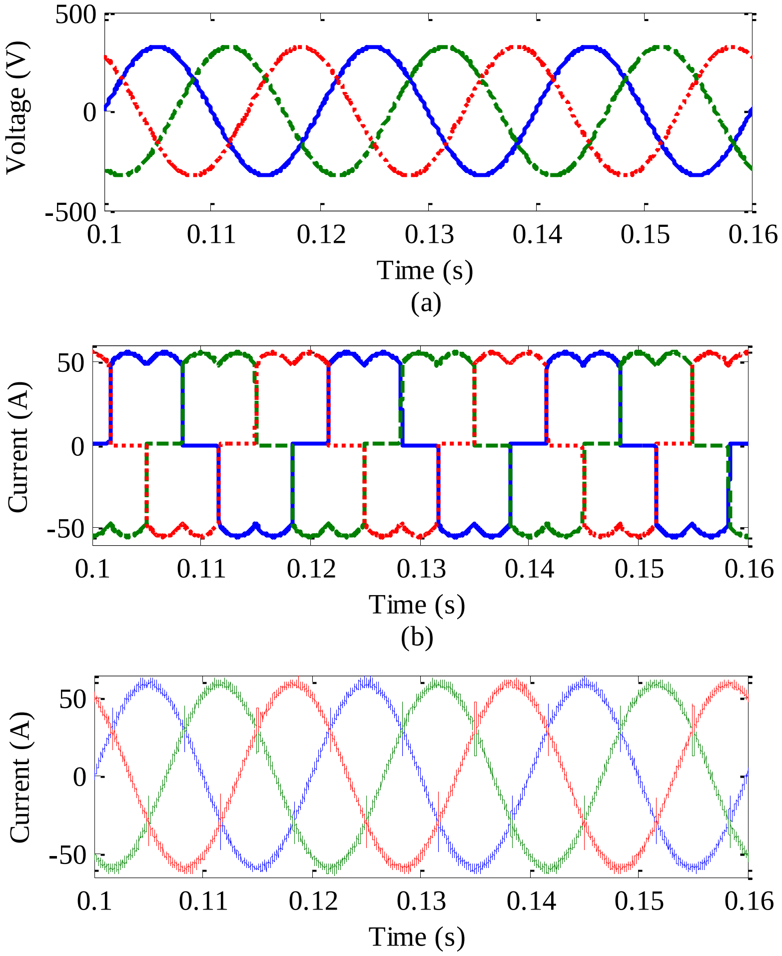

(a)

(b)

(c)

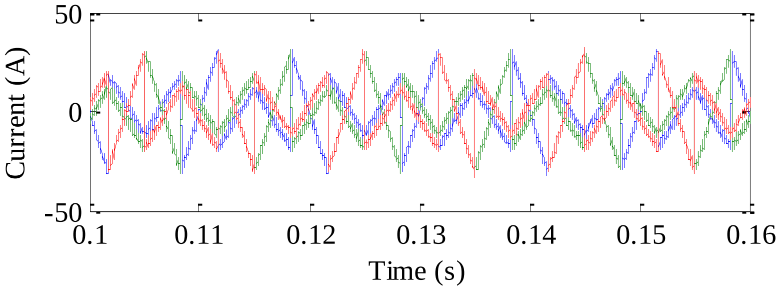

(d)

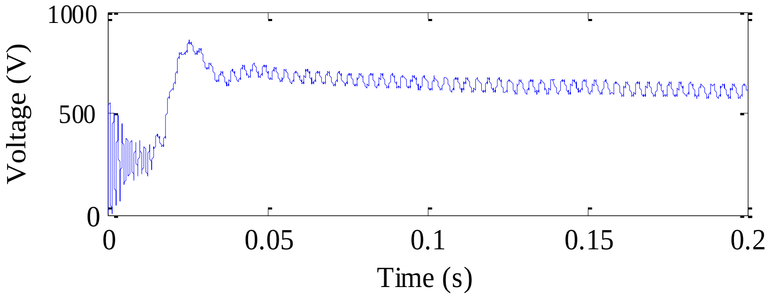

(e)

Fig. 2.8 Simulation results of L-type PV-DSTATCOM with nonlinear load and IRP theory (a) source voltage (b) load current before compensation (c) source current after compensation (d) filter current (e) voltage across dc bus.

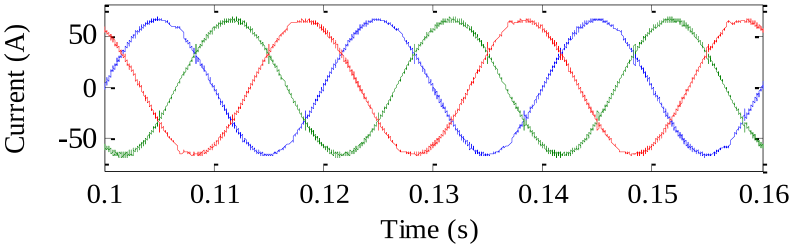

(a)

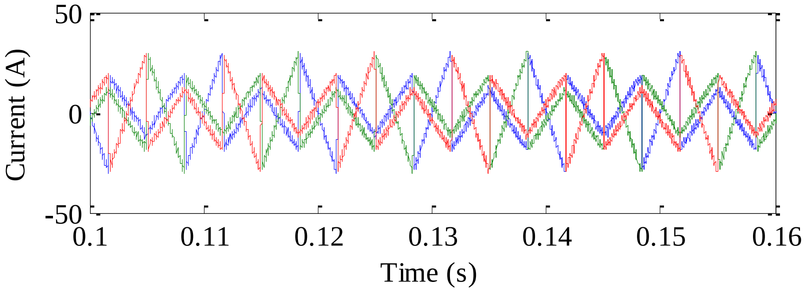

(b)

Fig. 2.9 Simulation results of L-type PV-DSTATCOM with nonlinear load and IcosΦ algorithm (a) source current after compensation (b) filter current

2.4.1.2 Performance with nonlinear plus linear load under ideal supply voltage

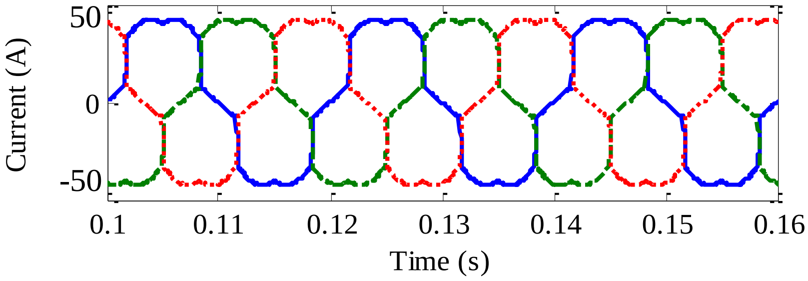

(a)

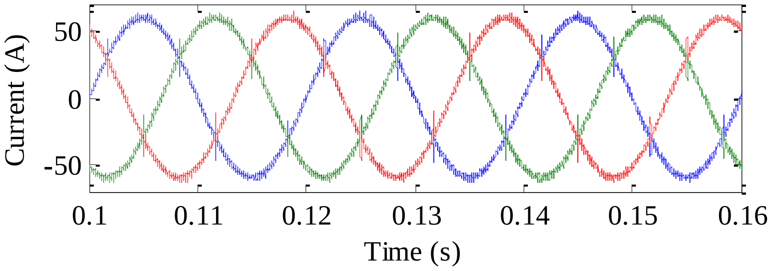

(b)

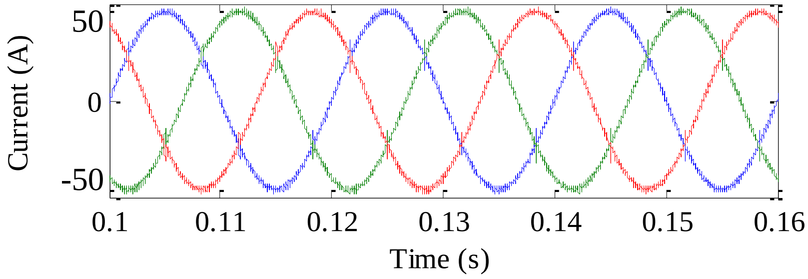

(c)

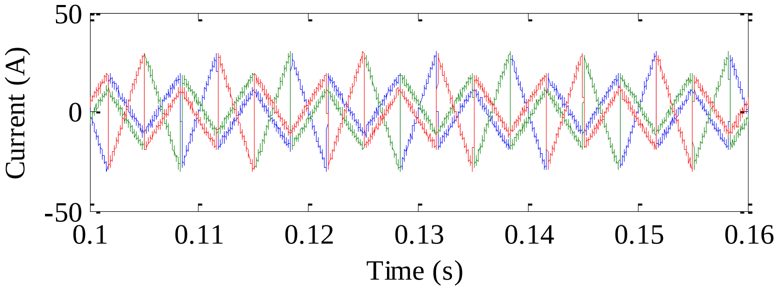

(d)

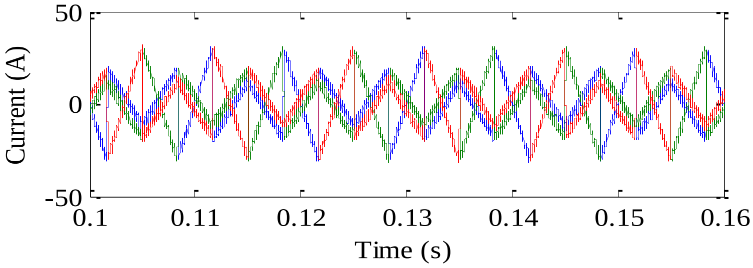

(e)

Fig. 2.10 Simulation results of L-type PV-DSTATCOM with nonlinear plus linear load (a) load current before compensation (b) source current after compensation with IRP theory (c) source current after compensation with IcosΦ algorithm (d) filter current with IcosΦ algorithm (e) filter current with IRP theory.

2.4.1.3 Performance with unbalance load under ideal supply voltage

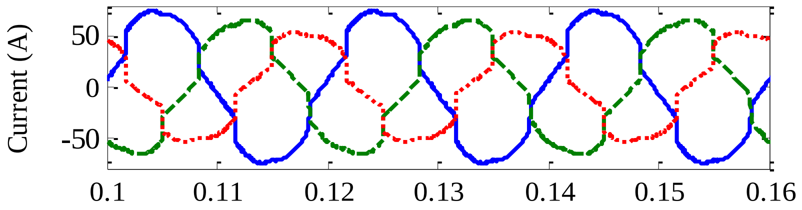

(a)

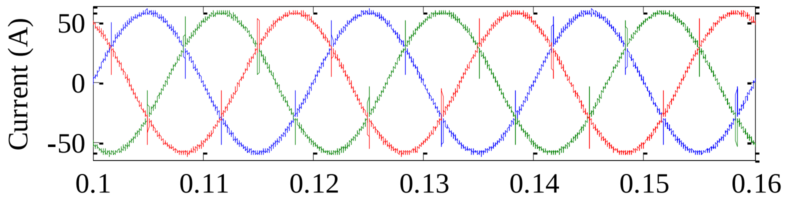

(b)

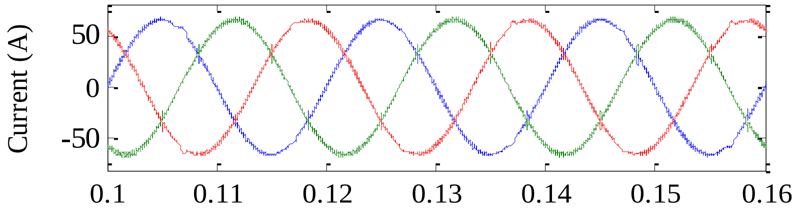

(c)

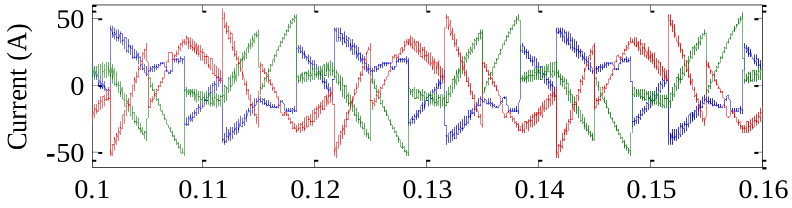

(d)

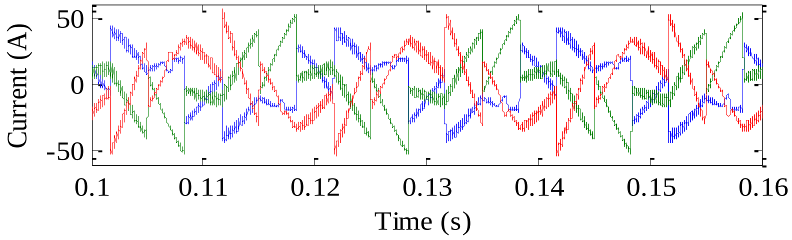

(e)

Fig. 2.11 Simulation results of L-type PV-DSTATCOM with unbalanced load (a) load current before compensation (b) source current after compensation with IRP theory (c) source current after compensation with IcosΦ algorithm (d) filter current with IRP theory (e) filter current with IcosΦ algorithm.

2.4.1.4 Performance with thyristor load under ideal supply voltage

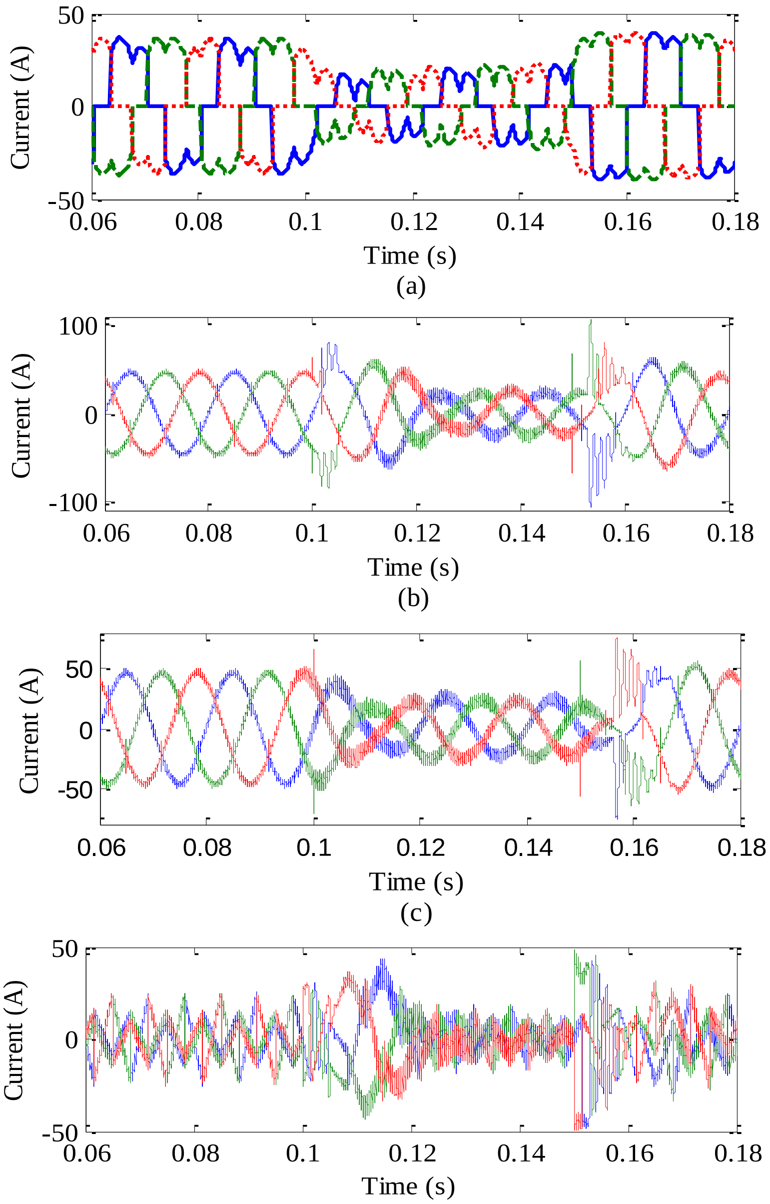

(d)

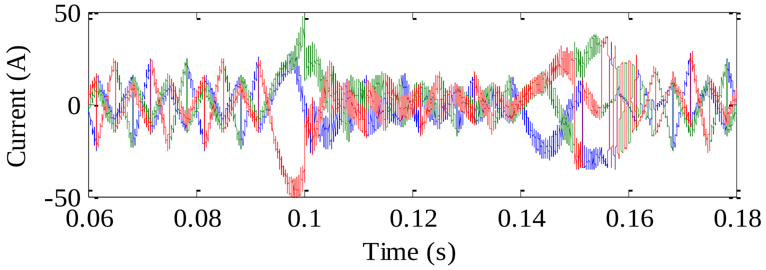

(e)

Fig. 2.12 Simulation results of L-type PV-DSTATCOM with thyristor load (a) load current before compensation (b) source current after compensation with IRP theory (c) source current after compensation with IcosΦ algorithm (d) filter current with IRP theory (e) filter current with IcosΦ algorithm.

2.4.1.5 Performance with nonlinear load under distorted supply voltage

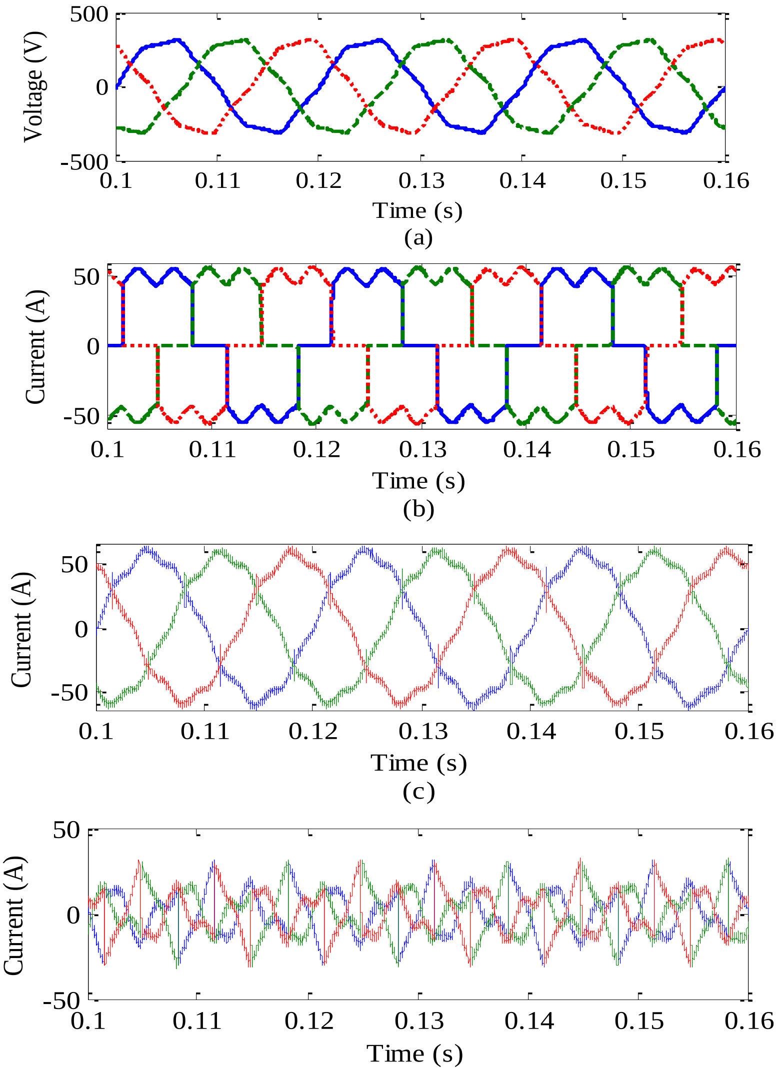

(d)

Fig. 2.13 Simulation results with nonlinear load and IRP theory under distorted supply (a) source voltage (b) load current before compensation (c) source current after compensation (d) filter current.

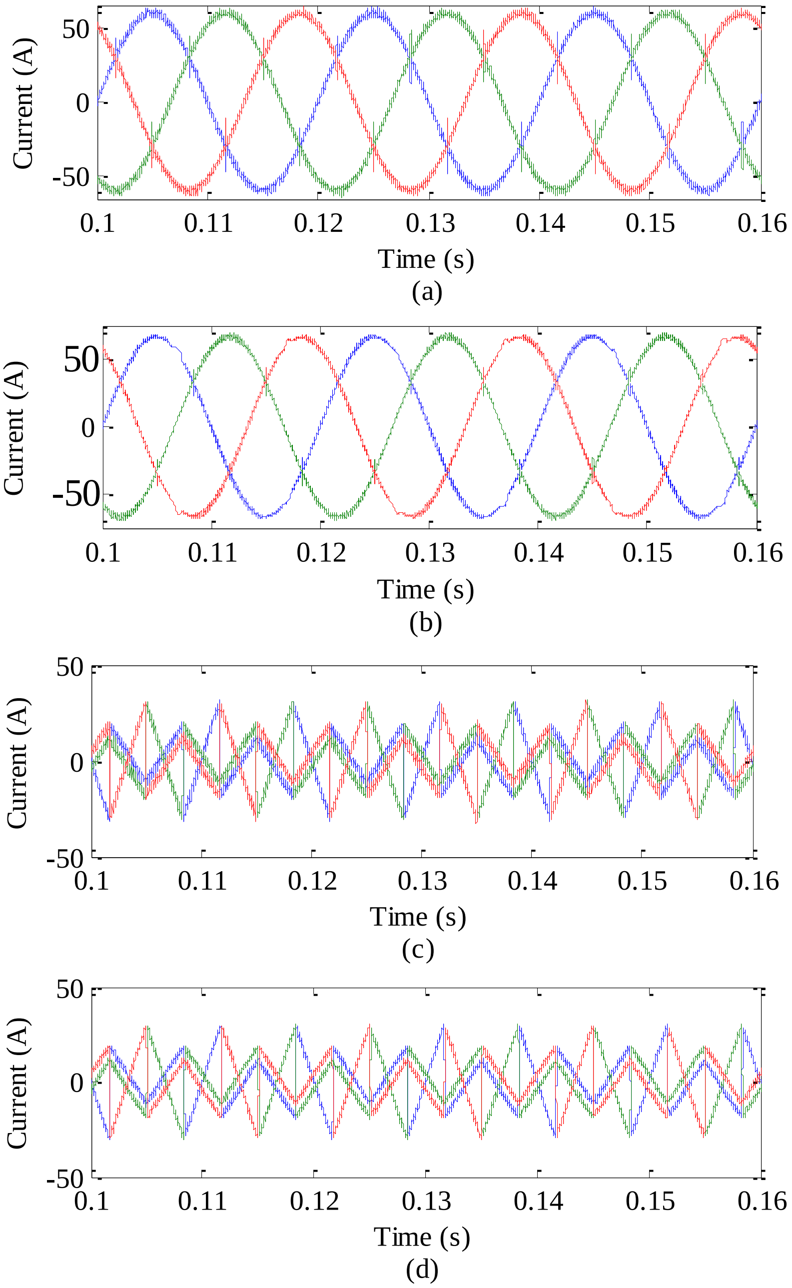

(a)

(b)

(c)

(d)

Fig. 2.14 Simulation results of L-type PV-DSTATCOM with nonlinear load under distorted supply (a) source current after compensation with MIRP theory (b) source current after compensation with IcosΦ algorithm (c) filter current with MIRP theory (d) filter current IcosΦ algorithm.

2.4.1.6 Performance with nonlinear plus linear load under distorted supply voltage

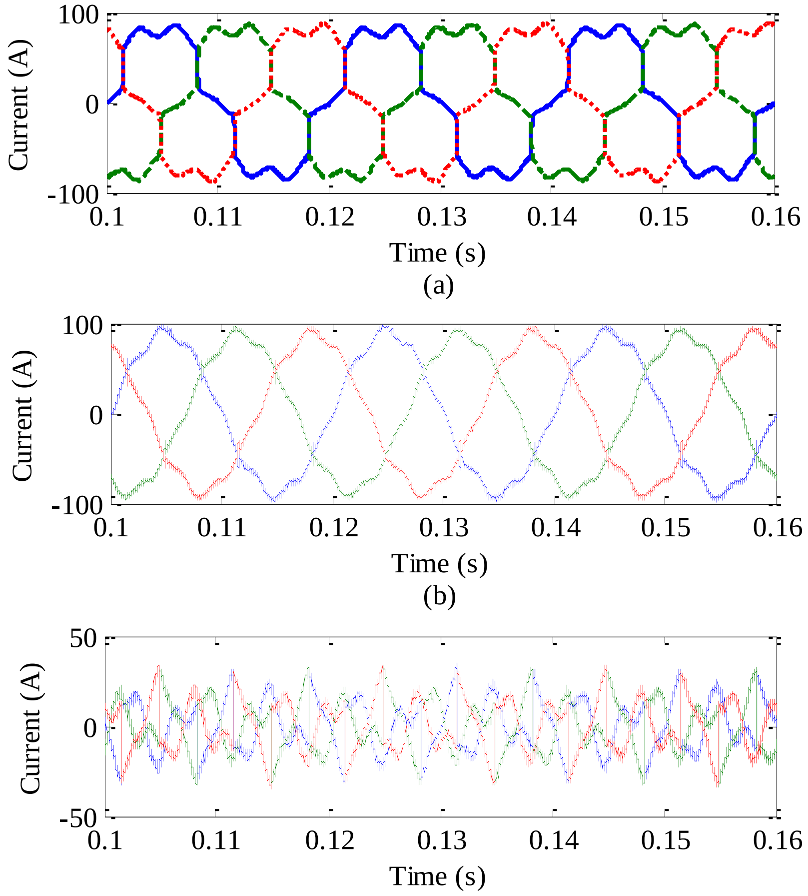

(a)

(b)

(c)

Fig. 2.15 Simulation results with nonlinear plus linear load and IRP theory under distorted supply (a) load current before compensation (b) source current after compensation (c) filter current

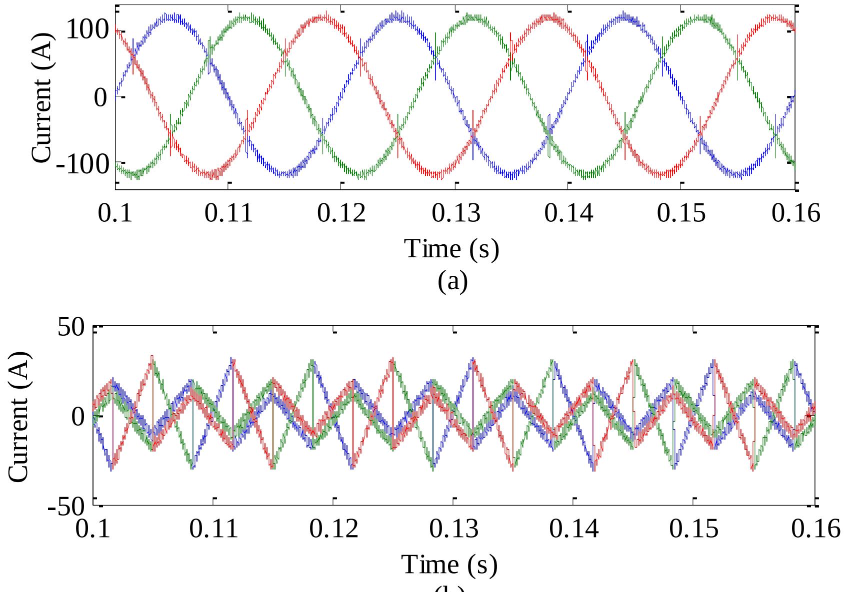

(a)

(b)

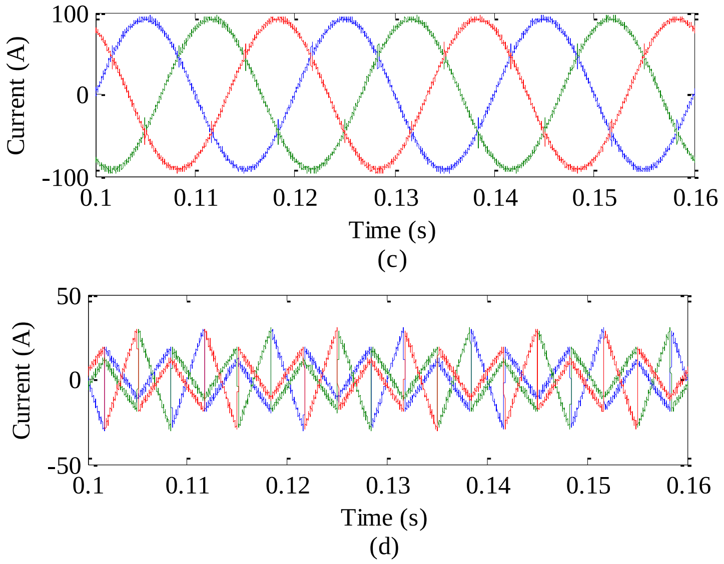

Fig. 2.16 Simulation results with nonlinear plus linear load under distorted supply (a) source current after compensation with MIRP theory (b) filter current with MIRP theory (c) source current after compensation with IcosΦ algorithm (d) filter current IcosΦ algorithm.

2.4.1.7 Performance with unbalanced load under distorted supply voltage

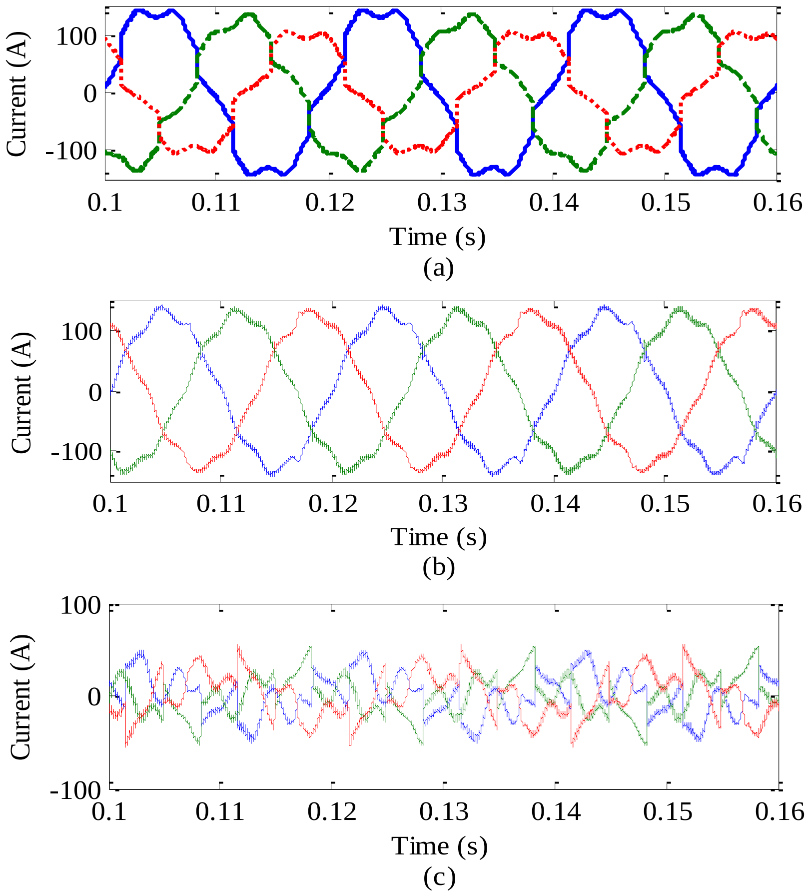

Fig. 2.17 Simulation results with unbalanced load and IRP theory under distorted supply (a) load current before compensation (b) source current after compensation (c) filter current.

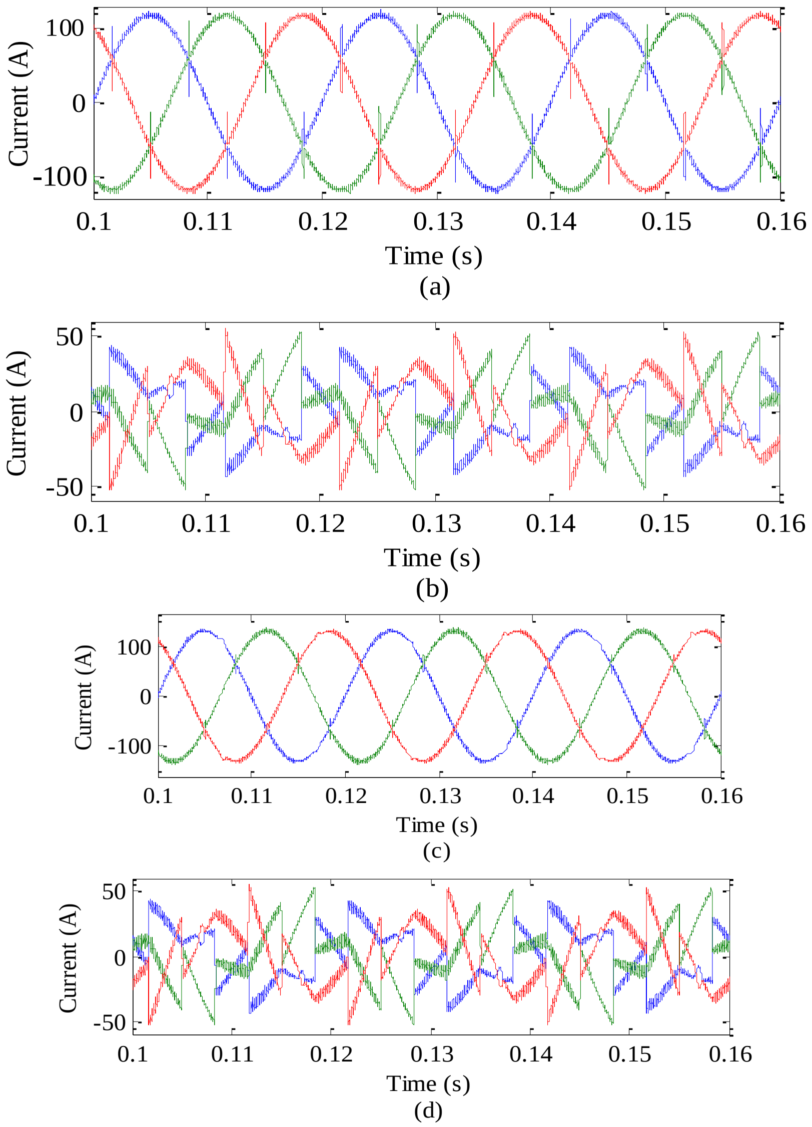

Fig. 2.18 Simulation results with unbalanced load under distorted supply (a) source current after compensation with MIRP theory (b) filter current with MIRP theory (c) source current after compensation with IcosΦ algorithm (d) filter current IcosΦ algorithm.

2.4.1.8 Performance with thyristor load under distorted supply voltage

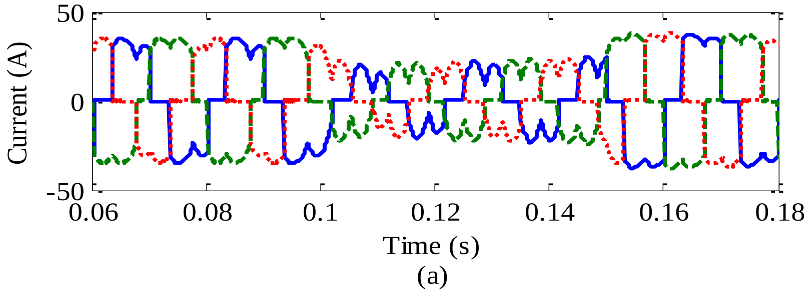

(a)

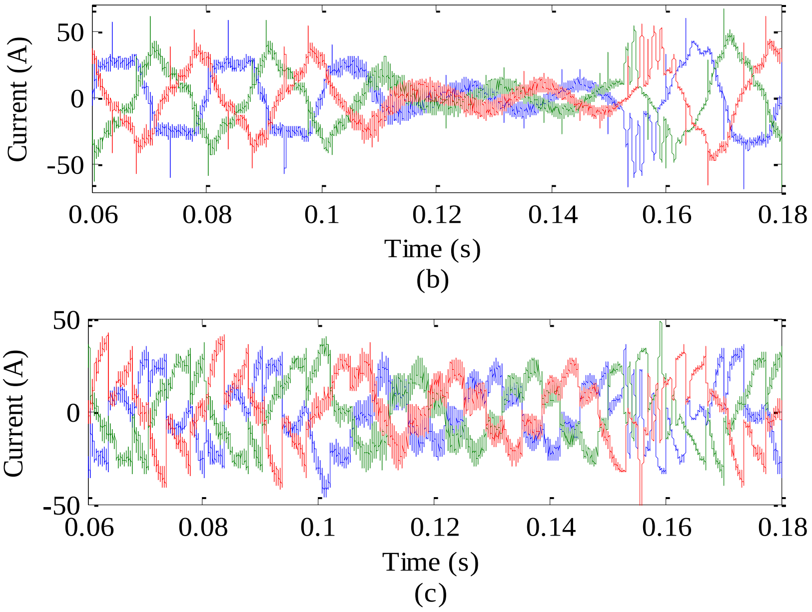

Fig. 2.19 Simulation results with thyristor load and IRP theory under distorted supply (a) load current before compensation (b) source current after compensation (c) filter current.

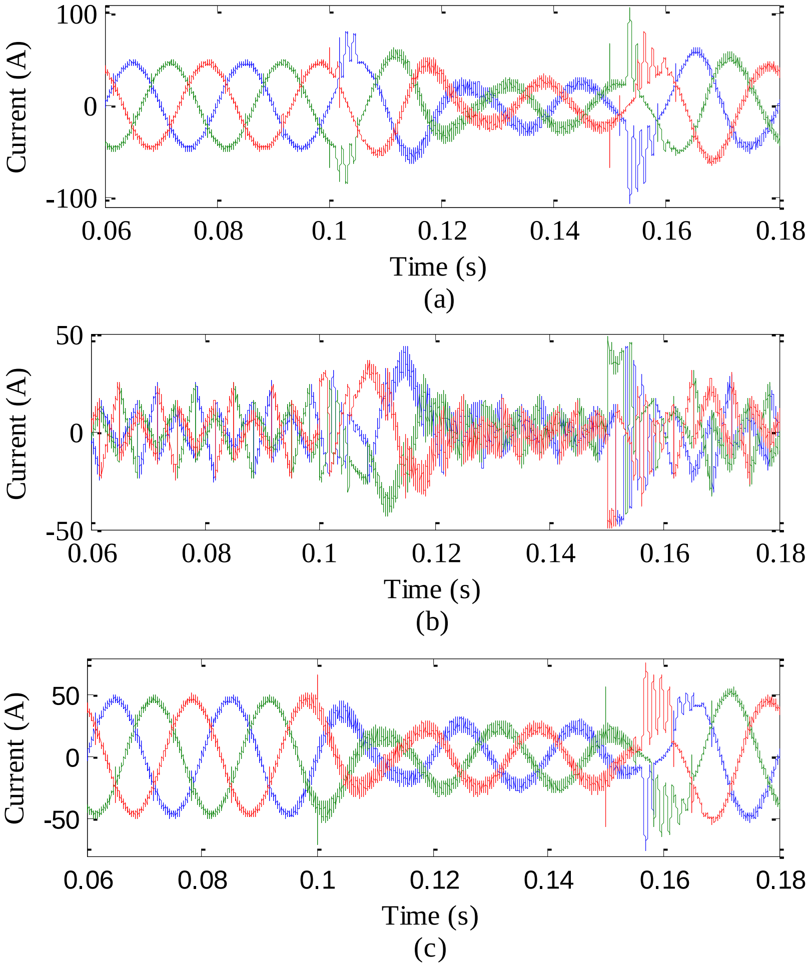

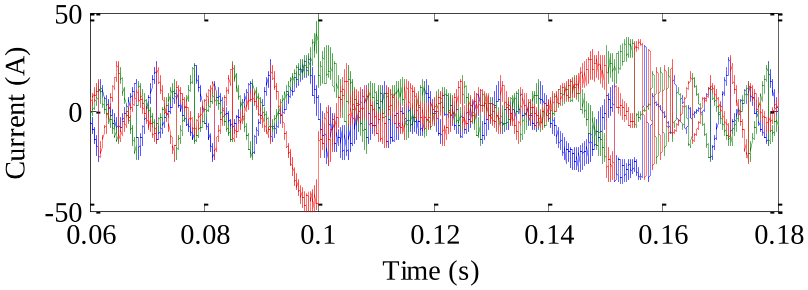

(d)

Fig. 2.20 Simulation results of L-type PV-DSTATCOM with thyristor load under distorted supply (a) source current after compensation with MIRP theory (b) filter current with MIRP theory (c) source current after compensation with IcosΦ algorithm (d) filter current IcosΦ algorithm.

Simulation results for L-type PV-DSTATCOM employing IRPT and IcosΦ schemes under ideal supply conditions are shown in Fig. 2.8 to Fig. 2.12. The nature of source current before compensation is exactly same as load current. From the results, it is observed that after compensation the harmonics from source current are eliminated for all type of loading conditions. Also both the control schemes are being able to reduce the reactive power burden on the system to a negligible amount. The PV-DSTATCOM with IcosΦ scheme performs better than the IRPT scheme and is easy to implement.

Simulation results for L-type PV-DSTATCOM employing IRPT, MIRPT and IcosΦ schemes under distorted supply conditions are shown in Fig. 2.13 to Fig. 2.20. Due to amplification of harmonic content during the calculation of instantaneous active and reactive powers under distorted supply conditions, the conventional IRPT scheme compensate harmonics imprecisely. This problem with IRPT control scheme can be verified from Fig. 2.13, Fig. 2.15, Fig. 2.17 and Fig. 2.19, in which for all loading conditions the source current is sinusoidal and contains high amount of harmonics even after compensation. These problems have been surpassed by both MIRPT and IcosΦ algorithm. But harmonics compensation performance of IcosΦ is better than the MIRPT control scheme with ease.

To rate the effectiveness of controllers, total harmonic distortion (THD) is considered as performance index. In order to calculate the overall THD of all three phases under all supply and loading conditions FFT analysis has been carried out. The bar diagrams presented in Fig. 2.21 to Fig. 2.28 show a comparison of the source current THDs for IRPT, MIRPT and IcosΦ control schemes with and without L-type PV-DSTATCOM. From the bar diagrams it is observed that PV-DSTATCOM with IcosΦ control algorithm compensates harmonics more efficiently than the other two control algorithms for all operational conditions.

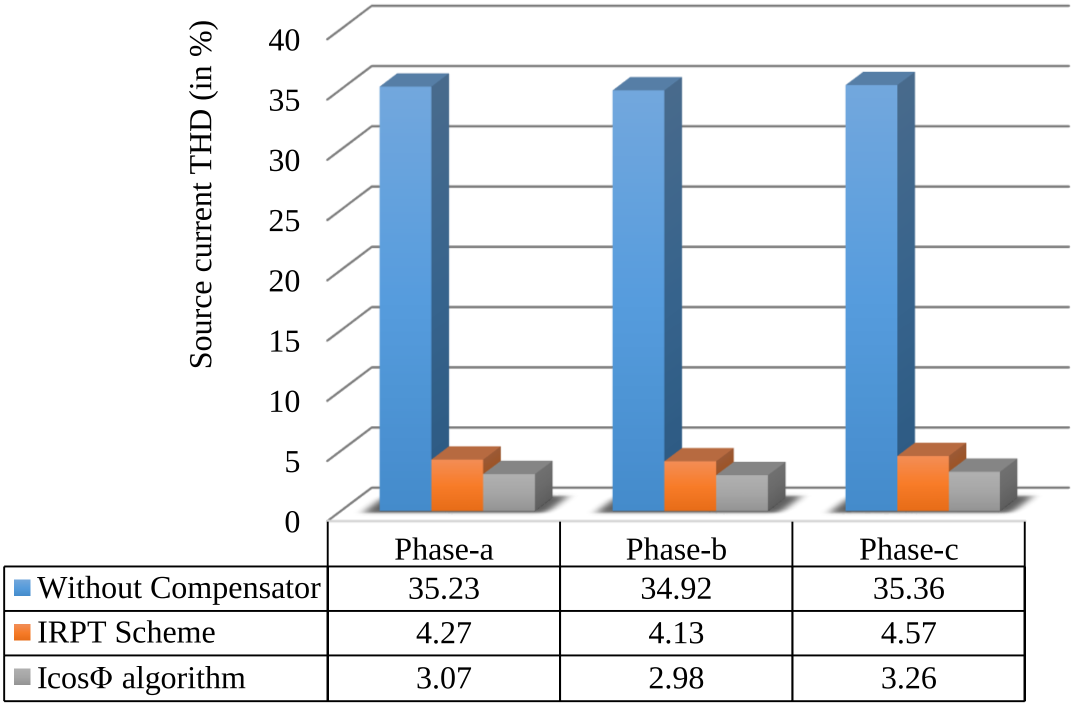

	Phase-a	Phase-b	Phase-c
🟦 Without Compensator	35.23	34.92	35.36
🟧 IRPT Scheme	4.27	4.13	4.57
⬜ IcosΦ algorithm	3.07	2.98	3.26

Fig. 2.21 Bar diagram showing source current THDs (in %) before and after compensation with IRPT and IcosΦ schemes for simulations with nonlinear load under ideal supply condition

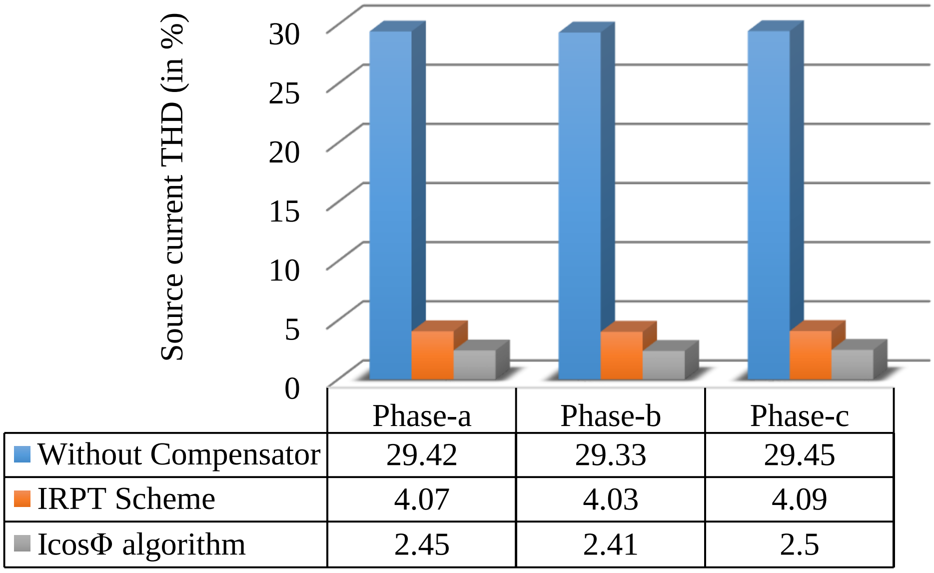

	Phase-a	Phase-b	Phase-c
🟦 Without Compensator	29.42	29.33	29.45
🟧 IRPT Scheme	4.07	4.03	4.09
⬜ IcosΦ algorithm	2.45	2.41	2.5

Fig. 2.22 Bar diagram showing source current THDs (in %) before and after compensation with IRPT and IcosΦ schemes for simulations with nonlinear and linear load under ideal supply condition

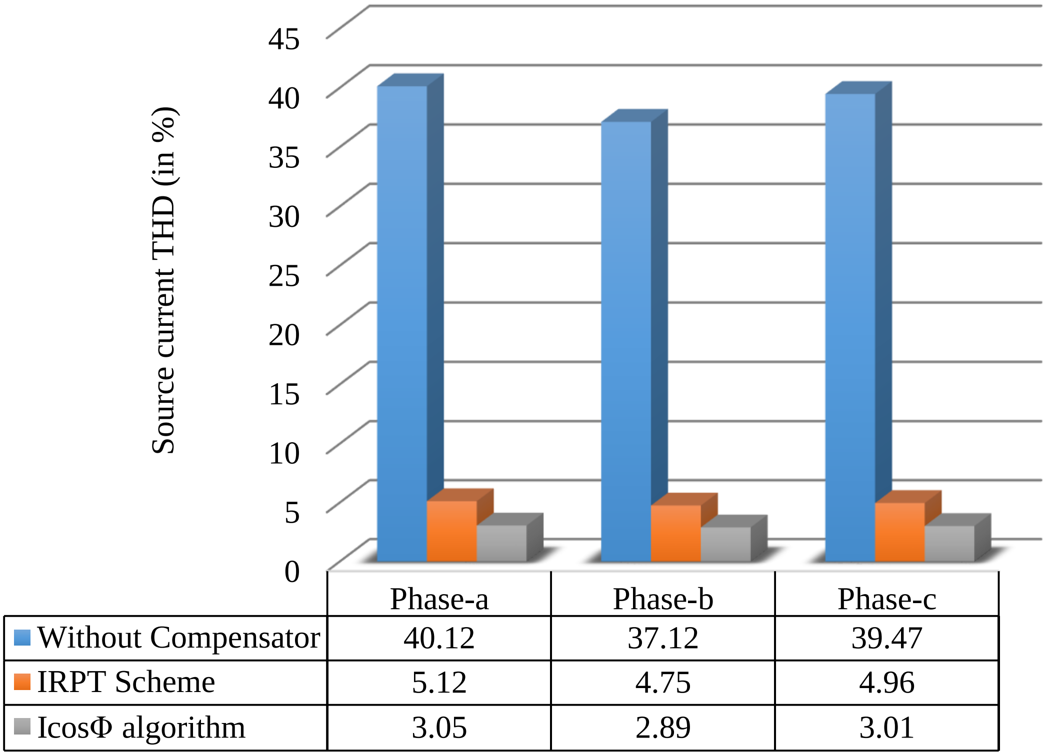

	Phase-a	Phase-b	Phase-c
🟦 Without Compensator	40.12	37.12	39.47
🟧 IRPT Scheme	5.12	4.75	4.96
⬜ IcosΦ algorithm	3.05	2.89	3.01

Fig. 2.23 Bar diagram showing source current THDs (in %) before and after compensation with IRPT and IcosΦ schemes for simulations with unbalanced load under ideal supply condition

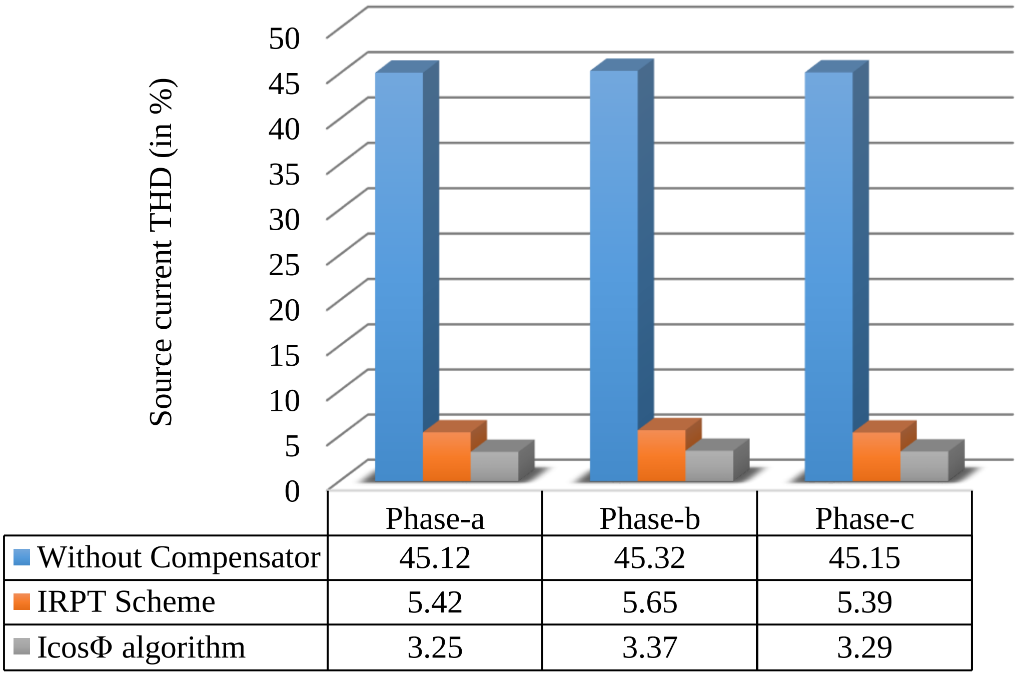

	Phase-a	Phase-b	Phase-c
🟦 Without Compensator	45.12	45.32	45.15
🟧 IRPT Scheme	5.42	5.65	5.39
⬜ IcosΦ algorithm	3.25	3.37	3.29

Fig. 2.24 Bar diagram showing source current THDs (in %) before and after compensation with IRPT and IcosΦ schemes for simulations with thyristor load under ideal supply condition

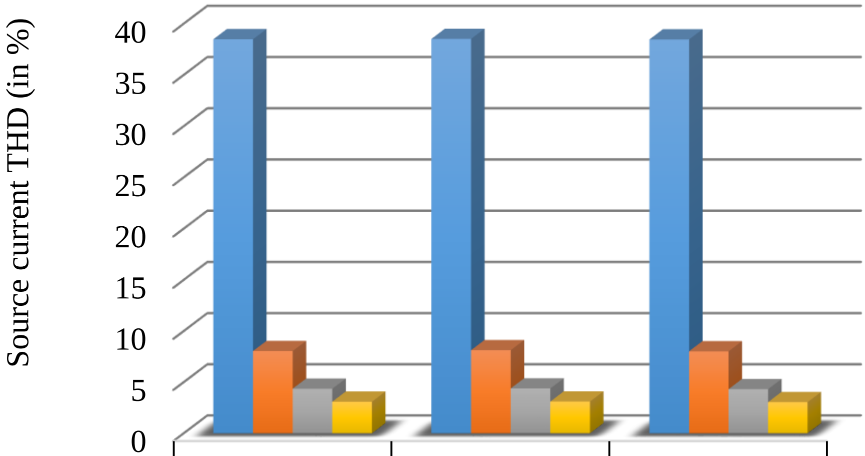

	Phase-a	Phase-b	Phase-c
🟦 Without Compensator	38.49	38.52	38.47
🟧 IRPT Scheme	8.05	8.13	8.02
⬜ MIRPT Scheme	4.36	4.39	4.32
🟨 IcosΦ algorithm	3.09	3.11	3.05

Fig. 2.25 Bar diagram showing source current THDs (in %) before and after compensation with IRPT, MIRPT and IcosΦ schemes for simulations with nonlinear load under distorted supply condition

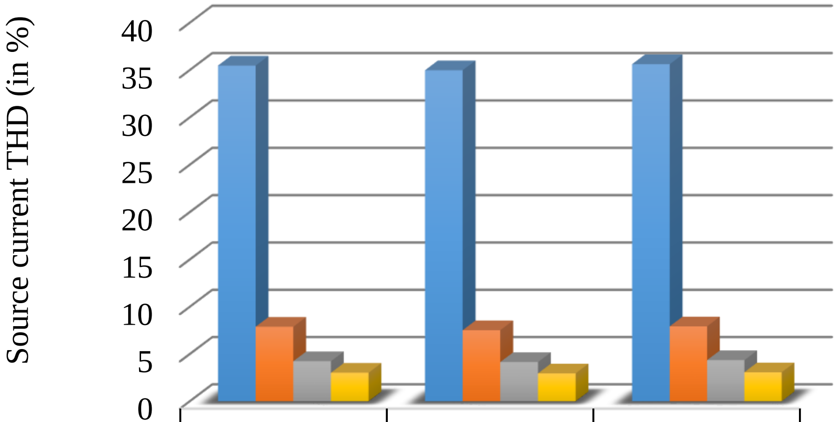

	Phase-a	Phase-b	Phase-c
🟦 Without Compensator	35.47	34.98	35.62
🟧 IRPT Scheme	7.89	7.52	7.93
⬜ MIRPT Scheme	4.24	4.15	4.35
🟨 IcosΦ algorithm	3.02	2.95	3.07

Fig. 2.26 Bar diagram showing source current THDs (in %) before and after compensation with IRPT, MIRPT and IcosΦ schemes for simulations with nonlinear and linear load under distorted supply condition

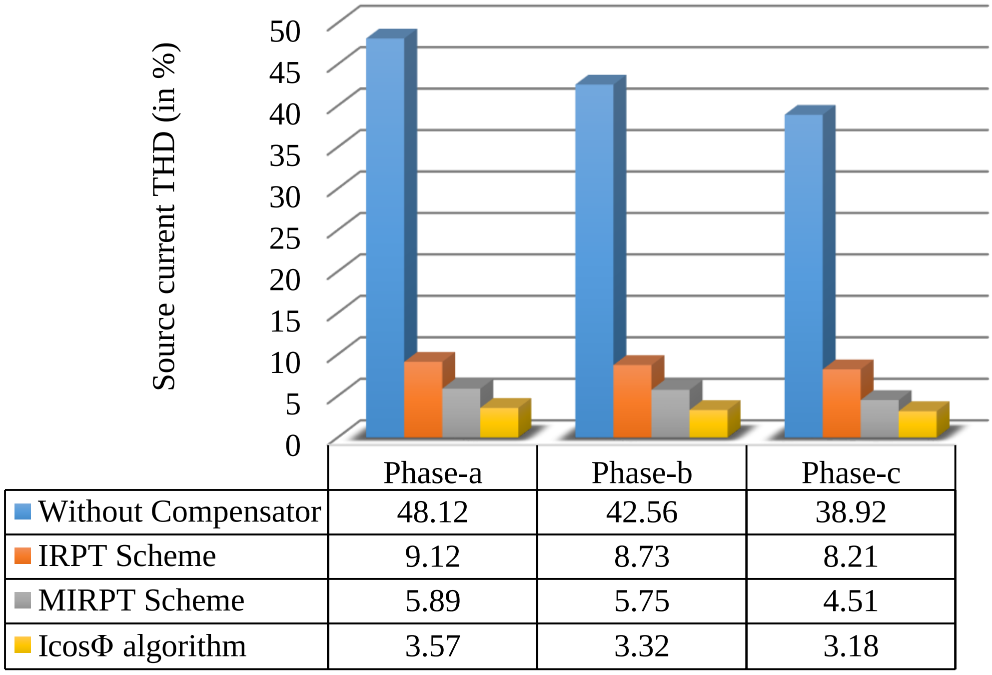

	Phase-a	Phase-b	Phase-c
🟦 Without Compensator	48.12	42.56	38.92
🟧 IRPT Scheme	9.12	8.73	8.21
⬜ MIRPT Scheme	5.89	5.75	4.51
🟨 IcosΦ algorithm	3.57	3.32	3.18

Fig. 2.27 Bar diagram showing source current THDs (in %) before and after compensation with IRPT, MIRPT and IcosΦ schemes for simulations with unbalanced load under distorted supply condition

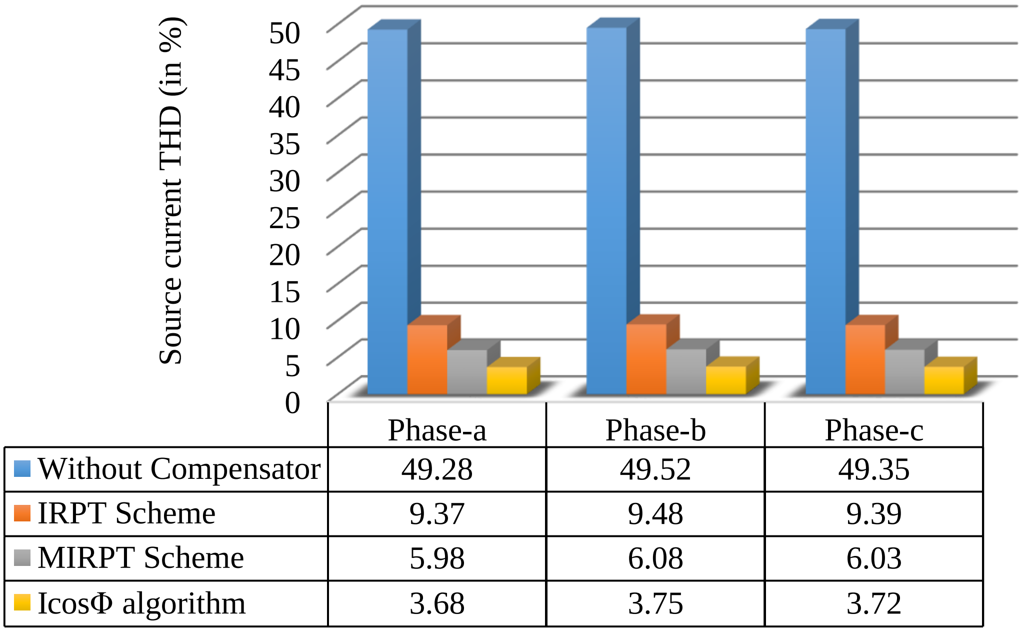

	Phase-a	Phase-b	Phase-c
🟦 Without Compensator	49.28	49.52	49.35
🟧 IRPT Scheme	9.37	9.48	9.39
⬜ MIRPT Scheme	5.98	6.08	6.03
🟨 IcosΦ algorithm	3.68	3.75	3.72

Fig. 2.28 Bar diagram showing source current THDs (in %) before and after compensation with IRPT, MIRPT and IcosΦ schemes for simulations with thyristor load under distorted supply condition

2.5 Chapter Summary

The chapter opens with the portrayal of basic operational details and design of L-type PV-DSTATCOM. Next section illustrates the control schemes for extraction of reference compensation currents using IRPT, modified IRPT and IcosΦ algorithms. The importance of dc link voltage and generation of switching signals for the solar inverter is also described. Section 2.4 analyzes the effectiveness of the L-type PV-DSTATCOM towards harmonic and reactive power compensation with the three control schemes under ideal and distorted supplies along with different load conditions (like nonlinear load, unbalanced load, linear plus nonlinear load and thyristor load). Sizable amount of simulation studies are carried out and from the obtained results it is concluded that for all conditions the IcosΦ scheme outperforms the other two control scheme. The THDs obtained from simulation shows the superiority of IcosΦ algorithm and are well under the IEEE 519 standard. Additionally the reference compensation current generation in IcosΦ scheme does not require a PLL whereas most of the PV-DSTATCOM control strategies including IRPT and modified IRPT schemes require a PLL for successful operation. This make the IcosΦ scheme capable of avoiding many synchronization problem. Also the IcosΦ based L-type PV-DSTATCOM found to be very simple and ease for implementation.

3 Chapter 3

LCL-type and LCLC-type PV-DSTATCOM: Realization and Control

- Design an LCL-type PV-DSTATCOM to inject solar power to grid, eliminate harmonics and compensate reactive power simultaneously.
- Design an LCLC-type PV-DSTATCOM to inject solar power to grid, eliminate harmonics and compensate reactive power simultaneously with reduced power rating of solar inverter.
- To simulate both the topology in MATLAB/Simulink for different load conditions.
- To develop an experimental setup for LCLC type PV-DSTATCOM to verify the performance in real time domain.

For an undisturbed distribution grid, the switching harmonics generated by the solar inverters must be properly filtered out. This can be done by compromising between the cost and the weight of the filter and fulfilment of international standards regarding the grid connections of power converters, like IEC/EN61000-3-4 [74] and IEEE 15471 [16]. In L-type PV-DSTATCOM, the L filter uses a large inductor. This inductor has a low slew rate for tracking the reference currents and produces a large voltage across it. Due to the large voltage drop the PV-DSTATCOM requires a higher value of the dc link voltage for proper compensation. Therefore, the L filter adds in cost, size and power rating. Moreover the system dynamic response may become poorer.

In this chapter, an LCL filter has been implemented at the front end of the solar inverter to overcome the limitations of an L filter [75]. It provides better reference tracking performance while using much lower value of passive components. Though the LCL-type passive ac interface filter reduces the cost, weight and size of the passive components still the disadvantage of high dc-link voltage is present. Therefore another topology named as LCLC-type PV-DSTATCOM is proposed latter in the chapter which overcomes this problem of LCL passive filter by keeping the advantage of LCL filter intact. But improper design of LCL filter or LCLC filter could lead to some inefficiency in PV-DSTATCOM performance, resonance, and instability amongst other possible consequences. So in the following section an efficient design procedure has been given for the designing of LCL-type and LCLC-type PV-DSTATCOM.

3.1 LCL-type PV-DSTATCOM Structure

Fig. 3.1 shows the line diagram of a three phase, three wire (3p3w) LCL-type PV-DSTATCOM. In the system, R_i & L_i represents the solar inverter side resistance and inductance respectively, R_g & L_g are the grid side resistance and inductance respectively, R_s & L_s are the grid resistance and inductance respectively, R_{sh} & C_{sh} are the shunt resistance and capacitance respectively.

The load is such that the load currents (I_{la}, I_{lb}, I_{lc}) may not be balanced, may contain harmonics and dc offset. i_1 is the current flowing through inverter side impedance, i_2 is the current flowing through grid side impedance. i_{pv}, i_{dc}, i_s are the currents flowing from photovoltaic source, dc capacitor and grid respectively. V_{sa}, V_{sb}, V_{sc} & V_{pv} are the three phase grid voltage and dc link voltage respectively. The discussion further progressed with design considerations and design procedure.

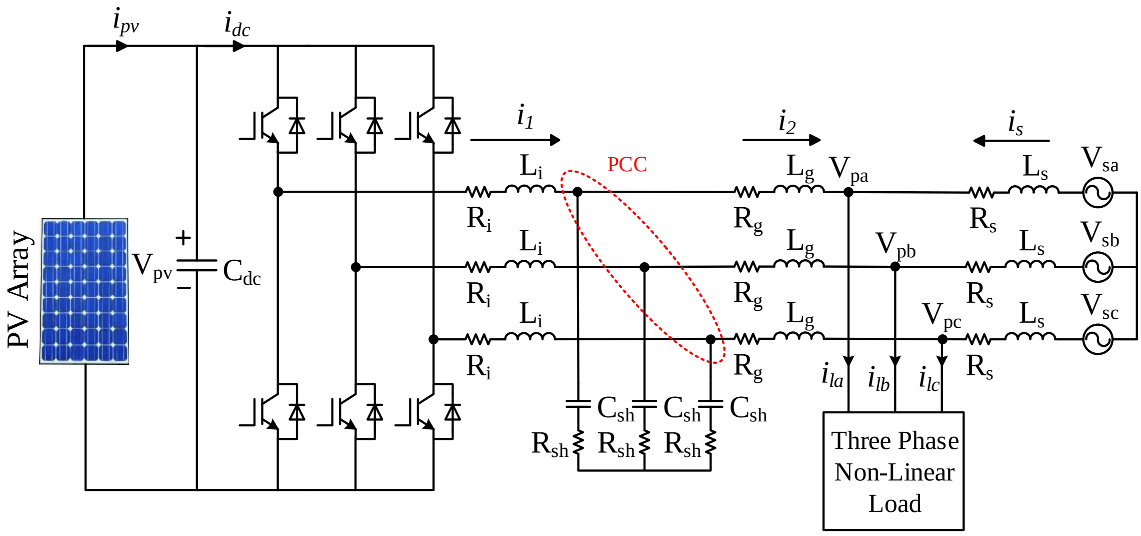

Fig. 3.1 Line diagram for the LCL-type PV-DSTATCOM

3.1.1 Design considerations of LCL-type PV-DSTATCOM

To design the passive LCL filter for PV-DSTATCOM applications, the following characteristics should be taken into consideration:

- *Cost of the total inductor*: Two parameters (L_d and k) are defined for the two inductances of the LCL filter (L_i and L_g) as:-
  $$L_d = L_1 + L_2, L_2 = kL_1 \tag{3.1}$$
  The total inductance L_d sets an upper limit to the switching frequency such that a bigger L_d is related to a lower switching frequency. Therefore, a minimum inductance is calculated using the parameters of both the converter and the switching modulation technique to limit the switching frequency to a certain value. Then, this minimum inductance is slightly increased to get a total inductance L_d that establishes a switching frequency margin to the upper limit. Thus, the total inductance obtained proves to be physically smaller and thus, less expensive.
- *Minimization of stabilizing resistor*: The equivalent impedance of the passive LCL-filter approaches zero at the resonance frequency and it will consequently lower the stability margin of the system down. To avoid instability, a resistor R_{sh} is used in series with the capacitor. The resistance R_{sh} is normally selected in proportion to the capacitive reactance of the PV-DSTATCOM at the resonance frequency ($1/2\pi f_{res}C_{sh}$). This resistance can be chosen such that it minimizes the power dissipation too.
- *Resonance frequency of the filter*: The frequency bandwidth in PV-DSTATCOMs is wide (defined by various harmonic standards). They are principally different from those of grid-connected reactive compensators. In this design, however, the resonance frequency (f_{res}) depends on the highest frequency component of the load which is compensated by the PV-DSTATCOM.

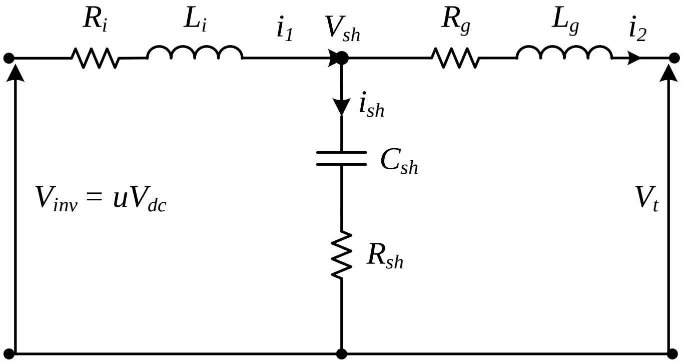

Fig. 3.2 Single phase circuit diagram of the passive filter

To describe the passive filter behavior three transfer functions are $(Y_{12}(s), Y_{21}(s), h_{22}(s))$ calculated using Fig. 3.2 which represents the single line circuit diagram for passive filter. Neglecting R_i and R_g at higher frequencies, by applying KVL the voltage equation can be expressed as:

$$V_{inv}(s) - sL_i i_1(s) - sL_g i_2(s) = 0 \tag{3.2}$$

By putting CDR rule at node V_{sh}

$$i_2(s) = \frac{i_1(s) * \frac{1}{sC_{sh}}}{sL_g + \frac{1}{sC_{sh}}} \tag{3.3}$$

Now inserting (3.3) in (3.2)

$$V_{inv}(s) - sL_i i_1(s) - sL_g \left(\frac{i_1(s) * \frac{1}{sC_{sh}}}{sL_g + \frac{1}{sC_{sh}}} \right) = 0$$

$$\Rightarrow V_{inv}(s) - sL_i i_1(s) - sL_g \left(\frac{\frac{i_1(s)}{sC_{sh}}}{\frac{s^2 L_g C_{sh} + 1}{sC_{sh}}} \right) = 0$$

$$\Rightarrow V_{inv}(s) - sL_i i_1(s) - sL_g \left(\frac{i_1(s)}{s^2 L_g C_{sh} + 1} \right) = 0$$

$$\Rightarrow V_{inv}(s) * \left(s^2 L_g C_{sh} + 1\right) - sL_i i_1(s) * \left(s^2 L_g C_{sh} + 1\right) - sL_g i_1(s) = 0$$

$$\Rightarrow V_{inv}(s) * \left(s^2 L_g C_{sh} + 1\right) = sL_i i_1(s) * \left(s^2 L_g C_{sh} + 1\right) + sL_g i_1(s)$$

$$\Rightarrow V_{inv}(s) * \left(L_g C_{sh} + \frac{1}{s^2}\right) s^2 = s i_1(s)\left[L_i\left(s^2 L_g C_{sh} + 1\right) + L_g\right]$$

$$\Rightarrow \frac{i_1(s)}{V_{inv}(s)} = \frac{s\left(L_g C_{sh} + \frac{1}{s^2}\right)}{L_i\left(s^2 L_g C_{sh} + 1\right) + L_g}$$

$$\Rightarrow \frac{i_1(s)}{V_{inv}(s)} = \frac{L_g C_{sh} s + \frac{1}{s}}{L_i + s^2 L_g L_i C_{sh} + L_g}$$

$$\Rightarrow \frac{i_1(s)}{V_{inv}(s)} = \frac{1 + s^2 L_g C_{sh}}{s\left[\left(L_i + L_g\right) + s^2 L_g L_i C_{sh}\right]}$$

$$\Rightarrow \boldsymbol{Y_{12}(s)} = \frac{\boldsymbol{i_1(s)}}{\boldsymbol{V_{inv}(s)}} = \frac{\boldsymbol{(1/L_i)\left(s^2 + \left(1/L_g C_{sh}\right)\right)}}{\boldsymbol{s\left[s^2 + \left(\left(L_i + L_g\right)/L_g L_i C_{sh}\right)\right]}} \tag{3.4}$$

Again the (3.3) can be rearranged as:

$$i_2(s)\left(sL_g + \frac{1}{sC_{sh}}\right) = i_1(s) * \frac{1}{sC_{sh}}$$

$$\Rightarrow i_2(s) s^2 L_g C_{sh} + 1 = i_1(s) \tag{3.5}$$

Now putting (3.5) in (3.2), (3.2) can be rewritten as:

$$V_{inv}(s) - sL_i\left(i_2(s) s^2 L_g C_{sh} + 1\right) - sL_g i_2(s) = 0$$

$$\Rightarrow V_{inv}(s) = sL_i\left(i_2(s) s^2 L_g C_{sh} + 1\right) + sL_g i_2(s)$$

$$\Rightarrow V_{inv}(s) = i_2(s)\left[sL_i\left(1 + s^2 L_g C_{sh}\right) + sL_g\right]$$

$$\Rightarrow V_{inv}(s) = i_2(s)\left[sL_i + s^3 L_i L_g C_{sh} + sL_g\right]$$

$$\Rightarrow V_{inv}(s) = i_2(s)\left[sL_i + s^3 L_i L_g C_{sh} + sL_g\right]$$

$$\Rightarrow \frac{i_2(s)}{V_{inv}(s)} = \frac{1}{sL_i + sL_g + s^3 L_i L_g C_{sh}}$$

$$\Rightarrow \frac{i_2(s)}{V_{inv}(s)} = \frac{1}{s\left(L_i + L_g\right) + s^3 L_i L_g C_{sh}}$$

$$\Rightarrow \frac{i_2(s)}{V_{inv}(s)} = \frac{1}{sL_i L_g C_{sh}\left[\left(L_i + L_g\right)/L_i L_g C_{sh} + s^2\right]}$$

$$\Rightarrow \boldsymbol{Y_{21}(s)} = \frac{\boldsymbol{i_2(s)}}{\boldsymbol{V_{inv}(s)}} = \frac{\boldsymbol{1/L_i L_g C_{sh}}}{\boldsymbol{s\left[s^2 + \left(L_i + L_g\right)/L_i L_g C_{sh}\right]}} \tag{3.6}$$

Similarly we can derive

$$\boldsymbol{h}_{22}(s) = \frac{\boldsymbol{i_2(s)}}{\boldsymbol{i_1(s)}} = \frac{\boldsymbol{\left(1/L_g C_{sh}\right)}}{\boldsymbol{s^2 + \left(1/L_g C_{sh}\right)}} \tag{3.7}$$

- *Inductance ratio*: The admittance $|Y_{12}(s)|$ includes three poles (p) and two zeros (z), while zeros are related to the nonzero poles as follows:
  $\boldsymbol{z} = \pm j\sqrt{\frac{1}{L_g C_{sh}}}$, $\boldsymbol{p} = \pm j\sqrt{\frac{L_i + L_g}{L_i L_g C_{sh}}}$, $\boldsymbol{p} = k'z$, $\boldsymbol{k'} = \sqrt{1 + \frac{L_g}{L_i}} = \sqrt{1 + k}$
  It can be seen that when the inductance ratio $(k = (L_g/L_i))$ becomes bigger, then the nonzero poles distance away from zeros. This would increase the overshoot amplitude and thus influences the performance of the PV-DSTATCOM. On the other hand, lowering k will decrease the overshoot inversely and proportional to k'.
- Current ripples of the capacitive branch (i_{sh}) passes through the stabilizing resistor R_{sh}, which will lead to power losses equal to $R_{sh} i_{sh}^2$. While the dc/ac converter supplies the dissipated power on R_{sh}, the dc voltage controller absorbs active power from the source in order to compensate the dc voltage drop. This will eventually cause an increase of the source current. Meanwhile, the low order harmonics should be highly attenuated by L_i, and the higher order of harmonics by L_g and C_{sh}. Since the magnitudes of high order harmonics are normally small, this will considerably lower the power dissipation on R_{sh}.
- Choosing the ratio k has no special effect on transfer function $Y_{21}(s)$.
- An LCL-filter comprises more energy storage elements than a passive L-filter, and his slows down the dynamic characteristics of the PV-DSTATCOM. Hence, switching frequencies are more limited for an LCL-filter with respect to a dynamically faster L-filter. Also, when an LCL-filter is designed using $k < 1(L_g > L_1)$, then the switching frequencies involved in current-controlled modulation become lower than those of $k < 1(L_g > L_i)$. This could be advantageous since very fast switches are not necessary, while it can also be argued that employing fast switches is, theoretically, advantageous.

Considering above points, choosing big values for L_g lowers i_2 distortion; although this constitutes higher cost and power losses for the system compared to smaller L_g. Thus, the relationship $L_g > L_i$ can be suggested to achieve high efficiency and to avoid possible overrating of the switches by choosing a low value for k.

- Two transfer functions $Y_{12}(s)$ and $h_{22}(s)$ in (3.4) and (3.7) show that bigger values of capacitance C, will further attenuates the higher frequencies.
- It is suggested in [76] that the value of damping resistor R_{sh} should be chosen proportional to the capacitive reactance at resonance frequency $(1/2f_{res}C_{sh})$.
- Moreover, it is necessary to design both i_{sh} and R_{sh} as low as possible to avoid additional power losses imposed to the source by R_{sh}.

3.1.2 Design procedure for LCL-type PV-DSTATCOM

As described in (3.1), the minimum value of total inductance is derived for an inductive filter in order to limit the maximum switching frequency. The inductor is designed to provide good tracking performance at maximum switching frequency, which is achieved at zero supply voltage in the HCC. Taking these into consideration, inductance (L_i) is given by:

$$L_i = \frac{V_{pv,ref}}{(2h_a)(2f_{max})} = \frac{V_{pv,ref}}{4h_a f_{max}} \tag{3.8}$$

where $V_{pv,ref}$ is the reference dc link voltage, $2h_a$ is the allowable ripple current, f_{max} is the maximum switching frequency achieved by the HCC.

The large ripple current will lower the IGBT switching frequency and lowers the losses. However, it can be seen from (3.8) that the smaller ripple current results in higher inductance and, thus, more core losses. Therefore, a ripple current of 20% is taken while compromising the ripple and inductor size.

Using the nonzero poles of $Y_{12}(s)$ in (3.4), the resonance frequency can be introduced as:

$$f_{res} = \frac{1}{2\pi}\sqrt{\frac{L_i + L_g}{L_i L_g C_{sh}}} = \frac{1}{2\pi}\sqrt{\frac{1 + (L_g/L_i)}{L_g C_{sh}}} \tag{3.9}$$

Multiplying both numerator and denominator of (3.9) by $\sqrt{1 + (L_g/L_i)}$, we get

$$f_{res} = \frac{1}{2\pi}\sqrt{\frac{\left(1+(L_g/L_i)\right)^2}{\left(1+(L_g/L_i)\right)L_gC_{sh}}} = \frac{1}{2\pi}\sqrt{\frac{\left(1+(L_g/L_i)\right)^2}{(L_i+L_g)(L_g/L_i)C_{sh}}} \tag{3.10}$$

Now substituting the (3.1) in (3.10), finally gives

$$f_{res} = \frac{1}{2\pi}\sqrt{\frac{(1+k)^2}{L_dkC_{sh}}} = \frac{1}{2\pi}\frac{1+k}{\sqrt{L_dkC_{sh}}} \tag{3.11}$$

The resonant frequency must be greater than highest order harmonics to be compensated. Selection of $L_g > L_i$ (i.e., $k > 1$) will reduce the capability of L_i to attenuate lower order harmonics. Therefore, lower order harmonics will be also attenuated by inductor L_g to achieve satisfactory compensation performance. Usually, the magnitude of the lower order harmonics in the LCL filter is used to be more as compared with the higher order harmonics. Hence, the current through the shunt capacitor and the inductor L_i will increase for $k > 1$. This will increase the damping power losses, the reactive power loss in inductor L_i, and the inverter current. Moreover, the source current will also increase as the damping power losses are extracted from the source. Hence, $L_g > L_i$ will result in more losses and cost. Therefore, to ensure low loss and high efficiency, a lower value of k is selected ($k < 1$). A higher C_{sh} will provide a low impedance path for harmonics but will draw more reactive current from the VSI, which further increases the loss in L_i and IGBT switch. However, a smaller capacitance will not provide sufficient attenuation, which, in turn, is compensated by selecting a larger inductor. As a tradeoff between these requirements the value C_{sh} is selected.

The equivalent impedance of the LCL filter approaches to zero at the resonance frequency f_{res}, and the system may become unstable. However, the system can be made stable by inserting a resistance R_{sh} in series with the capacitor. Usually, it is chosen in proportion to the capacitive reactance at f_{res} , i.e., $X_{c,res}$ such that the damping losses are minimum while assuring system stability. The capacitive reactance at resonance will be

$$X_{c,res} = \frac{1}{2\pi f_{res}C_{sh}} \tag{3.12}$$

The power loss in the damping resistor will be

$$P_{loss} = 3 * R_{sh} * \sum_{h=1}^{n} I_{sh}^{2} \tag{3.13}$$

where h is the harmonic order of the current flowing through R_{sh}. In the LCL filter-based PV-DSTATCOM topology, R_{sh} is chosen such that the damping losses are minimized while assuring that the sufficient resonance damping is provided to the system. The reason for considering damping power losses is that the significant current is drawn by the shunt part of the LCL filter. This further reduces the efficiency of the VSI. However, one of the major advantages of the proposed scheme is that the voltage across, and therefore the current through the shunt part of the LCL filter, is greatly reduced. This reduction in the shunt current significantly reduces the damping power losses. Therefore, sufficient resonance damping of the system is a prime concern while designing a damping resistor. By considering all the assumption and precaution the system parameters are calculated and presented in Table 3.1.

3.1.3 Results and Discussions

To observe the efficacy of the presented LCL-type PV-DSATCOM, a MATLAB/ SIMULINK is pursued. A balanced three phase voltage supply has been applied to a typical non-linear load composed of a three phase diode rectifier bridge feeding a R-L load. The values of the dc side ohmic-inductive load are 10Ω and 15mH respectively. The Simulation results for different loads and switching transients are shown in subsequent subsections.

Table 3.1 LCL-Type PV-DSTATCOM parameters used for simulation

System Parameters	**Values**	**System Parameters**	**Values**
Source voltage (V_s)	230V/rms	Source impedance (R_s, L_s)	0.008Ω, 0.18mH
System frequency (f)	50Hz	DC link capacitance (C_{dc})	2200μF
Inductance ratio (k)	0.49	Resonance frequency(f_{res})	1300Hz
Maximum switching frequency (f_{sw})	10Khz	Reference DC link voltage (V_{pv}^{*})	680V
LCL filter parameters	L_i=5.1mH, L_g=2.5mH, C_{sh}=10μF, R_{sh}=20Ω		

3.1.3.1 Performance analysis under Ideal mains voltage

In this section, the LCL-type PV-DSTATCOM is simulated under ideal mains voltage condition. Due to the nonlinear diode bridge rectifier load, a highly harmonic contaminated load current flows through the system as shown in Fig. 3.3 (b). After compensation the harmonics and reactive power are eliminated and the source current becomes sinusoidal. The simulation results for source current after compensation, voltage across dc-link and filter current are shown in Fig. 3.3 (c), (d) and (e) respectively.

From Fig. 3.3 (c), it can be verified that after compensation the switching harmonics are reduced as compared to L-type PV-DSTATCOM. The simulation results also shows that the load reactive power is compensated successfully by the compensator. With the compensator the total harmonic distortion of source current for all phases are reduced to the values within IEEE 519 standard as shown in Fig. 3.4.

3.1.3.2 Performance analysis during switch on transient

In general, when the compensator is integrated to the system and switched on for compensating purpose, it shows some transient behavior and take some time to settle down to its steady state operation. Here the transient behavior of the compensator is shown in Fig. 3.5. Initially when the PV-DSTATCOM is switched on the source current peak increases to 65A and then after 0.025 seconds it settles down to its actual value of 20A.

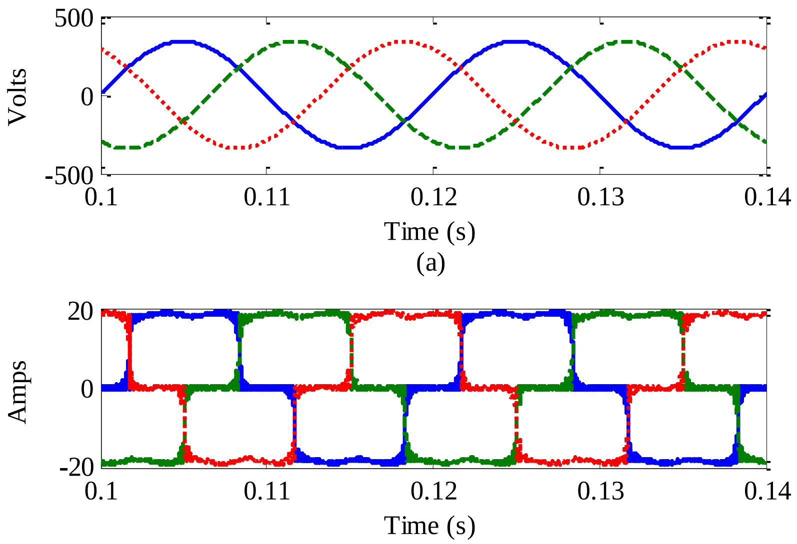

(a)

(b)

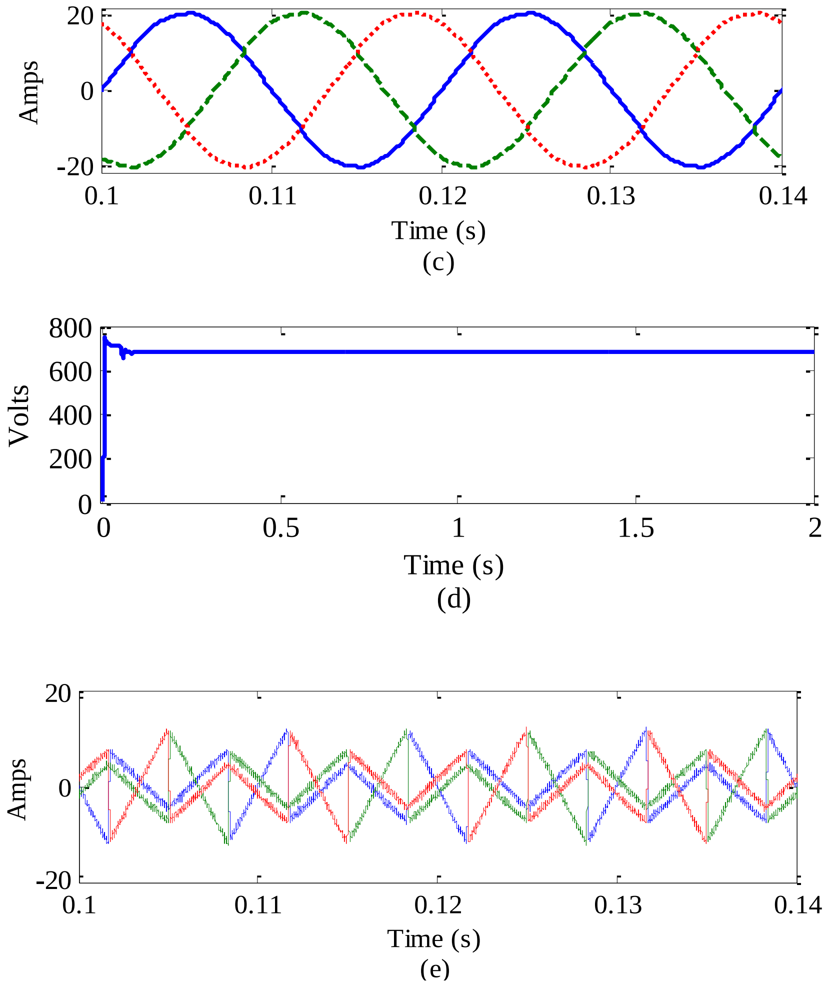

Fig. 3.3 Simulation results of LCL-type PV-DSTATCOM with nonlinear load and IcosΦ algorithm (a) source voltage (b) load current before compensation (c) source current after compensation (d) voltage across dc bus (e) filter current

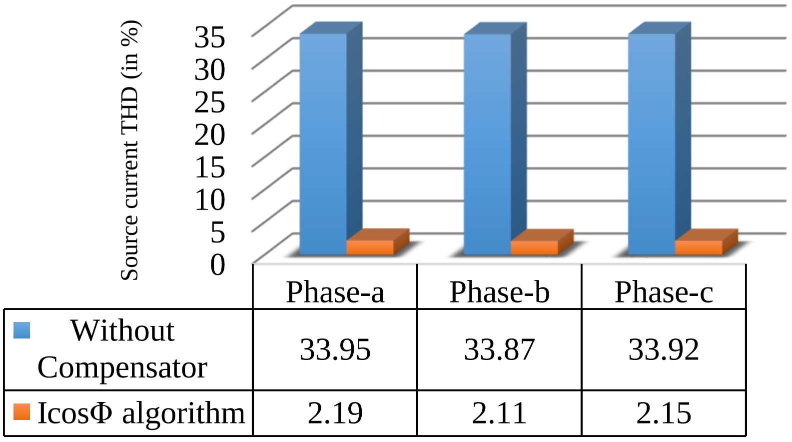

	Phase-a	Phase-b	Phase-c
🟦 Without Compensator	33.95	33.87	33.92
🟧 IcosΦ algorithm	2.19	2.11	2.15

Fig. 3.4 Bar diagram showing source current THDs (in %) before and after compensation with IcosΦ scheme for simulations with nonlinear load under ideal supply condition

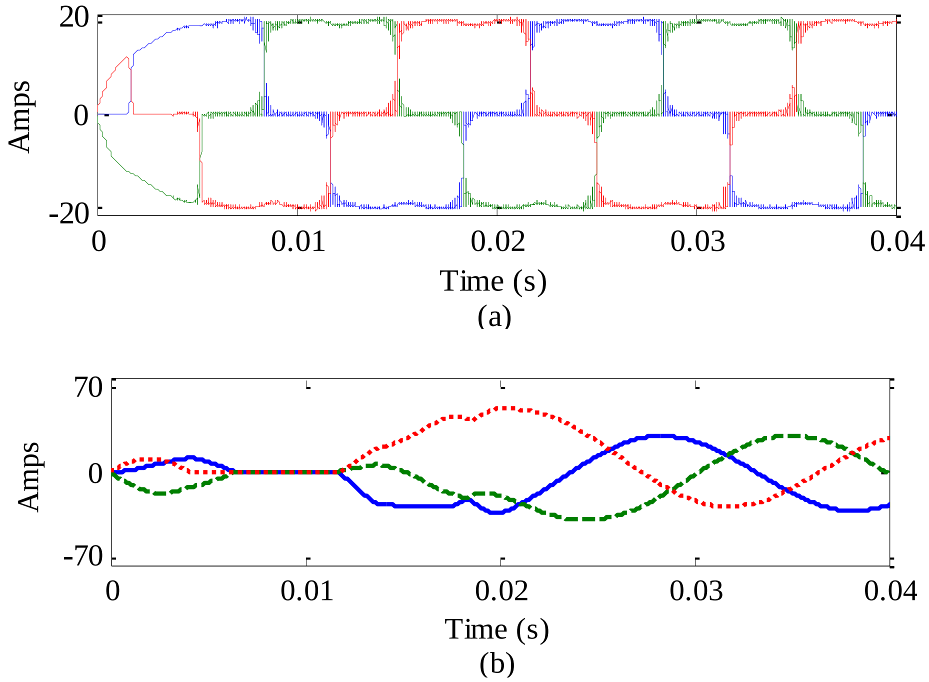

Fig. 3.5 Simulation results of LCL-type PV-DSTATCOM showing transient behavior with nonlinear load and IcosΦ algorithm (a) load current before compensation (b) source current after compensation

3.1.3.3 Performance analysis with thyristor load

To verify the compensating capability of the PV-DSTATCOM with different loads, a thyristor bridge rectifier with ohmic-inductive load is considered under this section for simulation. For the nonlinear load the dc side ohmic-inductive impedance is chosen as 12Ω and 20mH. To observe the influence of frequent changing load power consumption on compensator performance the firing angles of the load are changed to 0˚ to 60˚. From starting to 0.52 seconds the system is operated with 0˚. After that the firing angle is increased to 30˚ for 1.5 cycles and again the firing angle is increased to 60˚ for 0.03 seconds. After 0.58 seconds the firing angle is reduced to 0˚ and operated at the same for rest of the time period. The simulation results for source current before and after compensation are shown in Fig. 3.6. From the simulation result it is observed that though the power consumption load is varied abruptly the compensator is tracking the reference and compensating harmonics and reactive power successfully. The total harmonic distortion of source current before and after compensation is shown in Fig. 3.7.

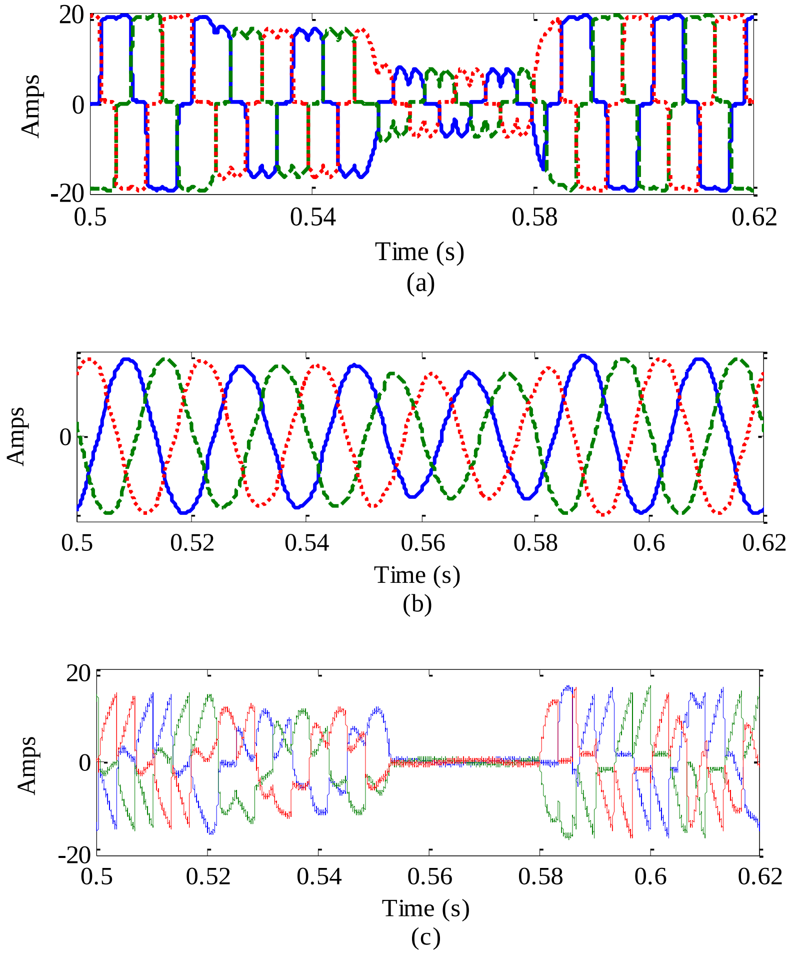

Fig. 3.6 Simulation results of LCL-type PV-DSTATCOM with thyristor load and IcosΦ algorithm (a) load current before compensation (b) source current after compensation (c) filter current

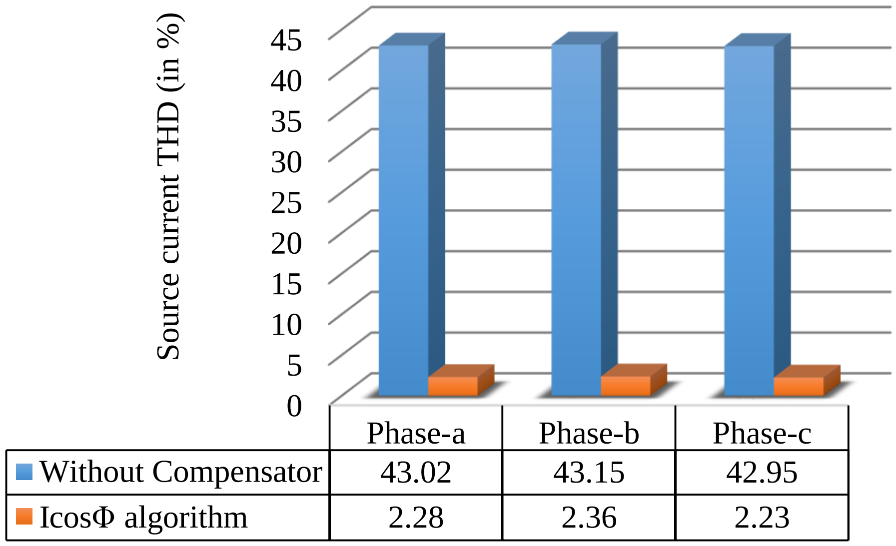

	Phase-a	Phase-b	Phase-c
🟦 Without Compensator	43.02	43.15	42.95
🟧 IcosΦ algorithm	2.28	2.36	2.23

Fig. 3.7 Bar diagram showing source current THDs (in %) before and after compensation with IcosΦ scheme for simulations with thyristor load under ideal supply condition

3.1.3.4 Performance analysis during frequently changing load condition

Under this section, the compensating performance of LCL-type PV-DSTATCOM is tested with different loads like linear unbalance load, linear plus nonlinear unbalanced load, balanced nonlinear load. In Fig. 3.8, initially the system is operated with nonlinear load (diode bridge rectifier with ohmic-inductive load) plus linear unbalance load (where R_a=30Ω, R_b=40Ω, R_c=50Ω and L_a=0.2H, L_b=0.25H, L_c=0.16H) and then at 0.2 seconds linear unbalanced load is switched off. Then at 0.4 seconds the nonlinear load is switched off and linear unbalance load is switched on. Again at 0.6 seconds the nonlinear load is switched on and the system is operated with nonlinear unbalanced load.

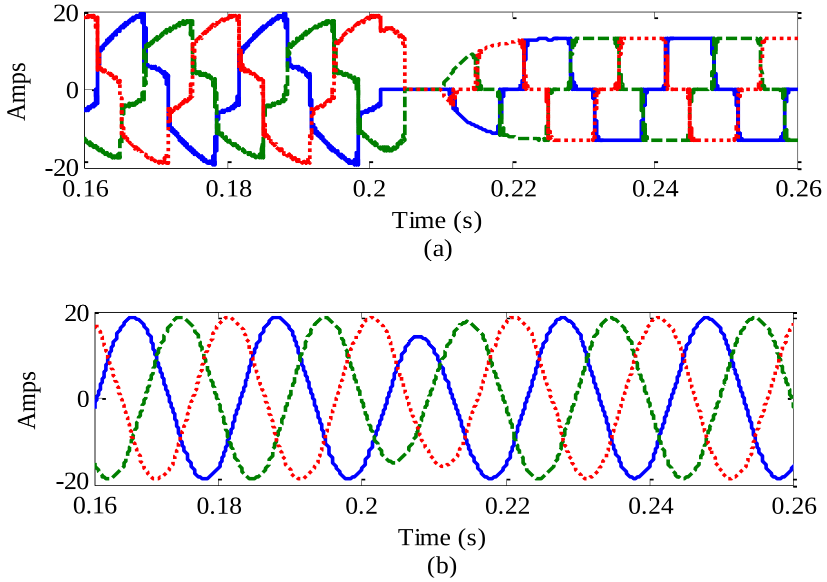

(a)

(b)

Fig. 3.8 Simulation results of LCL-type PV-DSTATCOM for load change from nonlinear unbalance to nonlinear load (a) load current before compensation (b) source current after compensation.

All these load transitions are shown in Fig. 3.9 and Fig. 3.10 respectively. From Fig. 3.8 (b), Fig. 3.9 (b) and Fig. 3.10 (b) it can be clearly ratified that the compensator is performing satisfactorily during all load transitions. The source current harmonics are reduced and reactive power is compensated after compensation. The switching harmonics are also reduced.

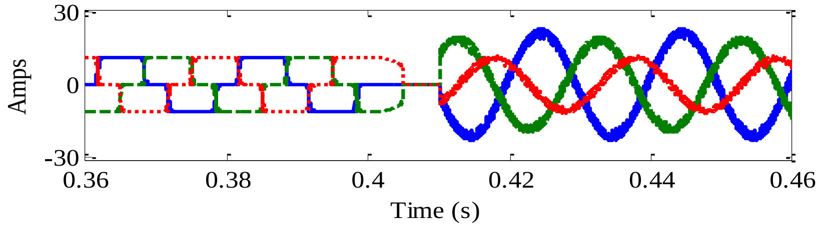

(a)

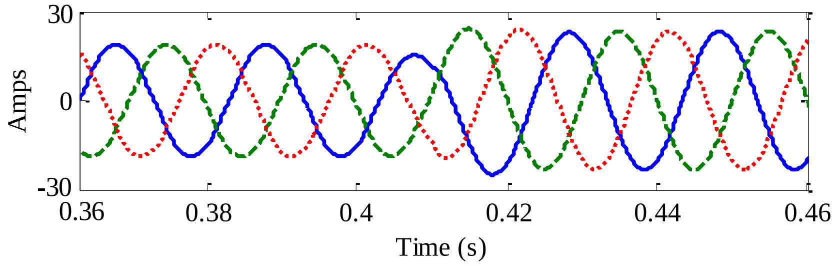

(b)

Fig. 3.9 Simulation results of LCL-type PV-DSTATCOM for load change from nonlinear to linear unbalance load (a) load current before compensation (b) source current after compensation.

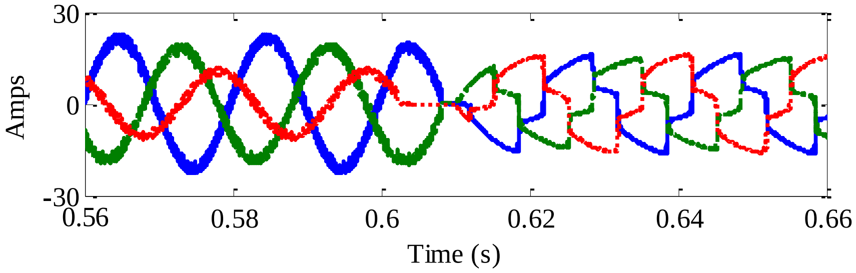

(a)

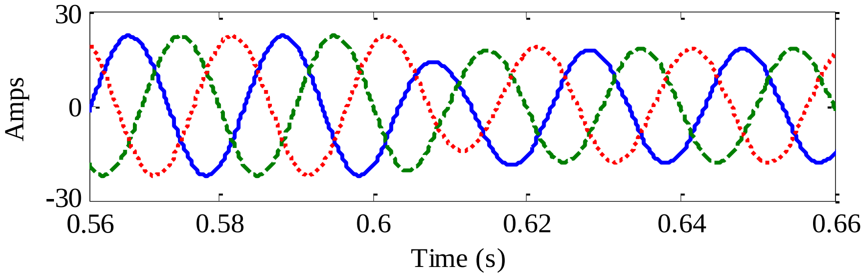

(b)

Fig. 3.10 Simulation results of LCL-type PV-DSTATCOM for load change from Linear unbalance to nonlinear unbalance load (a) load current before compensation (b) source current after compensation.

3.2 LCLC-type PV-DSTATCOM Structure

To overcome the limitations traditional L-type PV-DSTATCOM, an LCL filter has been implemented at the front end of solar inverter. Though LCL-type PV-DSTATCOM provides better tracking performance with much lower passive components, it uses a similar dc link voltage as that of L-type PV-DSTATCOM. The higher dc link voltage increases the rating of solar inverter. That makes the solar inverter heavy and results in higher voltage rating of insulated gate bipolar transistor (IGBT) switches. So the disadvantages due to high dc link are still present even when the LCL filter is used.

In this section, a hybrid topology is presented in which a capacitor is inserted in series with LCL filter at the front end of solar inverter to address aforementioned issue of L and LCL filter [77]. With the proposed LCLC-type PV-DSTATCOM, the size of passive components, rating of dc link voltage are reduced and reference tracking performance is improved simultaneously.

3.2.1 LCLC-type PV-DSTATCOM Structure

A three phase line diagram of the proposed LCLC-type PV-DSTATCOM is shown in Fig. 3.11. The proposed PV-DSTATCOM connects an LCL filter at the front end of solar inverter, which is followed by a series capacitor (C_{se}). Introduction of LCL filter reduces the size of passive components and addition of series capacitor reduces the dc link voltage thereby reducing the solar inverter rating.

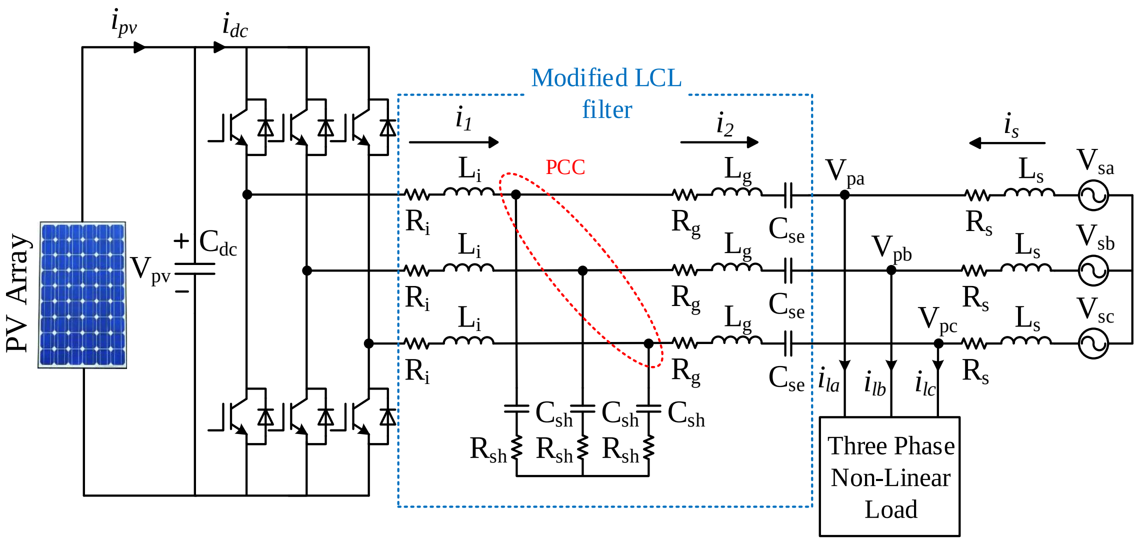

Fig. 3.11 Line diagram for LCLC-type PV-DSTATCOM.

3.2.2 Design procedure for LCLC-type PV-DSTATCOM

The L_i, L_g and C_{sh} passive components of LCLC –type PV-DSTATCOM are designed as mentioned in Section 3.1.2. For the design of series capacitor (C_{se}), it is necessary to take care of the fact that the series capacitor should provide a low impedance path for the fundamental frequency current component. From the design of shunt capacitor (C_{sh}) it is confirmed that it will provide a high impedance path for lower order harmonics. Therefore a negligible fundamental current will be drawn by shunt capacitor and can be neglected at fundamental frequency. The equivalent single phase circuit diagram of passive filters can be represented as shown in Fig. 3.12.

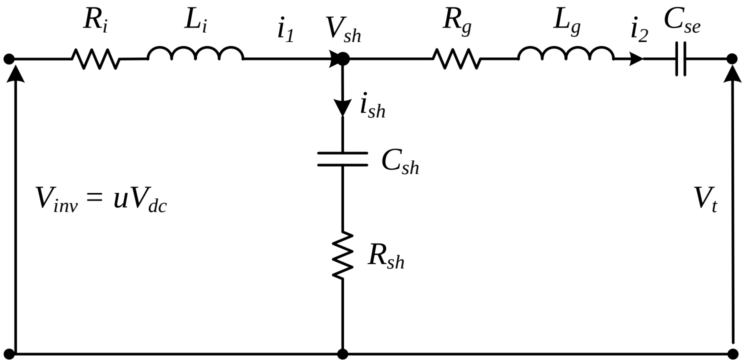

Fig. 3.12 Single phase circuit diagram of passive filter.

The fundamental current supplied by the filter can be calculated by applying KVL in Fig. 3.12 and neglecting C_{sh} as follows

$$V_{inv,1} - I_{f,1}R_f - I_{f,1}jX_{f12} + I_{f,1}jX_{se,1} - V_{t,1} = 0 \tag{3.14}$$

where $R_f = R_i + R_g$, $X_{f12} = \omega_1(L_i + L_g)$, $X_{se,1} = 1/\omega_1 C_{se}$, $V_{t,1}$ is the fundamental rms PCC voltage and $V_{inv,1}$ is the fundamental rms per phase voltage at the VSI terminal.

$$\Rightarrow V_{inv,1} - V_{t,1} = I_{f,1}R_f + I_{f,1}jX_{f12} - I_{f,1}jX_{se,1}$$
$$\Rightarrow V_{inv,1} - V_{t,1} = I_{f,1}(R_f + jX_{f12} - jX_{se,1})$$
$$\Rightarrow I_{f,1} = \frac{V_{inv,1} - V_{t,1}}{R_f + j(X_{f12} - X_{se,1})} \tag{3.15}$$

Multiplying conjugate of the denominator of (3.15), we get

$$I_{f,1} = \frac{(V_{inv,1} - V_{t,1})\left(R_f - j(X_{f12} - X_{se,1})\right)}{{R_f}^2 + (X_{f12} - X_{se,1})^2}$$
$$\Rightarrow I_{f,1} = \frac{R_f(V_{inv,1} - V_{t,1}) - j(X_{f12} - X_{se,1})(V_{inv,1} - V_{t,1})}{{R_f}^2 + (X_{f12} - X_{se,1})^2} \tag{3.16}$$

Separating real and imaginary parts, we can rewrite

$$Re[I_{f,1}] = \frac{R_f(V_{inv,1} - V_{t,1})}{{R_f}^2 + (X_{f12} - X_{se,1})^2} \tag{3.17}$$

$$Im[I_{f,1}] = -\frac{(X_{f12} - X_{se,1})(V_{inv,1} - V_{t,1})}{{R_f}^2 + (X_{f12} - X_{se,1})^2} \tag{3.18}$$

Interfacing resistance are very small compared with reactive part and therefore can be neglected. Considering this (3.17) and (3.18) can be rewritten as

$$Re\left[I_{f,1}\right] = \frac{R_f\left(V_{inv,1} - V_{t,1}\right)}{\left(X_{f12} - X_{se,1}\right)^2} \tag{3.19}$$

$$Im\left[I_{f,1}\right] = -\frac{V_{inv,1} - V_{t,1}}{X_{f12} - X_{se,1}} \tag{3.20}$$

It can be observed from (3.19) that to inject active current from the photovoltaic source to the load or the PCC the fundamental per phase rms voltage available at dc-link must be greater than the terminal voltage. In traditional topology (i.e., L-type PV-DSTATCOM and LCL-type PV-DSTATCOM) where series capacitor is not present, the maximum active current to be injected from the photovoltaic source only depends on dc-link voltage (since R_f, $V_{t,1}$ and X_{f12} are fixed). Therefore the dc-link voltage is maintained at a much higher value as compared with the terminal voltage. Due to the insertion of series capacitor in series with the interfacing passive LCL filter, the total impedance provided by the compensator is reduced which is also evident from (3.19). So for same active current injection the dc-link voltage can be reduced from its reference value.

Similarly from (3.20) it can be observed that for the injection of same reactive current from the compensator to the PCC, the dc-link voltage can be reduced from its reference value. As the main aim of the compensator is to provide load reactive power for power quality improvement, the value of series capacitor depends upon maximum reactive filter current and to the extent that the decrease in the dc-link voltage is required. To achieve unity power factor at load terminal, the maximum reactive current that the compensator can supply must be same as that of the maximum load reactive current. At minimum impedance i.e. at full load the load current will be maximum. Therefore maximum fundamental load current drawn by the load in a particular phase is expressed as:

$$I_{lm} = \frac{V_{t,1}}{R_{l,min} + jX_{l,min}} \tag{3.21}$$

Calculating the magnitude of imaginary load current from the preceding equation and equating with (3.20), we get:

$$\frac{V_{t,1}X_{l,min}}{Z_{l,min}^2} = \frac{V_{inv,1} - V_{t,1}}{X_{f12} - X_{se,1}} \tag{3.22}$$

By simplifying (3.22) a more generalized expression can be written as:

$$I_{lm}\sqrt{1-pf_{l,min}^2}=\frac{V_{inv,1}-V_{t,1}}{X_{f12}-X_{se,1}} \tag{3.23}$$

where $I_{lm}=V_{t,1}/Z_{l,min}$, and $pf_{l,min}$is the minimum load power factor given by $R_{l,min}/Z_{l,min}$. Hence $X_{se,1}$ can be calculated as:

$$X_{se,1}=X_{f12}-\frac{V_{inv,1}-V_{t,1}}{I_{lm}\sqrt{1-pf_{l,min}^2}} \tag{3.24}$$

In practical circumstances, for the consumers only nameplate details are available. Thus by using (3.24) the value of series capacitor can be calculated in real life.

3.2.3 Simulation Results and Discussions

The LCLC-type PV-DSTATCOM performance with reduced dc-link voltage is verified through Matlab simulation. For the generation of reference current IcosΦ algorithm is used as it has been proved as best technique in the Chapter-2. The close loop block diagram of switching pulse generation is shown in Fig. 3.13. By considering all the assumption and precaution the system parameters are calculated and presented in Table 3.2.

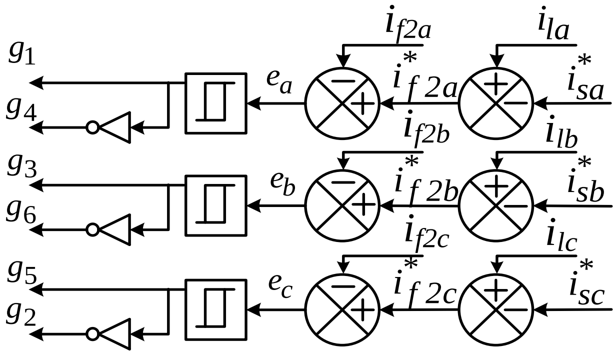

Fig. 3.13 Close loop block diagram of switching pulse generation

3.2.3.1 Performance analysis under Ideal mains voltage

In this section, the LCLC-type PV-DSTATCOM is simulated under ideal mains voltage condition. The highly harmonic contaminated load current, source current after compensation, dc-link voltage and filter current are shown in Fig. 3.14. From the simulation results it is clearly observed that with reduced dc-link voltage of 165V the LCLC-type PV-DSTATCOM is successfully compensating both current harmonics and load reactive power.

Table 3.2 LCLC-Type PV-DSTATCOM parameters used for simulation

System Parameters	**Values**	**System Parameters**	**Values**
Source voltage (V_s)	230V/rms	Source impedance (R_s, L_s)	0.008Ω, 0.18mH
System frequency (f)	50Hz	DC link capacitance (C_{dc})	3000μF
Inductance ratio (k)	0.49	Diode bridge rectifier load (R_{dc}, L_{dc})	10Ω, 15mH
Maximum switching frequency (f_{sw})	10Khz	Reference DC link voltage (V_{pv}^*)	165V
LCLC filter parameters	L_i=3mH, L_g=2.5mH, C_{sh}=10μF, R_{sh}=20Ω, C_{se}=55μF		
Unbalanced Load	R_a, L_a	30Ω, 0.2H	
	R_b, L_b	40Ω, 0.25H	
	R_c, L_c	50Ω, 0.16H	

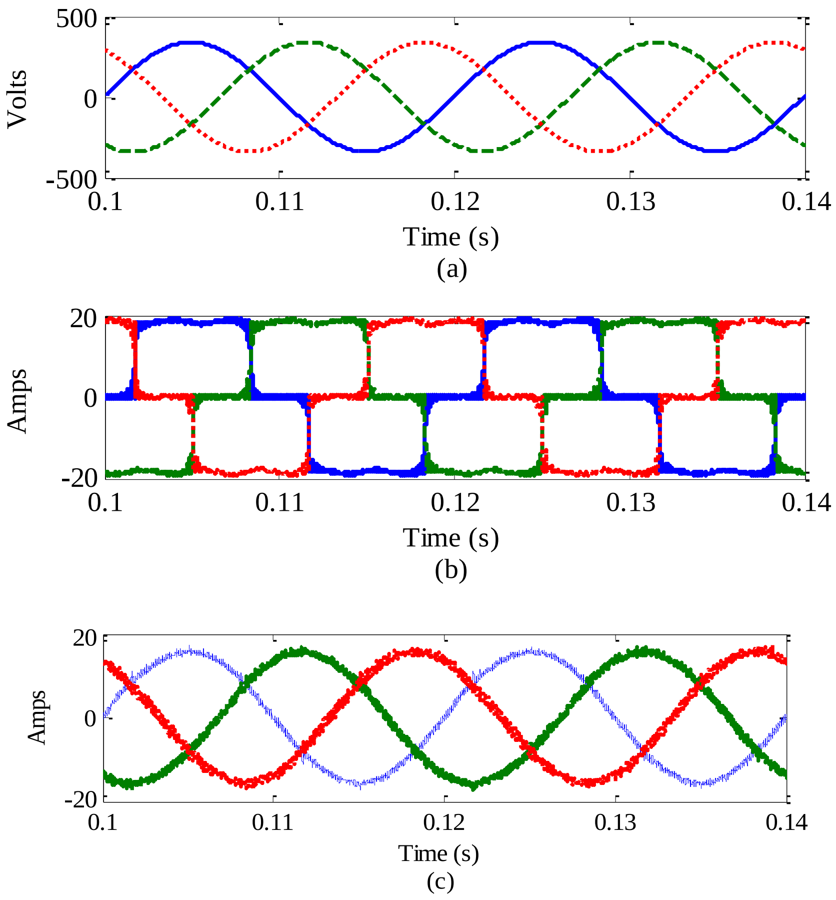

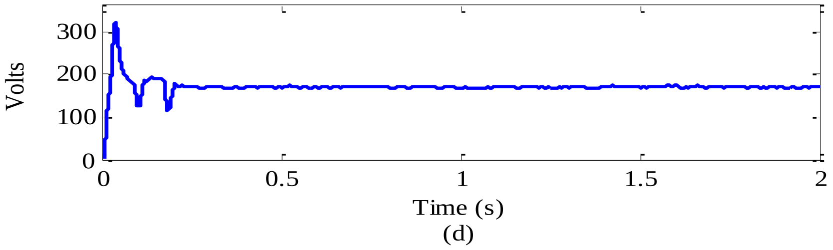

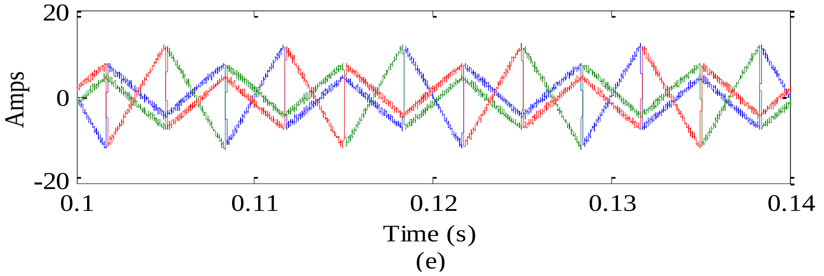

Fig. 3.14 Simulation results of LCLC-type PV-DSTATCOM with nonlinear load and IcosΦ algorithm (a) source voltage (b) load current before compensation (c) source current after compensation (d) voltage across dc bus (e) filter current

3.2.3.2 Performance analysis during switch on transient

Under this section the transient behavior of the compensator during switch on period is observed. From Fig. 3.15 it is seen that when the compensator is switched on, the peak of the source current reaches to 280A. After 0.01 seconds it settles down to its steady state value i.e. the source current settles down to original value more quickly with LCLC-type PV-DSTATCOM than LCL-type PV-DSTATCOM.

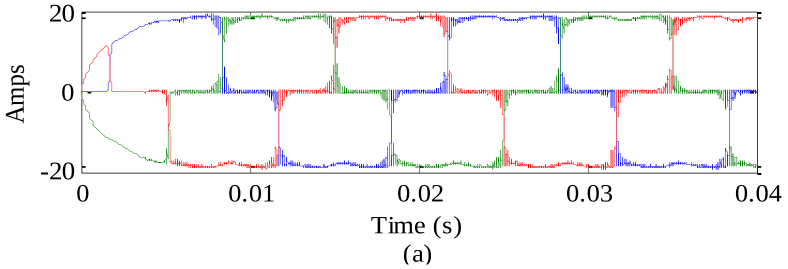

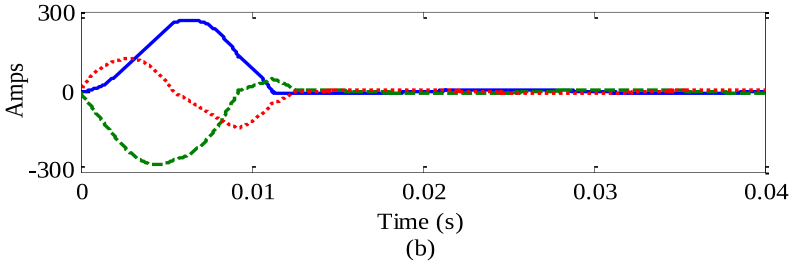

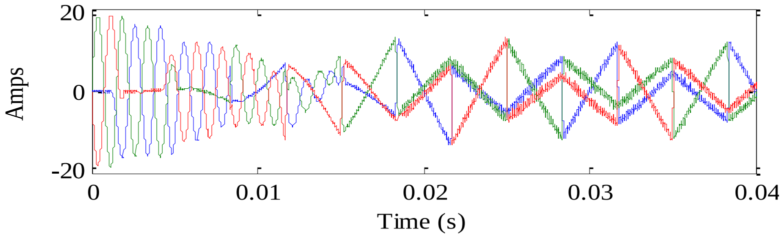

(c)

Fig. 3.15 Simulation results of LCLC-type PV-DSTATCOM showing transient behavior with nonlinear load and IcosΦ algorithm (a) load current before compensation (b) source current after compensation (c) filter current.

3.2.3.3 Performance analysis during frequently changing load condition

Under this section, the compensating performance of LCLC-type PV-DSTATCOM is tested with different loads like linear unbalance load, linear plus nonlinear unbalanced load, balanced nonlinear load. In Fig. 3.8, initially the system is operated with nonlinear load (diode bridge rectifier with ohmic-inductive load) plus linear unbalance load (where R_a=30Ω, R_b=40Ω, R_c=50Ω and L_a=0.2H, L_b=0.25H, L_c=0.16H) and then at 0.2 seconds linear unbalanced load is switched off. Then at 0.4 seconds the nonlinear load is switched off and linear unbalance load is switched on. Again at 0.6 seconds the nonlinear load is switched on and the system is operated with nonlinear unbalanced load.

From Fig. 3.16 it is observed that during load transition source current peak increases to 40A. Though it is being able to track reference but it is taking 0.02 seconds to settle down to steady state value.

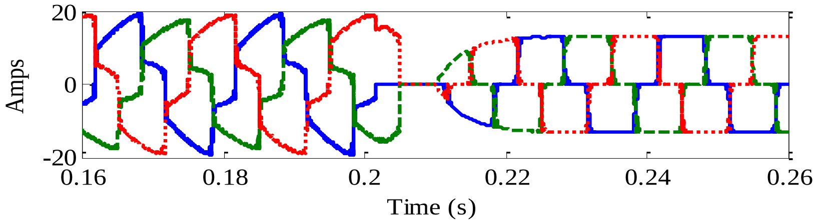

(a)

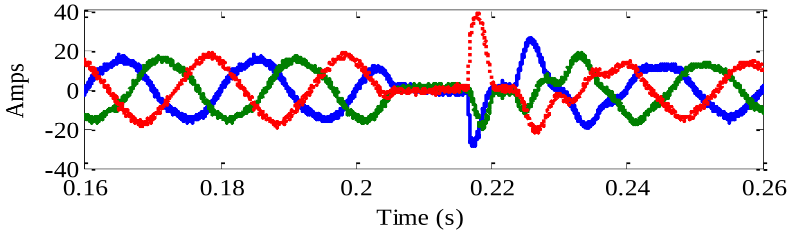

(b)

Fig. 3.16 Simulation results of LCLC-type PV-DSTATCOM for load change from nonlinear unbalance to nonlinear load (a) load current before compensation (b) source current after compensation.

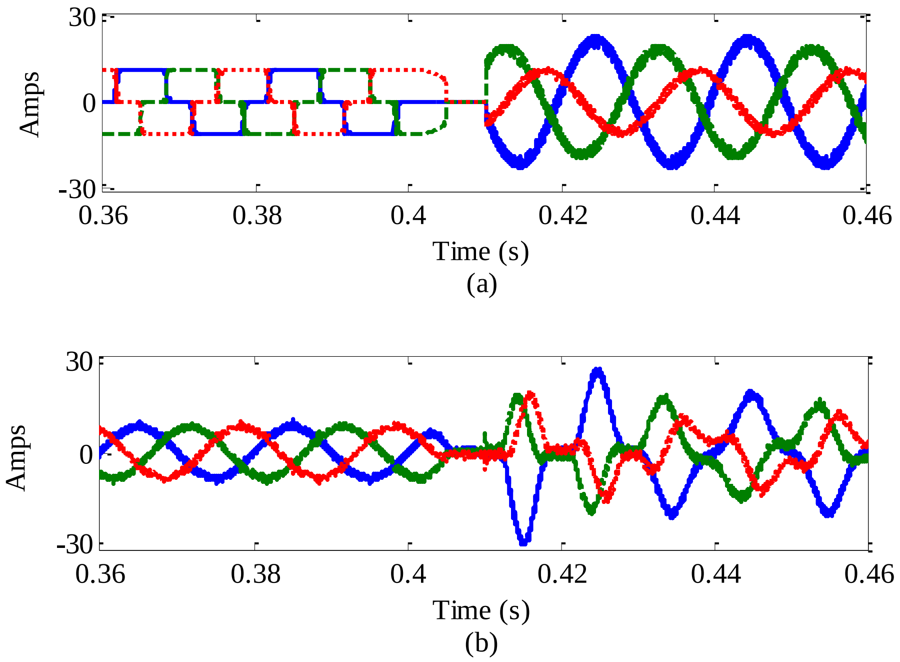

Fig. 3.17 Simulation results of LCLC-type PV-DSTATCOM for load change from nonlinear to linear unbalance load (a) load current before compensation (b) source current after compensation.

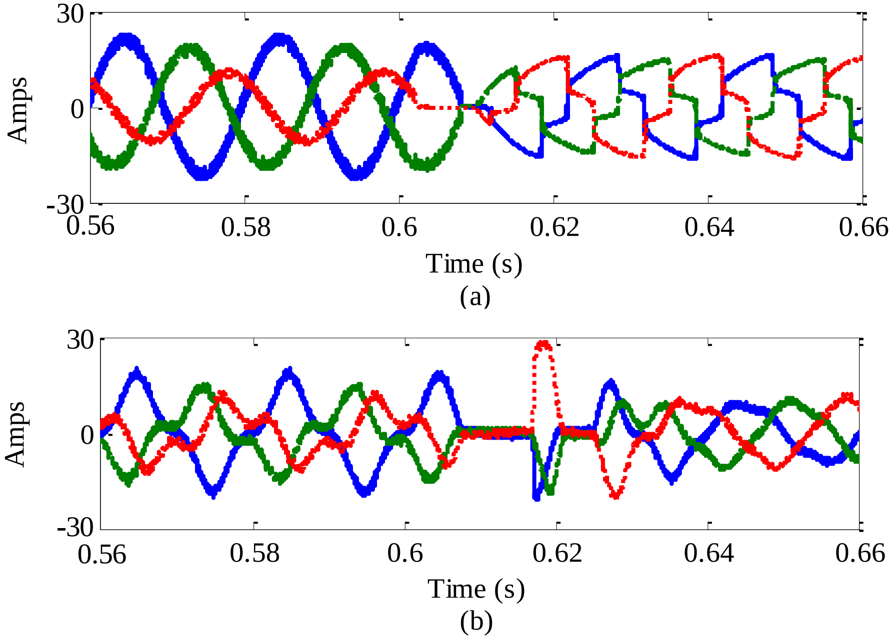

Fig. 3.18 Simulation results of LCLC-type PV-DSTATCOM for load change from Linear unbalance to nonlinear unbalance load (a) load current before compensation (b) source current after compensation.

From the Fig. 3.17 and Fig. 3.18, it is clearly visible that for linear unbalance load the compensator needs more time to settle down to the steady state value. But in all other loading condition the LCLC-type PV-DSTATCOM performs satisfactorily.

3.3 Real time Implementation

From the simulation results it is found that the LCLC-type PV-DSTATCOM is the best topology in terms of cost and power rating of the system and solar inverter. So for verification of the system under practical constraints, the real time response of the system needs to be observed. Therefore an experimental setup for LCLC-type PV-DSTATCOM is developed and dSPACE 1103 R&D board is used to interface with host computer. The overall block diagram of the hardware setup and interfacing details for power quality applications is shown in Fig. 3.19.

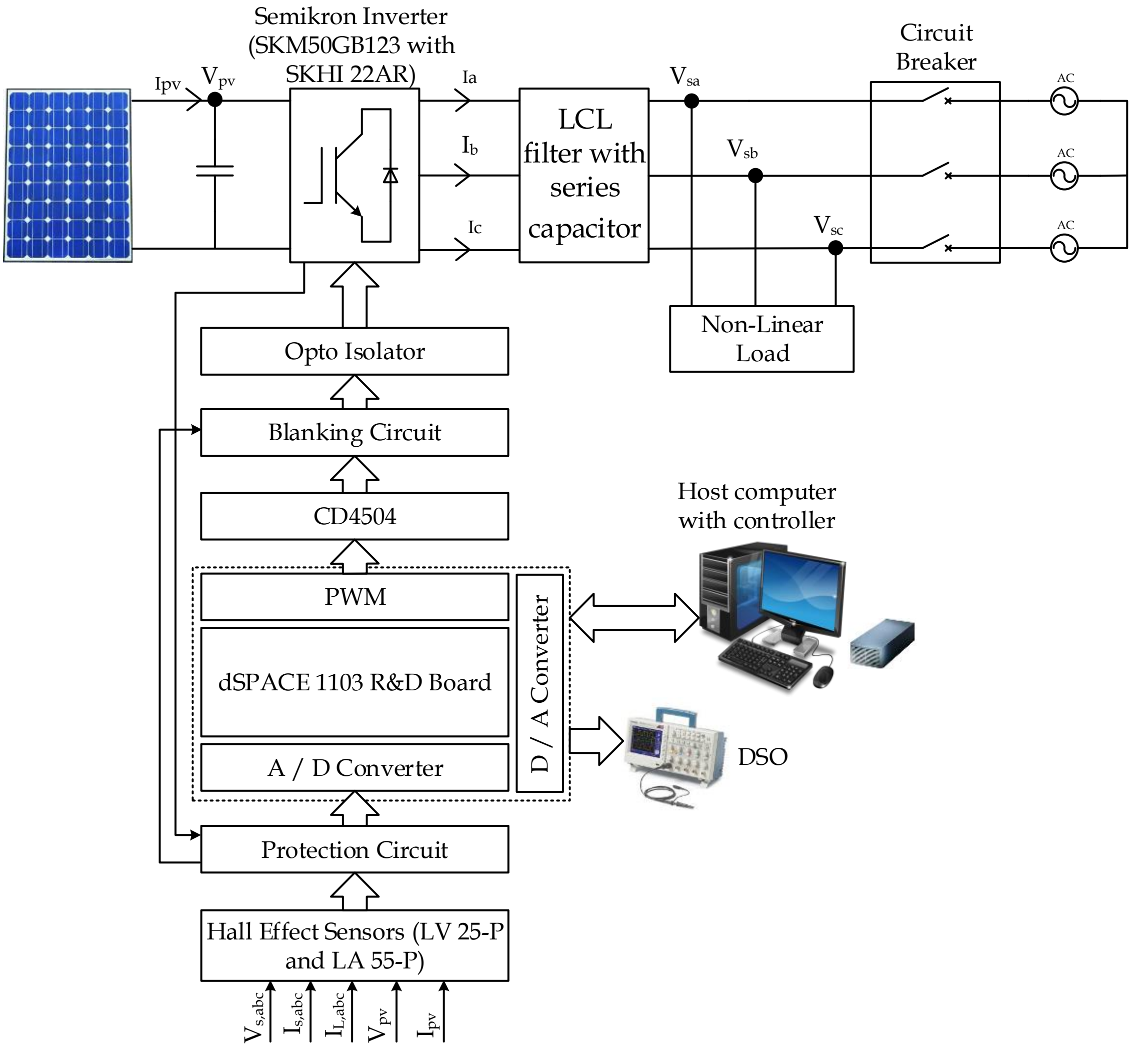

Fig. 3.19 Block Diagram of implemented experimental setup

The three phase power quantities (voltages and currents) are converted to low-level voltage signals using the Hall Effect voltage and current transducers. The dSPACE 1103 is connected to the host computer through a parallel port. The control algorithm in the dSPACE generates the VSI switching pulses. The IGBTs present in Semikron inverter need 15V pulses to trigger. Therefore the pulses are then passed through CD4504 ICs for amplifying its magnitude from 5V to 15V. Then the 15V pulses are passed through the blanking circuit to include a dead time in order to prevent short circuit of the capacitor through switches in the same VSI leg. The blanking circuit also receives stop (logical 0) signals from the protection circuit to ensure safe operation of the set-up, in case of any abnormality in the system. The blanking circuit output pulses are given to the VSI through the optoisolator circuit to isolate the high power network and the signal level circuits. The photograph of the experimental setup is shown in Fig. 3.20.

Fig. 3.20 Photograph of experimental set-up (a) solar panels (b) host computer with dSPACE R&D board and connector panel (c) auto transformer (d) interfacing inductor

The development and function of each component is described in the following subsections. The major components of the dSPACE-based power quality conditioner are given as follows:

- Solar Panel
- Voltage Source Inverter
- Transducer Circuit
- Protection Circuit
- Blanking Circuit
- Optoisolation Circuit
- Power Supply Circuit

3.3.1 Solar Panel

To generate the solar power, the solar panels from Solar Semiconductor bearing model number SSI-M6-205 are connected in series and parallel. A solar system of 2kw is installed on rooftop of the building consisting of 10 panels in series with two parallel connections. The detail parameter specification of SSI-M6-205 is given in Table 3.3. The photograph of the installed PV setup is shown in

Table 3.3 Parameters of the SSI-M6-205 solar panel at 1000W/m^2, 25˚C and 1.5 AM

Panel Parameters	**Values**
Rated Power (P_{mpp})	205W
Rated Voltage (V_{mpp})	28.04V
Rated Current (I_{mpp})	7.31A
Open Circuit Voltage (V_{oc})	35.55V
Short Circuit Current (I_{sc})	7.91A
Series Fuse Rating	15A
Diode Rating	15A

Solar Semiconductor Pvt.Ltd.
Made In India
SOLAR
SEMICONDUCTOR
SSI – M6 – 205
Tested at STC (1000 W/m², AM1.5, 25° C)
Rated Power (Pmp): 205Wp (Tolerance: +/– 3%)
Rated Voltage (Vmp): 28.04 V
Rated Current (Imp): 7.31 A
Open Circuit Voltage (Voc): 35.55 V
Short Circuit Current (Isc): 7.91 A
Max System Voltage (Vdc): 600V (USA),
1000V (EU)
Series Fuse Rating 15 A
Diode Rating 15 A
Conforming to IEC 61215,61730 and UL 1703
Fire Hazard Rating: Class C
CE
S1 – 3M020910 – 0411356

(a) (b) (c) (d)

Fig. 3.21 Photograph of installed solar system (a) solar panels (b) lightening arrestor and data logger (c) nameplate specification of solar panel (d) pyranometer

3.3.2 Voltage Source Inverter

The voltage source inverter generates compensating voltage/current as dictated by the control algorithm. The inverter used for the experimental setup consists of three Semikron IGBT modules (SKM200GB125D) and three drivers (SKYPER 32R). The gate driver controls the dynamic behavior of IGBTs and takes care of protections like over voltage, over current and short circuit protection etc. In an IGBT module two IGBT switches are connected suitably with antiparallel diodes. The specifications of the S KM200GB125 are given in Table 3.4.

Table 3.4 Parameter specification for inverter

DC-link	4700µF/450V(2nos)	Output Current	35A Max
Input DC voltage	600V	Output Frequency	50Hz
Output AC voltage	415V, 3-Φ	Switching Frequency	25Khz Max

3.3.3 Transducer Circuit

The Hall effect voltage transducer and current transducer sense and transform the high level voltage and current to low level signals. The Hall effect transducers also provide isolation between power network and the signal level circuits. These transducers offers many advantages like very good linearity, low temperature drift, excellent accuracy etc.

3.3.4 Voltage transducer circuit design

The LV 25-P is used as Hall effect voltage transducer and its schematic diagram is shown in Fig. 3.22.

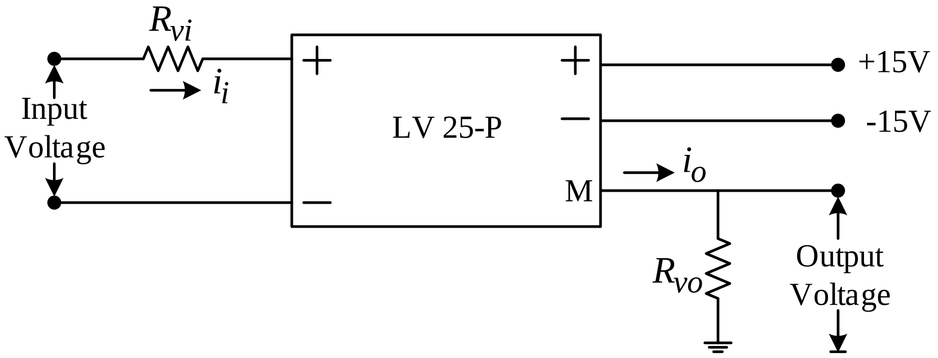

Fig. 3.22 Schematic diagram of voltage transducer

The power voltage is stepped down from 100V to ±5V range in experimental setup. The input resistance is chosen as 100kΩ and the input current is calculated as [78]:

$$i_i = \frac{V_i}{R_{vi}} = \frac{100}{100 \times 10^3} = 1mA$$

The conversion ratio (CR_v) of the Hall effect current transducer is 2500:1000. So the output current is found as

$$i_o = i_i \times CR_v = 1 \times 10^{-3} \times \frac{2500}{1000} = 25mA$$

To level down the voltage to 5V at output the output measuring resistance is computed as:

$$R_{vo} = \frac{V_o}{i_o} = \frac{5}{25 \times 10^{-3}} = 200\Omega$$

3.3.5 Current transducer circuit design

The LA 55-P is used as Hall effect current transducer and its schematic diagram is shown in Fig. 3.23.

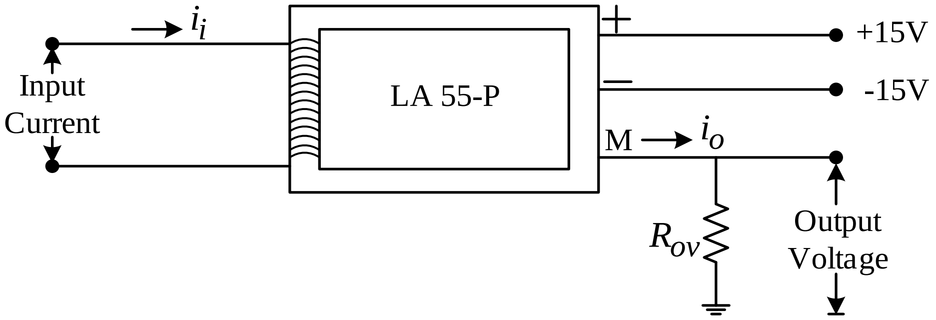

Fig. 3.23 Schematic diagram of current transducer

The current of 10A in power network is leveled down to ±5V. The number turns (N_p) is chosen as 5 such that the output resistance falls in the range of 50-160Ω [79]. The conversion ratio (CR_i) for the current transducer is 1:1000. By considering these values the output current is obtained as follows:

$$i_o = \frac{N_p \times i_i}{CR_i} = \frac{5 \times 10}{1000} = 0.05A$$

To obtain 5V output voltage the output measuring resistance is computed as follows:

$$R_{ov} = \frac{V_o}{i_o} = \frac{5}{0.05} = 100\Omega$$

3.3.6 Protection Circuit

The protection circuit plays an important role in giving security to the inverter from the infringement of cutoff points in the compensator currents, source voltages, and capacitor voltage(s). The basic building block of the protection circuit is given in Fig. 3.24. If the magnitude of any of the above parameters violates the positive/negative limits, the comparator (OPAMP-TL064) gives a logic high output which passes through the diode (IN4007) to clip its negative portion and then through the buffer (CD4050). These signals are then NORed utilizing IC 4075 and IC 7404 to form the clock pulse for the JK flip-flop (74LS76). This being a negative edge triggered flip-flop, Q is set and Q is reset when the negative edge of the clock appears. The Q signal is used as the STOP pulse to the blanking circuit (described below) for stopping the gate signals to IGBTs.

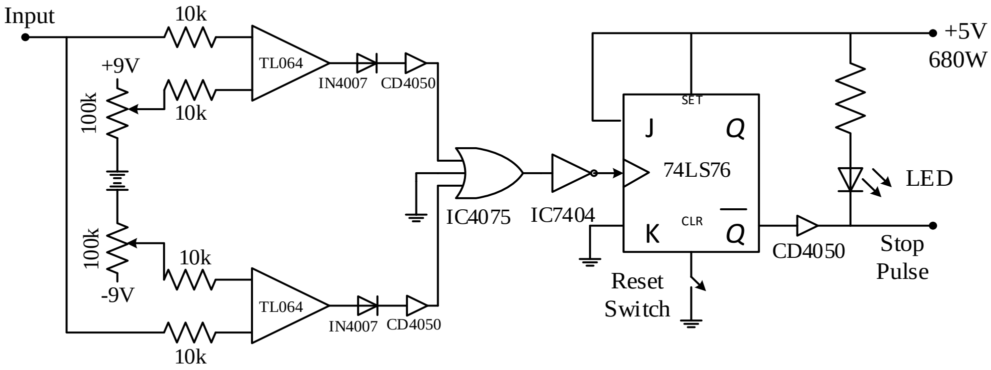

Fig. 3.24 Protection circuit schematic diagram

3.3.7 Blanking Circuit

The control algorithm developed in the host computer generates the switching pulses and are taken out for inverter IGBT modules through dSPACE CLP1103 connector panel. However, these pulses are not specifically given to the IGBT modules so as to prevent the short circuit of the capacitor during the turn ON and OFF of both the switches in the same leg. A dead band is given in between the turning ON and turning OFF of the switches in the same leg. Fig. 3.25 shows the blanking circuit used for phase-a. Its inputs are the switching pulses S_a and $\overline{S_a}$ generated from the dSPACE1103. The detailed circuit diagram for two channels of the blanking circuit using mono-stable multi-vibrator (SN74LS123) is shown in Fig. 3.26. This unit generates two shot pulses S_{as} and $\overline{S_{as}}$ with a duration of t_d.

The gate signal G_a is generated by ANDing S_a and S_{as} using IC 7408 and passing this signal through a buffer (CD4050). Similarly, the complementary gate signal Ga can be achieved. In this experiment, a dead beat time of 4μs is chosen by considering the values of $R_{E1}$and C_{E1} as 18 kΩ and 470 pF respectively.

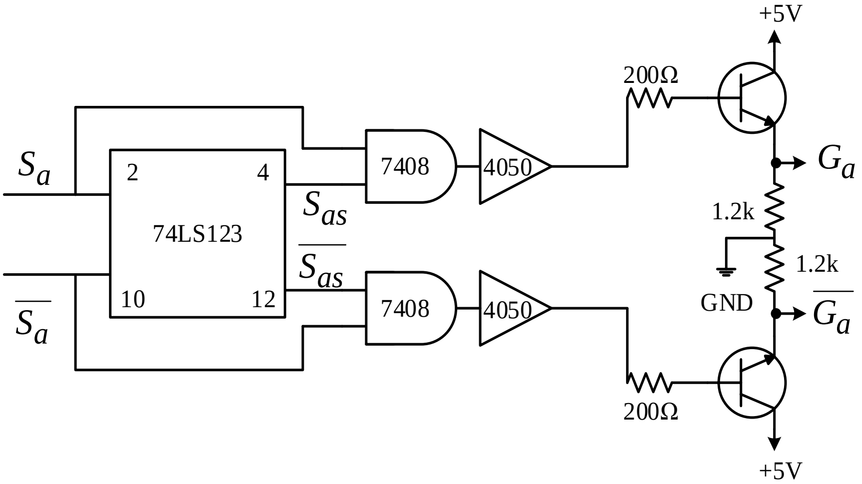

Fig. 3.25 Schematic diagram of blanking circuit

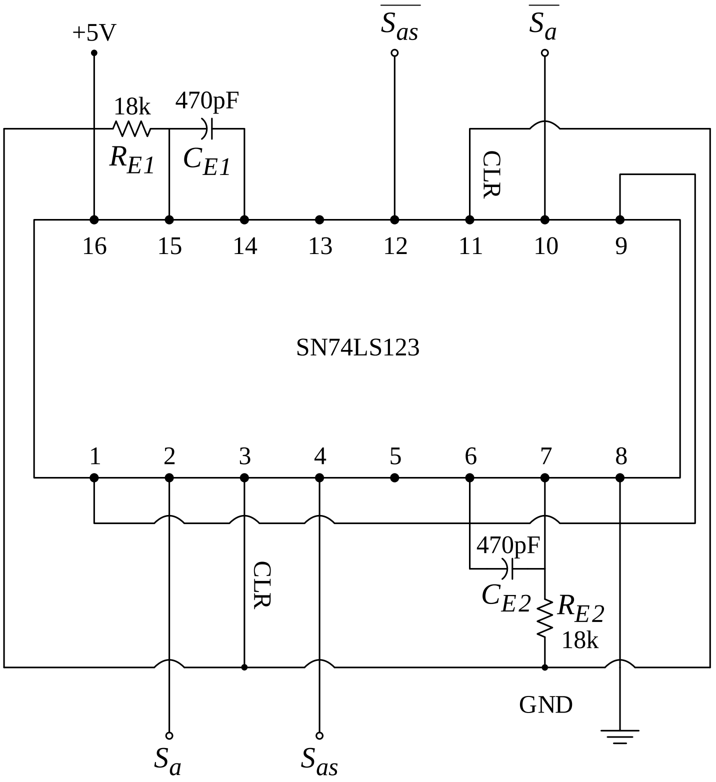

Fig. 3.26 Circuit connection diagram of SN74LS123

3.3.8 Optoisolation Circuit

The logical gate signals accessible from the blanking circuit cannot be directly applied to gates of the IGBT switches which are a part of the high-power network. Thus, high speed optocouplers (IC HCPL2601) with isolated dc power supplies are utilized for giving isolation between the logic control circuits and the power network. The internal and external circuit details of the optocoupler are shown in Fig. 3.27.

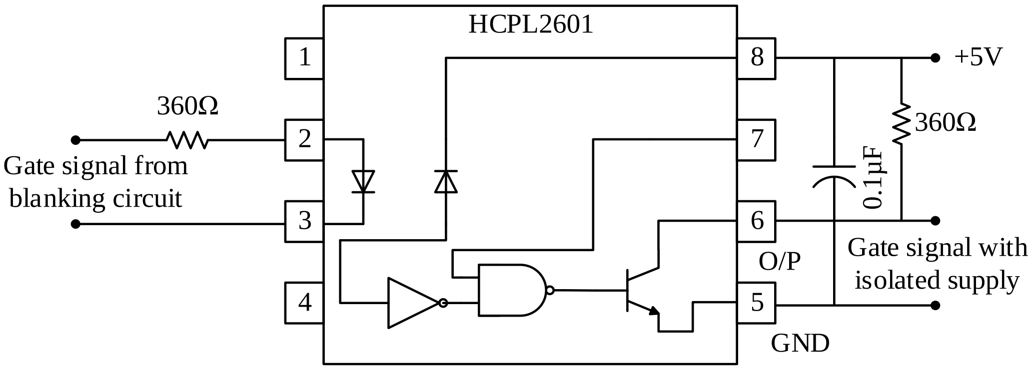

Fig. 3.27 Schematic diagram of optocoupler circuit

3.3.9 Power Supply Circuit

For the experimental set-up regulated dc power supplies of different voltage levels are required as given in Table 3.5. To generate a bipolar ±15V dc supply, a 230/18-0-18V center tapped step down transformer; full bridge diode rectifier consisting of four diodes (IN4007); two electrolytic capacitor of value 2200µF, 25V and two voltage regulators (7815 and 7915) are required. Once the ac voltages are converted to low level dc voltages then they are passed through the capacitors for smoothening purpose. A local ground is created by connecting the center tap of the transformer and capacitors as shown in Fig. 3.28. Then the dc voltage is given to the ICs 7815 and 7915 to produce regulated dc voltage of +15V and -15V respectively. Similarly +5V and -5V can be generated through ICs 7805 and 7905 respectively.

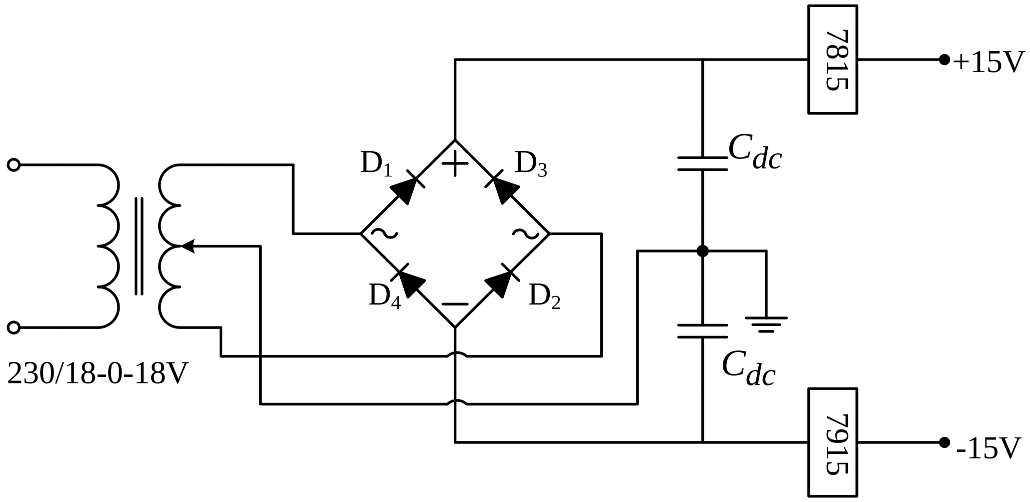

Fig. 3.28 Schematic diagram for dc regulated power supply

Table 3.5 Requirement of regulated dc power supply

Module	**Required Voltage Level**
Hall effect transducer circuit	±15V
Blanking circuit	+5V
Optocoupler	+5V
Protection circuit	±5V
Reference for protection circuit	±9V
Driver circuit	±15V

3.3.10 Experimental Results

The proposed LCLC-type PV-DSTATCOM with IcosΦ algorithm is developed in the laboratory. The efficacy of the proposed topology in real time domain is verified through the obtained experimental results. The design specification and parameter values of the experimental model are same as simulation prototype.

3.3.10.1 Real time performance analysis under ideal supply

In this section, the LCLC-type PV-DSTATCOM is operated at a lower voltage level of 100V. The three phase nonlinear load is drawing a nonlinear current of 5A. Fig. 3.29 and Fig. 3.30 are showing the experimental results for ideal three phase source voltage and nonlinear load current.

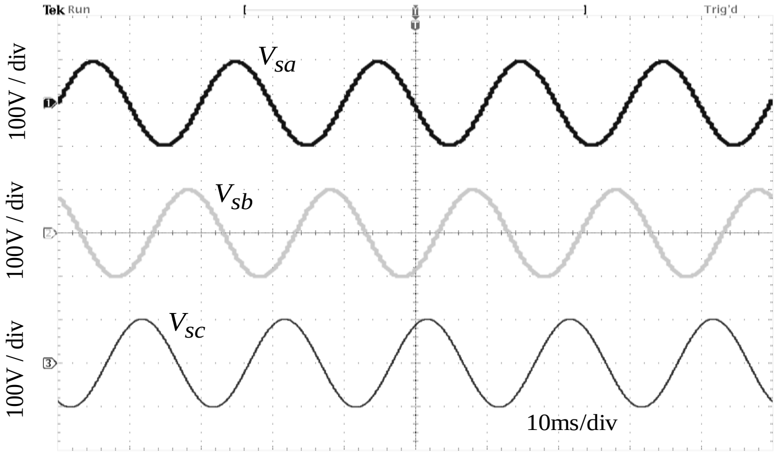

Fig. 3.29 Experimental result for ideal source voltage

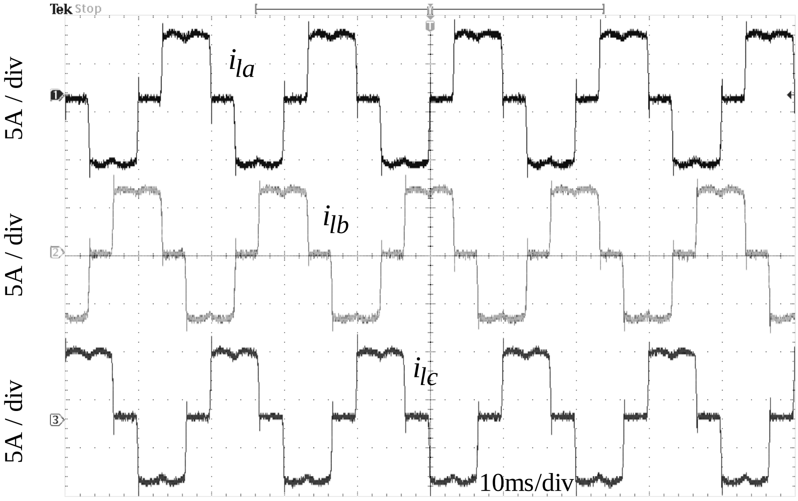

Fig. 3.30 Experimental result for load current

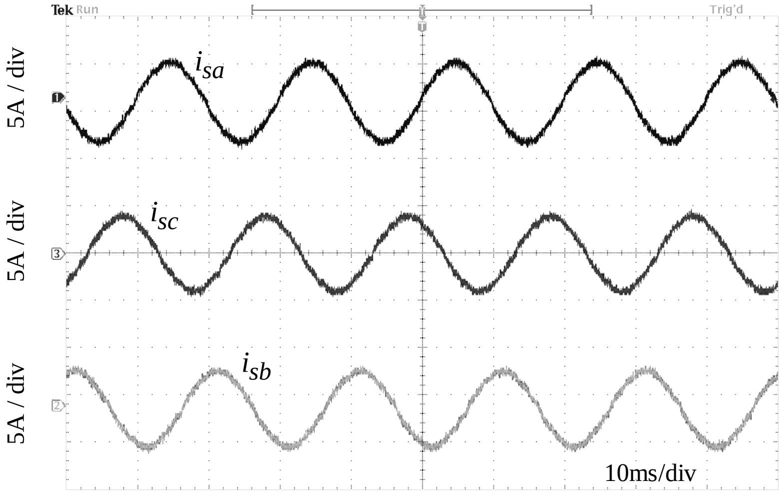

Fig. 3.31 Experimental result for source current

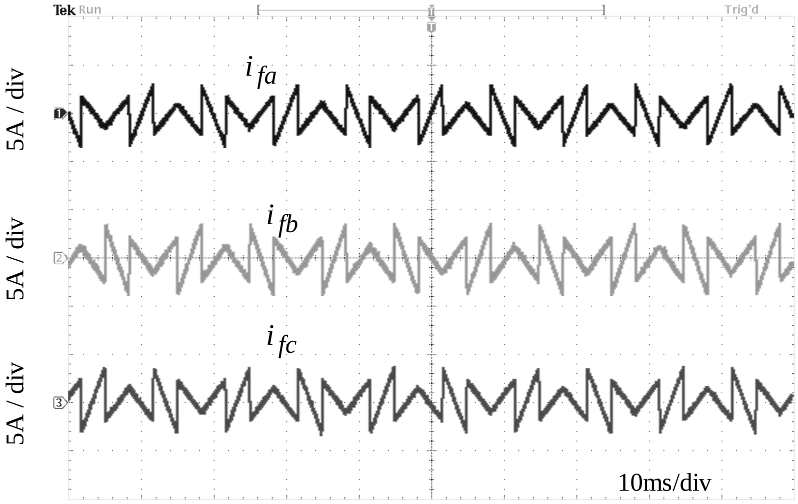

Fig. 3.32 Experimental result for filter current

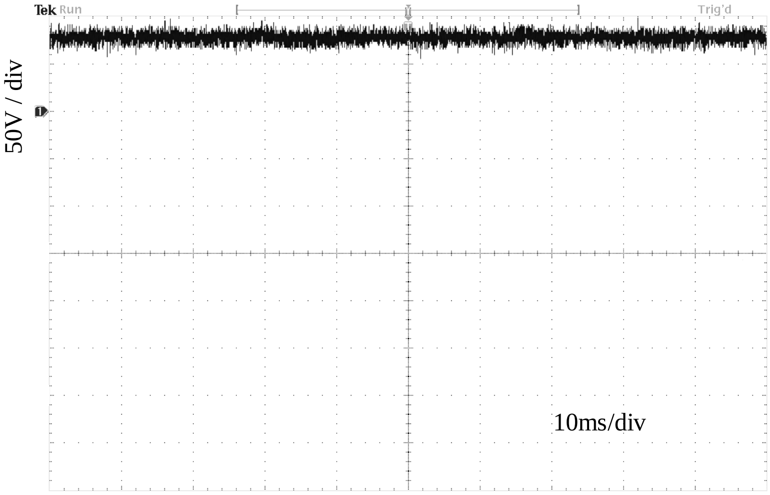

Fig. 3.33 Experimental result for dc-link voltage

The source current after compensation with proposed topology is shown in Fig. 3.31. From the result it is observed that after compensation the source current is sinusoidal and free from harmonics. The dc-link voltage is maintained at 75V and the waveform is shown in Fig. 3.33. The filter current injected from the compensator at PCC is shown in Fig. 3.32.

3.3.10.2 Real time performance analysis during load transient

Under this section, the compensating ability of the system is tested during sudden change of the load. Initially the PV-DSTATCOM is operated with unbalance nonlinear load. After some time the unbalance load is switched off and nonlinear load is switched on as shown in Fig. 3.34. Fig. 3.35 shows the source current which are sinusoidal and in phase with source voltage. From the experimental results it is depicted that with proposed topology the PV-DSTATCOM is being able to perform satisfactory in real time domain. The experimental results for phase-'a' are shown in Fig. 3.36.

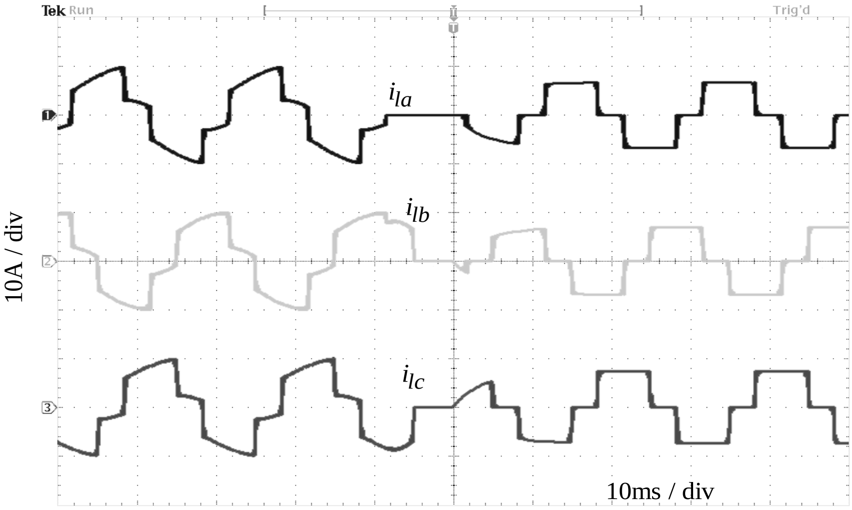

Fig. 3.34 Experimental result for load current during load transient

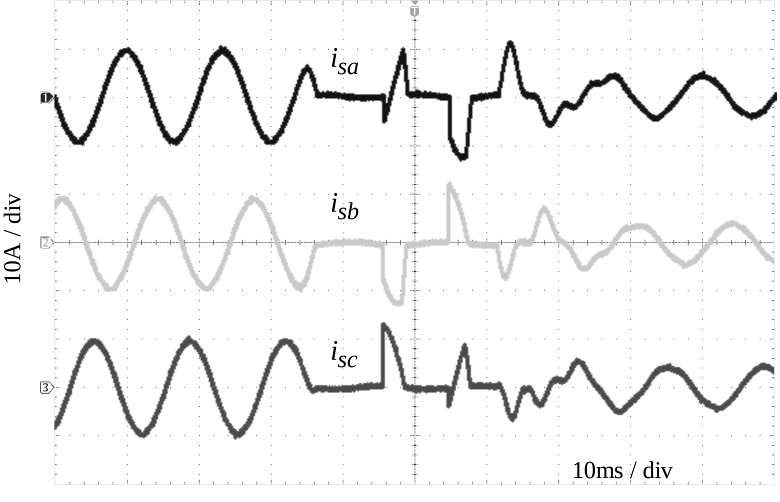

Fig. 3.35 Experimental result for source current during load transient

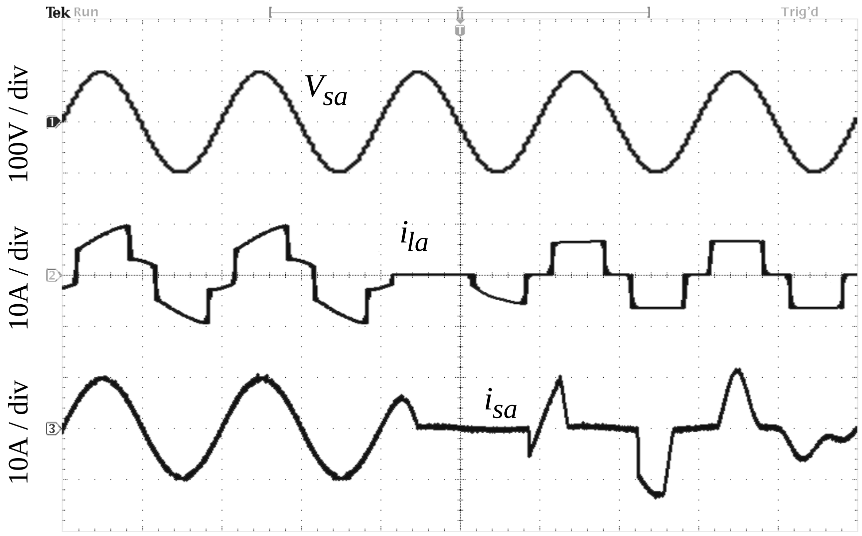

Fig. 3.36 Experimental result for phase-a during load transient

3.4 Chapter Summary

This chapter is presented in three major sections out of which Section 0 describes about LCL-type PV-DSTATCOM; Section 3.2 presents the LCLC-type PV-DSTATCOM and in Section 3.3 a real time prototype for LCLC-type PV-DSTATCOM has been developed. The mathematical designing and parameter selection procedure for both LCL-type and LCLC-type PVSTACOM has been discussed.

Though the LCL-type PV-DSTATCOM successfully overcomes the lacunas associated with L-type PV-DSTATCOM, still the voltage across dc-link capacitor is same as L-type compensator. Therefore LCLC-type PV-DSTACOM is proposed which includes a capacitor in series with LCL passive ac interface filter. Due to the insertion of the series capacitor the dc-link voltage has been reduced to 165V for the same amount of compensation. Because of reduction in dc-link voltage, the rating of the solar inverter has been reduced as the rating of inverter switches (IGBTs) reduced. Also due to lower dc-link voltage low rating solar systems can be integrated into the grid in single stage conversion process. The effectiveness of the system has been observed through both simulation and experimental results. From the results, it has been concluded that with proposed topology the power quality (i.e. current harmonics and load reactive power) of the system can be improved to limit within IEEE 519 standard. Hence the proposed LCLC-type PV-DSTATCOM is more effective than the other two topologies (L-type and LCL-type) of PV-DSTACOM.

4 Chapter 4

Performance Enhancement of LCLC-type PV-DSTATCOM Using Optimization Algorithm

- Develop an optimized LCLC-type PV-DSTATCOM to enhance the harmonic and reactive power compensating ability of the compensator universally.
- To apply an optimization tool to LCLC-type PV-DSTATCOM whose optimizing capability is independent of algorithm specific control parameters and compare its superiority over other optimization tools.
- To simulate the proposed system in MATLAB/Simulink for different load conditions.
- To analyze the effectiveness of the optimized PV-DSTATCOM in real time domain through experimentation.

For continuous and effective compensation of power quality issues, the dc-link voltage of PV-DSTATCOM is required to be maintained at its ideal value and as well as it is important that the passive ac interface filter parameter values should be chosen correctly. From the results obtained in Chapter 3 for LCLC-type PV-DSTATCOM, it is found that though the dc-link voltage is maintained at its reference value, when another passive component is inserted (series capacitor) due to the mismatching of passive filter values the compensation is not good as LCL-type PV-DSTATCOM. Because in general, the filtering parameters of the PV-DSTATCOM and gains of the PI controller are designed using a linearized mathematical model of the system. Such a design may not yield satisfactory results under changing operating conditions. To overcome this, evolutionary algorithms have been adopted for DSTATCOM in the literature [80] [81] [82] [83] [84] [85]. The advantage of optimization based controllers over conventional controllers are that they (a) don't need accurate mathematical modeling (b) can work with imprecise inputs (c) can handle nonlinearity (d) are more robust than conventional controllers. The nature-inspired optimization algorithms (such as genetic Algorithms (GA), Particle Swarm Optimization (PSO), Bacteria Forging Optimization (BFO), Firefly Algorithm etc.) performance is affected by their specific control parameters. Due to improper selection of those algorithm-specific control parameters (like mutation and crossover probability, selection operator in GA; inertia weight, social and cognitive parameter in PSO; chemotaxis, swarming and elimination in BFO etc.), these optimization techniques may lead to sluggishness of the system or convergence to a local minima. In addition to this, the selection of appropriate algorithm-specific parameters is difficult when the system becomes more complex. So, there is an urge to develop an optimized PV-DSTATCOM whose performance will be free from algorithm-specific control parameters.

In this Chapter, the JAYA optimization technique has been proposed for finding the optimal values of filter parameters and gains of the PI controller of the PV-DSTATCOM. JAYA has the benefits of being free from the selection of algorithm-specific control parameters plus suitable for fewer design variables, computational inexpensiveness, ease of solving discrete optimization problems and convergence to global optimum value, as compared to other optimization algorithms, such as gradient search method and nature inspired optimizations. To validate the superiority of JAYA algorithm, the results obtained are compared with other optimized systems performances like GEM based PV-DSTATCOM and TLBO based PV-DSTATCOM. The performance index for design, considered in this Chapter includes harmonic elimination, improvement of power factor, enhancement of switch on response and transient behavior of compensator.

4.1 Formulation of Objective Function

The compensating ability of LCLC-type PV-DSTATCOM depends on the both dc-link voltage and passive ac interface filter. If the dc-link voltage is not maintained at its reference value or the passive filters (L_i, L_g, C_{sh} and C_{se}) values are not chosen properly then the compensator may operates at less efficiency or may not compensate by any means. The dc-link voltage is regulated using a PI controller. A PI controller offers dual advantages as the Proportional (P) action provides fast response and the Integral (I) action provides zero steady-state error. But the conventional PI controller is criticized for being case dependent because, when they are applied to same model with different parameters, the result varies. So in this Chapter, the optimization algorithms are used to optimize the gains of PI controller (K_p and K_i) and the filter parameters (L_i, L_g, C_{sh} and C_{se}) as they directly affect the compensation ability of compensator. The mean square error (MSE) performance index presented in (4.1) is used as the objective function 'J' for optimization.

$$J = MSE = \sum_{i=1}^{iter} e_r^2 \tag{4.1}$$

where

$$Error\ (e_r) = \frac{\left|i_{f2a}^{*} - i_{f2a}\right| + \left|i_{f2b}^{*} - i_{f2b}\right| + \left|i_{f2c}^{*} - i_{f2c}\right| + \left|V_{pv}^{ref} - V_{pv}\right|}{iter}$$

As the necessity for better compensation is to reduce or minimize the error, a minimizing cost function is chosen. The objective of the optimizations is to find out the values for parameters that are to be optimized so that the $Error\ (e_r)$ will be minimized to the lowest value (i.e. zero).

4.2 Grenade Explosion Method Optimization

Parameter optimization consists of certain goals (objective functions), a search space (feasible solutions) and a search process (optimization methods). The feasible solutions are the set of all parameters characterized by all possible values of the design variables. The optimization method searches for the optimal parameter value from all available feasible parameter values. In population based optimization algorithm, the disadvantage is crowding of agents, which shows the convergence of the algorithm to a point in the crowded region. If it happens in the early iterations of the algorithm, solution to which the algorithm has converged is probably a local minimum, because the design space has not been explored adequately. Furthermore, in the final population, similar agents don't present different solutions, which can be a disadvantage especially when the objective function has several global minima. Therefore an evolutionary algorithm is developed namely Grenade Explosion Method (GEM) which will take care of the above said problem [86].

4.2.1 Basic working ideas of GEM optimization

The idea of the presented algorithm is based on observation of a grenade explosion, in which the thrown pieces of shrapnel destruct the objects near the explosion location. L_e is the length of explosion along each coordinate, in which the thrown piece of shrapnel may destruct the objects. The loss caused by each piece of shrapnel is calculated. A high value for loss per piece of shrapnel in an area indicates there are valuable objects in that area. To make more loss, the next grenade is thrown where the greatest loss occurs. Although the objects near grenade's location are more likely to be damaged, the probability of destruction is still kept for farther objects by choosing a high value for L_e. This process would result in finding the best place for throwing the grenades, even though shrapnel cannot discover this area in early iterations. The loss caused by destruction of an object is considered as the fitness of the objective function at the object's location. Suppose that X is the current location of a grenade

$$X = \{X_m\}, \qquad m = 1, 2, \dots, n$$

In which n is the search space dimension, equal to the number of independent variables. Now N_q pieces of shrapnel are produced by the grenade explosion and destruct objects that are in X'_j location:

$$X'_j = \{X_m + sign(r_m) \times |r_m|^p \times L_e\}, \qquad j = 1, 2, \dots, N_q \tag{4.2}$$

where r_m is a uniformly distributed random number in [-1,1] and p is a constant. A high value for p lets pieces of shrapnel search the region near the exploded grenade more accurately, while a low one lets them to explore farther regions better.

Considering Eq. (4.2), it is obvious that exploration for more valuable items performs in an n-dimensional cubic space extended $2L_e$ units along each coordinate and the grenade is located at the center of this cube. To use this algorithm, an independent variable range is scaled to [-1, 1]. Using Eq.(4.2), some produced shrapnel may collide to objects outside the feasible space. To increase the convergence rate and exploration of near-boundary regions more accurately, such a collision location is transported to a new location inside the feasible region according to the following scheme:

$$\text{if } X'_j \notin [-1,1]^n \Rightarrow \left(B'_j = \frac{X'_j}{\left|\text{Largest component of } X'_j \text{ in value}\right|}\right)$$

$$\rightarrow B''_j = r'_j \times \left(B'_j - X\right) + X \tag{4.3}$$

$$\begin{cases} j = 1 \text{ to } N_q \text{ (Srapnel Number)} \\ 0 < r'_j < +1 \text{ (Random Number)} \end{cases}$$

where X'_j is the collision location outside the feasible space and B'' is the new location inside the feasible space. Fig. 4.1 depicts this procedure schematically.

One of the special concepts of this algorithm which can hardly be seen in other EAs is the agent's territory radius (R_t), which means an agent (in this algorithm agents are grenades) does not let other agents come closer than a specific distance, which is specified by R_t. When several agents are exploring the feasible space, a high value for this parameter makes sure that grenades are spread quite uniformly in the feasible space and the whole space is being explored, while a low value for this parameter lets the grenades get closer to search the local region all together. Fig. 4.2 depicts the range of explosion and territory radius in the two-dimensional space.

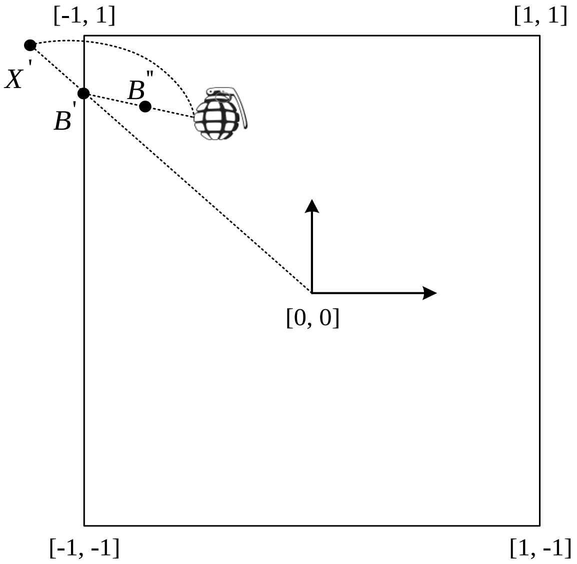

Fig. 4.1 Transportation of an unfeasible point ($\boldsymbol{X'}$) to a feasible location ($\boldsymbol{B''}$)

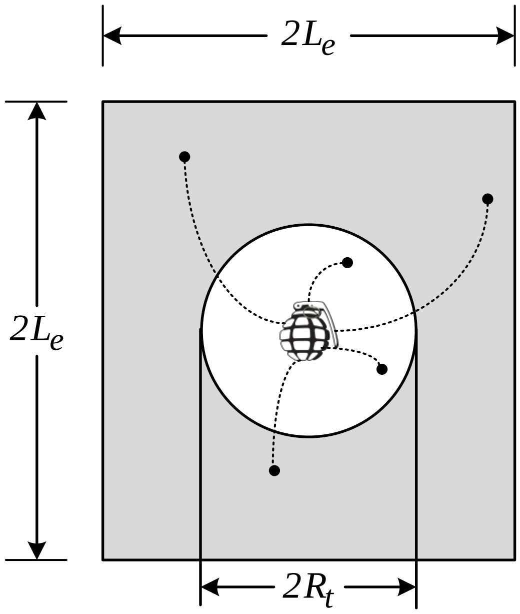

Fig. 4.2 Range of explosion and territory radius in the two-dimensional space

A higher value for the explosion range makes it possible to explore farther regions (better exploration), while a lower one lets the grenades focus on the region nearby (better exploitation). The value of exponent p determines the intensity of exploration. This parameter is updated based on the value of T_w:

$$p = max\left\{1, n \times \frac{log(R_t/L_e)}{log(T_w)}\right\} \tag{4.4}$$

where T_w is the probability that a produced piece of shrapnel collides an object in an n-dimension hyper-box which circumscribes the grenade’s territory.

To increase the global search ability, a high value for R_t should be chosen at the beginning ($R_{t,initial}$) and reduced gradually to let the grenades search the probable global minimum location found altogether for a precise answer. A simple method to reduce R_t, which is used in this article is:

$$R_t = \frac{R_{t,initial}}{(R_{rd})^{(\text{iteration No/total no.of iteration})}} \tag{4.5}$$

The value of R_{rd} is set before the algorithm starts. This parameter represents the ratio of the value of R_t in the first iteration to its value in the final iteration. Furthermore, L_e is reduced according to the following equation:

$$L_e = \left(L_{e,initial}\right)^m (R_t)^{1-m}, \qquad 0 \leq m \leq 1 \tag{4.6}$$

Which indicates that L_e is reduced more slowly than R_t during the iterations in order to save the global search ability. m can be constant during the algorithm, or reduced from a higher value to a lower one.

4.2.2 Steps for GEM optimization

- **Step-1:** Scale the independent variables' ranges to [-1, 1].
- **Step-2:** Select problem parameters: ($N_g, N_q, L_{e,initial}, R_{t,initial}, R_{rd}, m_{max}, m_{min}$, T_w).
- **Step-3:** Let $L_e = L_{e,initial}, R_t = R_{t,initial}$, iteration_number $= 1$.
- **Step-4:** Generate N_g grenades in random locations in an n-dimension space $\vec{X}_i \in [-1,1]^n$ which are a distance of at least R_t apart from each other.
- **Step-5:** While iteration_number $\leq$ max_iterations.
- **Step-6:** Arrange the grenades based on their fitness.
- **Step-7:** Let $i = 1$.
- **Step-8:** While N_q accepted points are generated around ith grenade generate a point (X') around ith grenade according to Eq. (4.2).
- **Step-9:** If (X') is outside $[-1,1]^n$, transport it into $[-1,1]^n$, according to Eq.(4.3).
- **Step-10:** If X' is a distance of at least R_t apart from the location of grenades$1,2,\ldots,i-1$, then X' is accepted.
- **Step-11:** End while $\%N_q$ pieces of shrapnel are thrown.
- **Step-12:** Calculate the fitness of the new generated points around the ith grenade. If the fitness of the best point is better than current location of the ith grenade, move the grenade to the location of the best point.
- **Step-13:** Let $i = i + 1$.

- **Step-14:** If $N_g \geq i$ the go to Step-8.
- **Step-15:** Reduce R_t according to Eq. (4.5).
- **Step-16:** Calculate exponent m according to the relation:

  $$m = m_{max} - \left(\frac{Iteration\_number}{Max\_iterations}\right)(m_{max} - m_{min}).$$

- **Step-17:** Update L_e according to Eq. (4.6).
- **Step-18:** Update exponent p according to Eq. (4.4).
- **Step-19:** End while % number of iteration.

4.3 Teaching Learning Based Optimization

Prior, numerous traditional (deterministic) optimization techniques have been successfully utilized, the most popular were: gradient based methods, Newton based method, simplex method, sequential linear programming, sequential quadratic programming, and interior point methods. Although, some of these deterministic techniques have excellent convergence characteristics and many of them are widely used in the industry however, they experience the ill effects of few shortcomings. Some of their disadvantages are: they cannot promise global optimality i.e. they may converge to local optima, they cannot readily handle binary or integer variables and finally they are developed with some theoretical assumptions, such as convexity, differentiability, and continuity, among other things, which may not be appropriate for the real power system conditions.

Moreover, the fast development of recent computational intelligence tools have motivated significant research in the area of non-deterministic that is, heuristic optimization methods. Some of these techniques are: Genetic Algorithm (GA), Particle Swarm Optimization (PSO), Grenade Explosion Method (GEM), Artificial Bee Colony (ACO), Harmony Search (HS), Bacterial Foraging Algorithms (BFA), Differential Evolution (DE), Evolutionary Algorithms (EAs), Gravitational Search Algorithm (GSA). These methods are known for: their capabilities of finding global solutions and avoid to be trapped with local ones, their ability of fast search of large solution spaces and their ability to account for uncertainty in some parts of the power system.

But these evolutionary optimization techniques performance is dependent on algorithm specific control parameters (such as: PSO uses inertia weight, social and cognitive parameters; GA uses crossover rate and mutation rate etc.; GEM uses length of explosion, number of grenades thrown, pieces of shrapnel per grenade etc., ABC requires optimum controlling parameters of number of bees (employed, scout, and onlookers), limits etc., HS requires harmony memory consider rate, pitch adjusting rate etc.). Because of the difficulties in selecting the optimum algorithm specific control parameters these heuristic algorithms give near optimal solution for complex systems. An adjustment in algorithm parameter changes the viability of the algorithm.

Teaching-Learning-Based Optimization is a rising star among metaheuristic techniques with highly competitive performances [87] [88] [89]. This method is based on the impact of an educator on learners. Like other nature-inspired algorithms, TLBO is also a population-based method and uses a population of solutions to proceed to the global solution. The population is considered as a group of learners or a class of learners. The process of TLBO is divided into two sections: the initial segment consists of the ‘Teacher Phase’ and the second part consists of the ‘Learner Phase’. ‘Teacher Phase’ means learning from the teacher and ‘Learner Phase’ means learning by the interaction between learners. The basic philosophy of the TLBO method is explained in detail in next section.

4.3.1 Basic working procedure of TLBO method

Assume two different teachers, T_1 and T_2, teaching a subject with the same content to the same merit level learners in two distinct classes. Fig. 4.3 demonstrates the distribution of marks got by the learners of two different classes evaluated by the teachers. Curves 1 and 2 represent the marks acquired by the learners taught by teacher T_1 and T_2 respectively. It is seen from Fig. 4.3 that curve-2 represents better results than curve-1 and so it can be said that teacher T_2 is superior to teacher T_1 in terms of teaching. The main difference between both the results is their mean (M_2 for Curve-2 and M_1 for Curve-1), i.e. a decent teacher delivers a better mean for the results of the learners. Learners additionally learn from interaction between themselves, which also helps in their results.

Consider Fig. 4.4, which demonstrates a model for the marks obtained for learners in a class with curve-A having mean M_A. The teacher is considered as the most proficient individual in the society, so the best learner is mimicked as a teacher, which is shown by T_A in Fig. 4.4. The teacher tries to disseminate knowledge among learners, which will thus expand the knowledge level of the entire class and help learners to get good marks or grades. So a teacher increases the mean of the class according to his or her capability. In Fig. 4.4, teacher T_A will try to move mean M_A towards their own level according to his or her capability, thereby increasing the learners’ level to a new mean M_B. Teacher T_A will put maximum effort into teaching his or her students, but students will acquire knowledge according to the quality of teaching delivered by a teacher and the quality of students present in the class. The quality of the students is judged from the mean value of the population. Teacher T_A puts effort in so as to increase the quality of the students from M_A to M_B, at which stage the students require a new teacher, of superior quality than themselves, and i.e. in this case the new teacher is T_B. Hence, there will be a new curve-B with new teacher T_B.

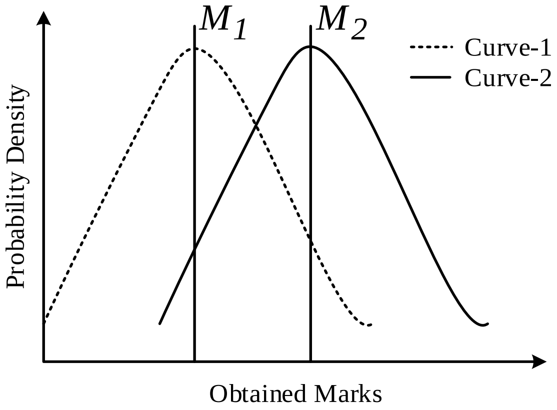

Fig. 4.3 Distribution of marks obtained by learners taught by two different teachers

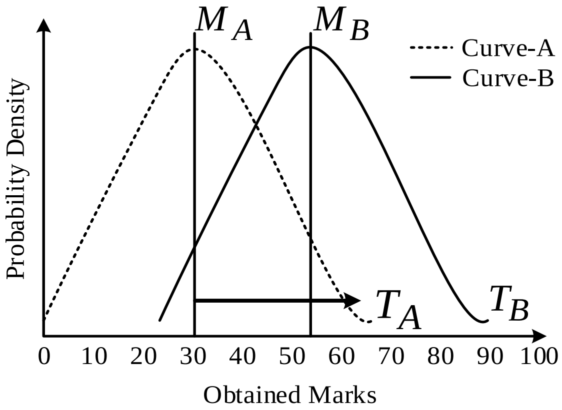

Fig. 4.4 Model for the distribution of marks obtained for a group of learners

In TLBO, different design variables will be analogous to different subjects offered to learners and the learners' result is analogous to the 'fitness', as in other population-based optimization techniques. The teacher is considered as the best solution obtained so far.. The flowchart of TLBO method is shown in Fig. 4.5.

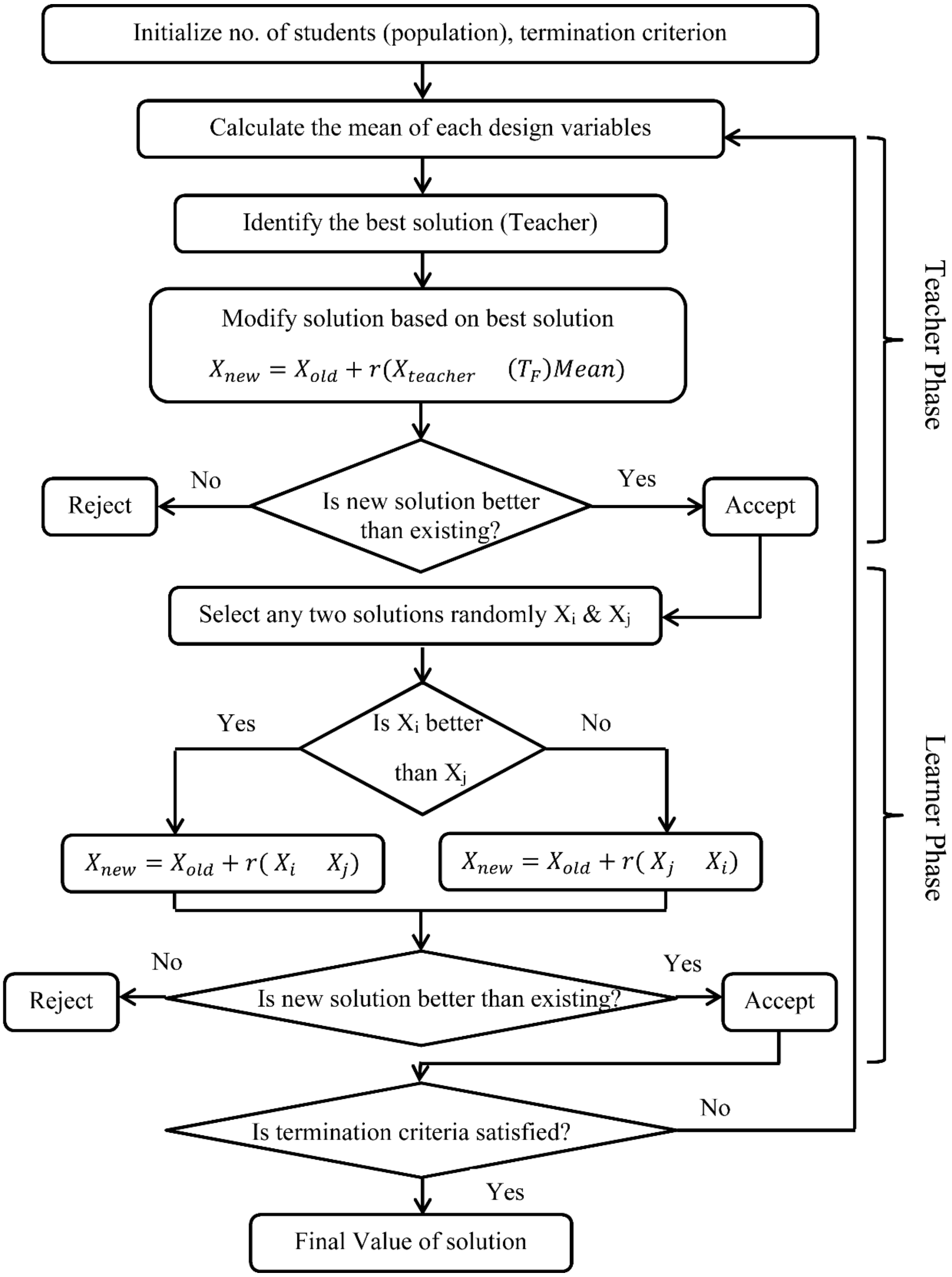

Fig. 4.5 Flowchart for Teaching Learning Based Optimization

4.3.1.1 Teacher Phase

As shown in Fig. 4.4, the mean of a class increases from M_A to M_B depending upon a good teacher. A good teacher is one who brings his or her learners up to his or her level in terms of knowledge. But in practice this is not possible and a teacher can only move the mean of a class up to some extent depending on the capability of the class. This follows a random process depending on many factors.

Let M_i be the mean and T_i be the teacher at any iteration 'i'. T_i will try to move mean M_i towards its own level, so now the new mean will be T_i designated as M_{new}. The solution is updated according to the difference between the existing and the new mean given by

$$Difference - mean_i = r_i(M_{new} - T_F M_i) \tag{4.7}$$

where T_F is a teaching factor that decides the value of mean to be changed, and r_i is a random number in the range [0, 1]. The value of T_F can be either 1 or 2, which is again a heuristic step and decided randomly with equal probability as T_F = round [1 + rand (0, 1) {2-1}].

This difference modifies the existing solution according to the following expression

$$X_{new,i} = X_{old,i} + Difference - mean_i \tag{4.8}$$

4.3.1.2 Learner Phase

Learners increase their knowledge by two different means: one through input from the teacher and the other through interaction between themselves. A learner interacts randomly with other learners with the help of group discussions, presentations, formal communications, etc. A learner learns something new if the other learner has more knowledge than him or her. Learner modification is expressed as

```
for $i = 1{:}P_n$
    Randomly select two learners $X_i$ and $X_j$, where $i \neq j$
    if $f(X_i) < f(X_j)$
        $X_{new,i} = X_{old,i} + r_i(X_i - X_j)$
    else
        $X_{new,i} = X_{old,i} + r_i(X_j - X_i)$
    End if
End for
Accept $X_{new}$ if it gives better function value
```

4.3.1.3 Pseudocode for TLBO

n: dimension of the problem

```
m: population size
MAXITER: maximum number of iterations
Initialization ( )
while $ITER < MAXITER$
    Elite ← Select Best (P, Elite)
    for $i = 1:m$
        $T_F$ = round (1 + rand)
        $X_{mean}$ ← mean ($X_i$)
        $X_{teacher}$ ← best ($X_i$)
        $X_{new,i} = X_i$ + rand ($X_{teacher}$ - ($T_F \cdot X_{mean}$))
        if $f(X_{new,i}) < f(X_i)$
            $X_i$←$X_{new,i}$
        end if
        j ← randi (m)
        if j ≠ i
            if $f(X_i) < f(X_j)$
                $X_{new,i} = X_i$ + rand ($X_i - X_j$)
            else
                $X_{new,i} = X_i$ + rand ($X_j - X_i$)
            end if
        end if
        if $f(X_{new,i}) < f(X_i)$
            $X_i$←$X_{new,i}$
        end if
    end for
    P ← Replace worst with Elite (P, Elite)
    P ← Remove duplicate individuals (P)
    ITER = ITER + 1
end while
```

4.4 JAYA Optimization

At a point when there is a battle, game, competition or obstacle, then the act of defeating the opponent enemy or expelling the impediment from the craved way is known as victory. This idea has been effectively consolidated in an optimization tool called as JAYA (means victory) optimization [90]. This optimization algorithm only requires the common control parameters to move towards the best solution avoiding the worst. JAYA algorithm operates only in one phase, unlike teaching-learning based optimization (TLBO) algorithm which requires two phases (i.e. teacher phase, learner phase) to find the optimum solution. In spite of the fact that both TLBO and JAYA algorithm are not dependants on algorithm-specific parameters, the less implementation complexity, less computation time and faster convergence characteristics of the JAYA algorithm makes it dominant over the TLBO one.

In any evolutionary algorithms, the convergence rate is given prime importance for solving an optimization problem over the quality of solutions. JAYA optimization algorithm is seen to yield improved results as compared to other evolutionary computing (EC) techniques like genetic algorithm (GA), particle swarm optimization (PSO), differential evolution (DE), grenade explosion method (GEM), artificial bee colony (ABC) and teaching-learning based optimization (TLBO).

4.4.1 Implementation of JAYA algorithm

A stepwise procedure is given in this section for the implementation of JAYA algorithm. Further details regarding convergence is given in [90].

Step-1: Define the objective function as minimize $f(X)$. Initialize the population size ($p = 1, 2, \ldots, n$), number of design variables ($d = 1, 2, \ldots, m$), upper and lower limits of design variables(U_L, L_L) and k numbers of iteration (i.e. $i = 1, 2, \ldots, k$) as termination criterion.

Step-2: Generate a random population according to the population size and number of design variables. The population size indicates the number of candidate solutions.

Step-3: Find the candidates, which obtain the best and the worst value of $f(X)$. Since the objective function is a minimizing function, the candidate with lowest $f(X)$ is considered as the best and the candidate with the highest $f(X)$ is considered as the worst.

Step-4: Assuming the random variables (r_1 and r_2) in the range of [0 to 1], the values for design variables are modified as follows:

$$\begin{aligned} X'_{d,p,i} = X_{d,p,i} + \underbrace{r_{1,d,i}\left(X_{d,best,i} - \left|X_{d,p,i}\right|\right)}_{A} \\ - \underbrace{r_{2,d,i}\left(X_{d,worst,i} - \left|X_{d,p,i}\right|\right)}_{B} \end{aligned} \tag{4.9}$$

where $X_{d,p,i}$ is the value of d^{th} variable for p^{th} candidate at i^{th} iteration, $X_{d,best,i}$ is the value of d^{th} variable for the best candidate, $X_{d,worst,i}$ is the value of d^{th} variable for the worst candidate.

The part 'A' of (4.9) corresponds to the characteristics of the algorithm to move towards best solution and the part 'B' is responsible for the tendency of algorithm to avoid worst solution.

Step-5: After getting new values of design variables, the corresponding objective function is calculated and compared with the previous values. From the comparison, the lowest of each are considered and the values for design variables and objective function are updated at the end of i^{th} iteration based on their fitness.

Step-6: From the updated values of f (X), the best and worst solutions are selected. The corresponding candidates are considered as best and worst candidate for the next iteration. After choosing the new values for random variables, the design variables are updated according to Step-4 and Step-5.

Step-7: The Steps-4, 5, and 6 are repeated till the termination criteria reached. The flowchart of JAYA algorithm is shown in Fig. 4.6.

4.5 Results and Discussions

The advantages of JAYA optimized PV-DSTATCOM are that it uses a lower ratings of VSI, operate with a lower value of dc link voltage, faster convergence to the global optimum, improved current compensation and invariable performance with changing load. All these advantages are verified through Matlab/Simulink power system toolbox. The parameters of all optimization algorithm are given in Table 4.1.

Table 4.1 Parameters used for all optimization

	Population Size	No. of design variable	No. of iteration	L_e	R_t	N_g	N_q	R_{rd}	T_w
GEM	50	4	1000	5	1.8	3	50	4500	0.3
TLBO	50	4	1000	--	--	--	--	--	--
JAYA	50	4	1000	--	--	--	--	--	--

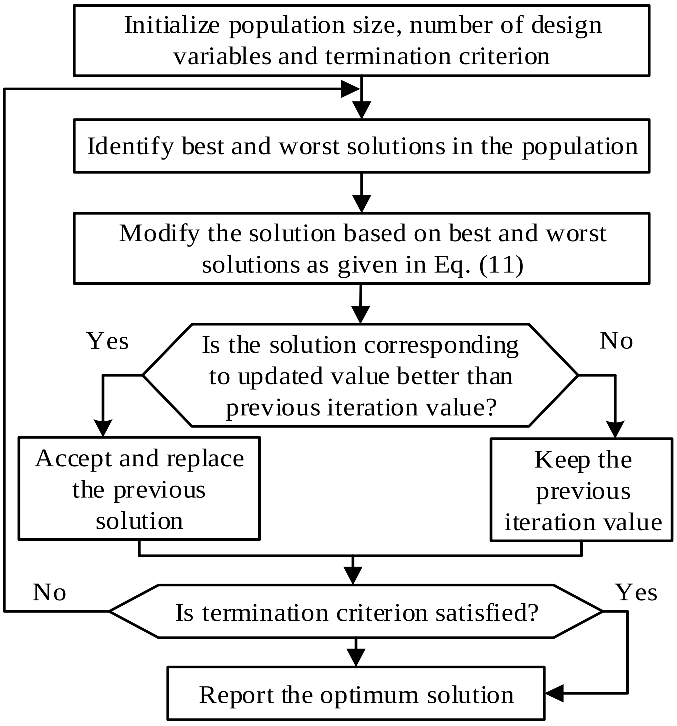

Fig. 4.6 Flowchart of JAYA optimization algorithm

4.5.1 Simulation Results

TLBO is the highly established and well-known optimization tool. Like JAYA, it depends on common controlling parameters such as population size, number of iterations. But TLBO algorithm operates in two phases, one is learner phase and the other one is teacher phase. This makes the algorithm more complex than JAYA to implement. Again TLBO technique optimizes the cost function by improving the mean for results of the learners. In the process, though the objective function reaches optimized value, the design variables may not achieve the best individual value in situations. Unlike JAYA and TLBO, the grenade explosion (GEM) requires additional controlling parameters to be set and also depends on algorithm-specific parameters (such as length of the explosion, pieces of shrapnel thrown, grenades territory radius etc.) [86]. Therefore, the convergence of GEM to its optimum value is slower than the other two optimization tool.

4.5.1.1 Comparison of Convergence characteristics

Generally, the effectiveness of the optimization algorithm depends on how fast it converges to the optimum value. The optimum value of the cost function J is plotted against the number of iteration in Fig. 4.7. From Fig. 4.7, it can be seen that the JAYA based PV-DSTATCOM converges faster than the other two optimized (TLBO and grenade explosion method (GEM) based PV-DSTATCOM) systems. Again for this particular problem, the GEM based PV-DSTATCOM is not being able to reach optimum solution.

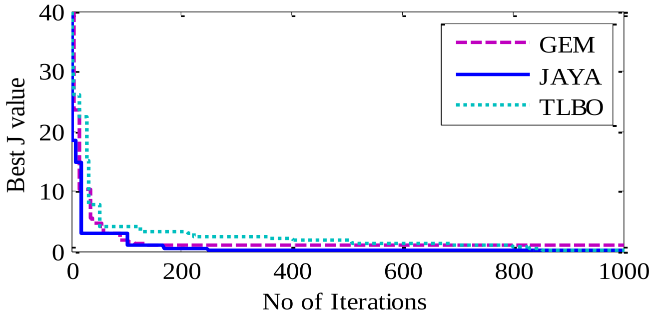

Fig. 4.7 Convergence characteristics for different optimization techniques.

From Fig. 4.7, it can be clarified that, though the JAYA and TLBO algorithm achieve the optimum solution before 300th and 850th iteration respectively, till 1000th iteration GEM is not being able to converge to best cost function value. The optimized filter parameters and PI gains are presented in Table 4.2 for a comparison.

Table 4.2 Optimized parameter values for different optimizations

Optimization Algorithm	GEM	TLBO	JAYA
K_p	0.4	1.2	0.9
K_i	25	12	11
L_i (in mH)	1.5	3.2	2.9
L_g (in mH)	0.4	1.8	2
C_{pv} (in µF)	2800	3050	3050
C_{sh} (in µF)	12	11	11
C_{se} (in µF)	56	58	52

4.5.1.2 Performance analysis under ideal mains voltage

Under this section, the PV-DSTATCOM is operated under a balanced and ideal source voltage. The source current is non-sinusoidal and heavily contaminated with harmonics when the compensator is not switched on, this can be clearly observed from Fig. 4.8 (b). The performance of the compensator can be ratified from Fig. 4.9. Fig. 4.9 shows that without the optimized PI controller gain and filter parameters, the source current after compensation carries high switching harmonics whereas with GEM based PV-DSTATCOM it considerably decreases. Using TLBO and JAYA optimization, the switching harmonics becomes negligible and thereby the source current becomes pure sinusoidal after compensation. By observing the Fig. 4.9 (c), we found that the source current of the TLBO optimized PV-DSTATCOM is slightly out of shape after compensation. Whereas the source current of the JAYA optimized PV-DSTATCOM is pure sinusoidal after compensation. Fig. 4.10 shows the voltage dynamics across the dc bus for all system.

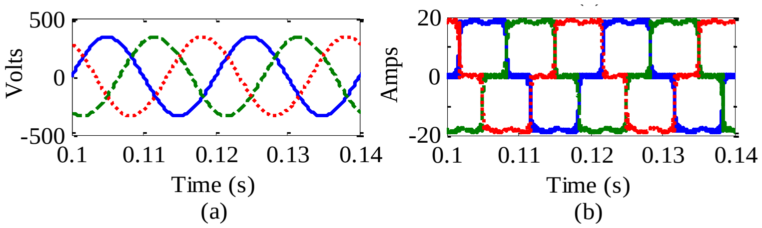

Fig. 4.8 Simulation results for (a) Source voltage, (b) Source current before compensation

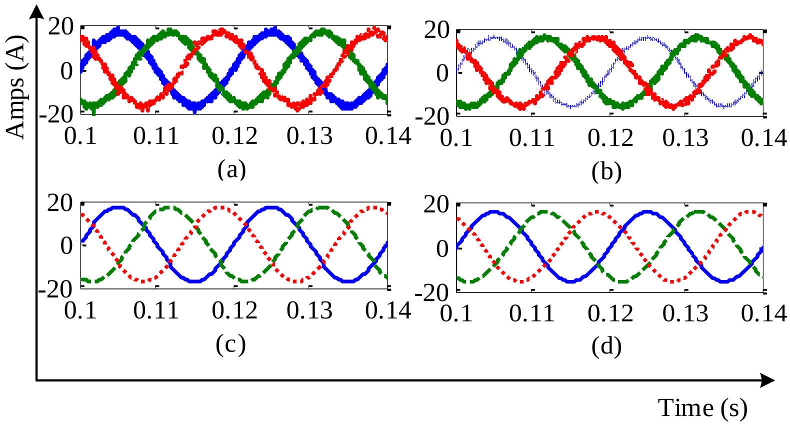

Fig. 4.9 Simulation results for source current after compensation. (a) Without optimization. with (b) GEM. (c) TLBO. (d) JAYA.

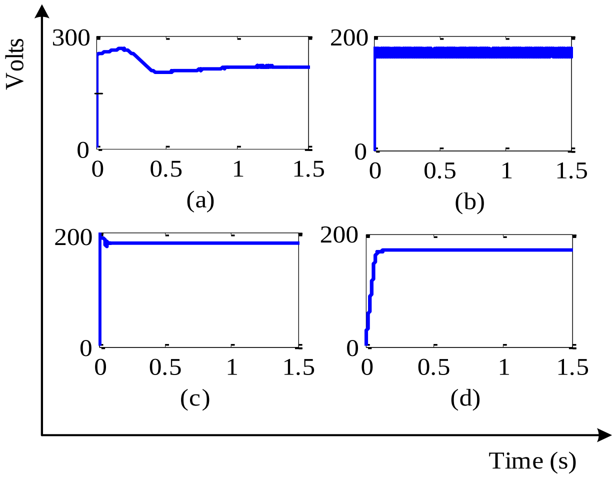

Fig. 4.10 Simulation results for voltage across dc link (a) without optimization. With (b) GEM. (c) TLBO. (d) JAYA

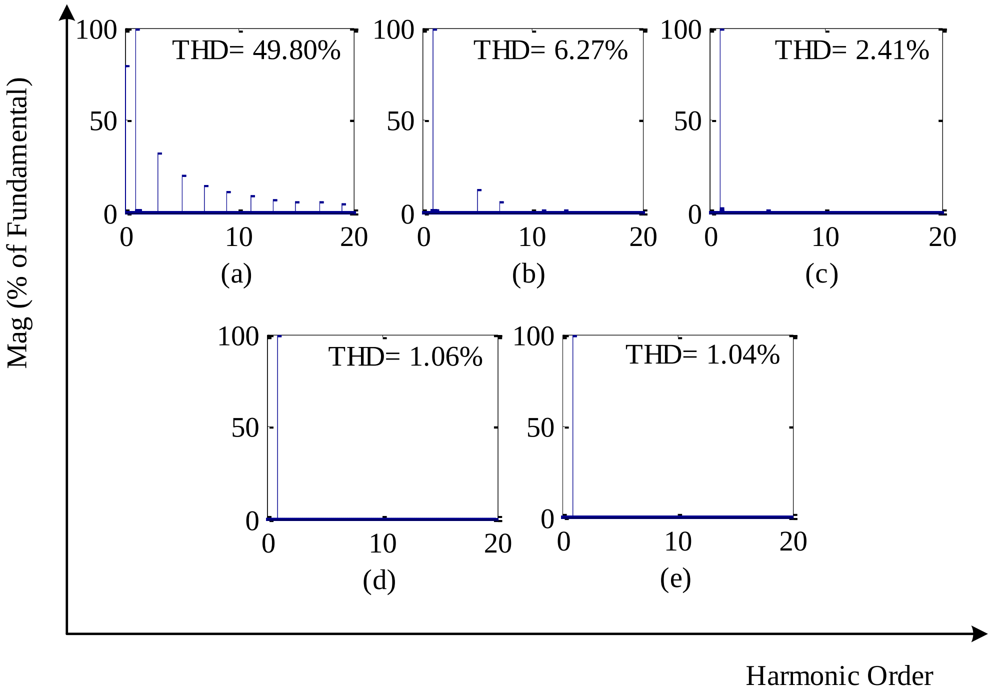

Fig. 4.11 Spectral analysis of source current (a) before compensation. (b) without optimization. With (c) GEM. (d) TLBO. (e) JAYA

The FFT analysis of the current signals before and after compensation are shown in Fig. 4.11. From the FFT analysis, it is found that the total harmonic distortion (THD) of source current after compensation is less for JAYA optimized PV-DSTATCOM as compared to TLBO optimized one.

4.5.1.3 Performance analysis during switch on transient

Initially, when the compensator is switched on, it takes some time to operate at its full efficiency. So under this section, it is shown that how fast the compensator achieves the steady state with different optimized PV-DSTATCOMs. The switch on transient for source current without compensator is shown in Fig. 4.12. From Fig. 4.13 (a), it is observed that without optimized parameter the source current magnitude increases to a peak of 280A during switch on transient. After 0.6 cycles, the source current settles to its original value. With GEM optimized PV-DSTATCOM, the peak of source current settles at 120A as shown in Fig. 4.13 (b) and the current regains its original shape and magnitude after 0.3 cycles. The transient peak of the source current further reduces with TLBO based PV-DSTATCOM to 60A but settling time increases to 1.5 cycles. The JAYA optimized PV-DSTATCOM gives the best switch on transient response as there is no sudden rise of current magnitude and also no oscillation.

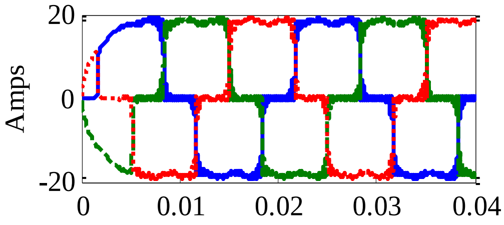

Fig. 4.12 Source current before compensation

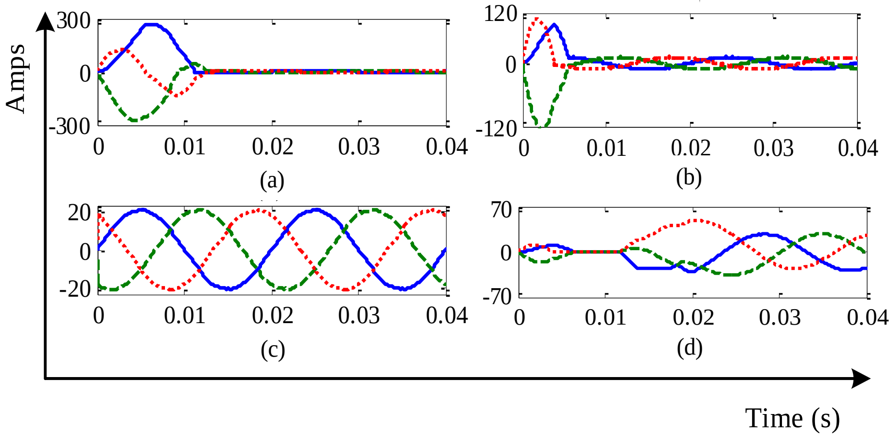

Fig. 4.13 Simulation results for switch on transient of source current after compensation. (a) Without optimization. With (b) GEM. (c) JAYA. (d) TLBO.

4.5.1.4 Performance analysis with thyristor load

In an electrical power system, the thyristorized converters are used to control the load as per the requirement. The thyristor based loads are controlled by controlling the firing angles of the converter to ensure the required output. For this case, a thyristor based rectifier with a resistor of 12Ω in series with an inductor of 20mH is considered as the load for simulation. To observe the robustness of the proposed JAYA based PV-DSTATCOM, the system is operated with different firing angles. The system is simulated with the firing angle of 0^0 till 0.52 seconds and then increased to 30^0 for 1.5 cycles. At 5.55 second again the load is operated with a firing angle of 60^0 for 0.03 seconds and then after 1.5 cycles the system is operated at 0^0 firing angle. The simulation results of source current before and after compensation for the proposed JAYA based PV-DSTATCOM along with GEM and TLBO optimized PV-DSTATCOM are presented in Fig. 4.14 and Fig. 4.15 respectively. From Fig. 4.15, it is clearly noticeable that the JAYA optimized DSTOSTCOM gives better performance than the other two optimized system. With the proposed system the switching harmonics and the (THD) are less. The bar graph of THD for source current with thyristor load after compensation is shown in Fig. 4.16. Comparing the Fig. 4.11 and Fig. 4.16, it is concluded that though JAYA is much simpler for implementation than TLBO, it remains unaffected to load change like TLBO. The proposed controller tracks the reference efficiently as compared to GEM and TLBO algorithm.

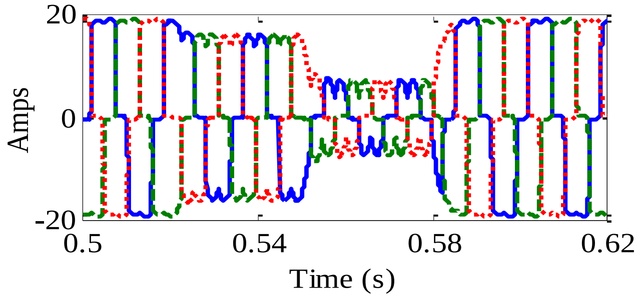

Fig. 4.14 Simulation results for source current before compensation with thyristor load

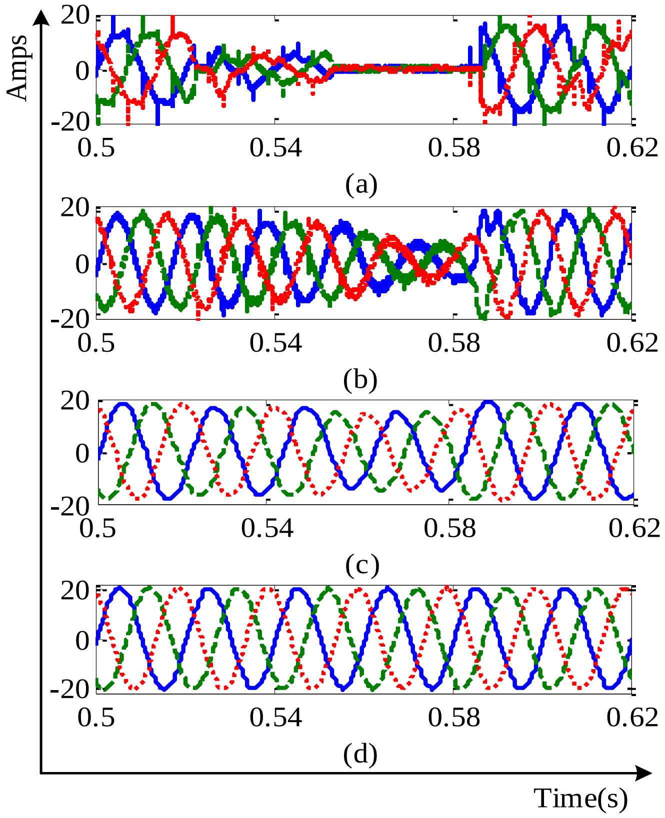

Fig. 4.15 Simulation results for source current after compensation with thyristor load. (a) Without optimization. With (b) GEM. (c) TLBO. (d) JAYA

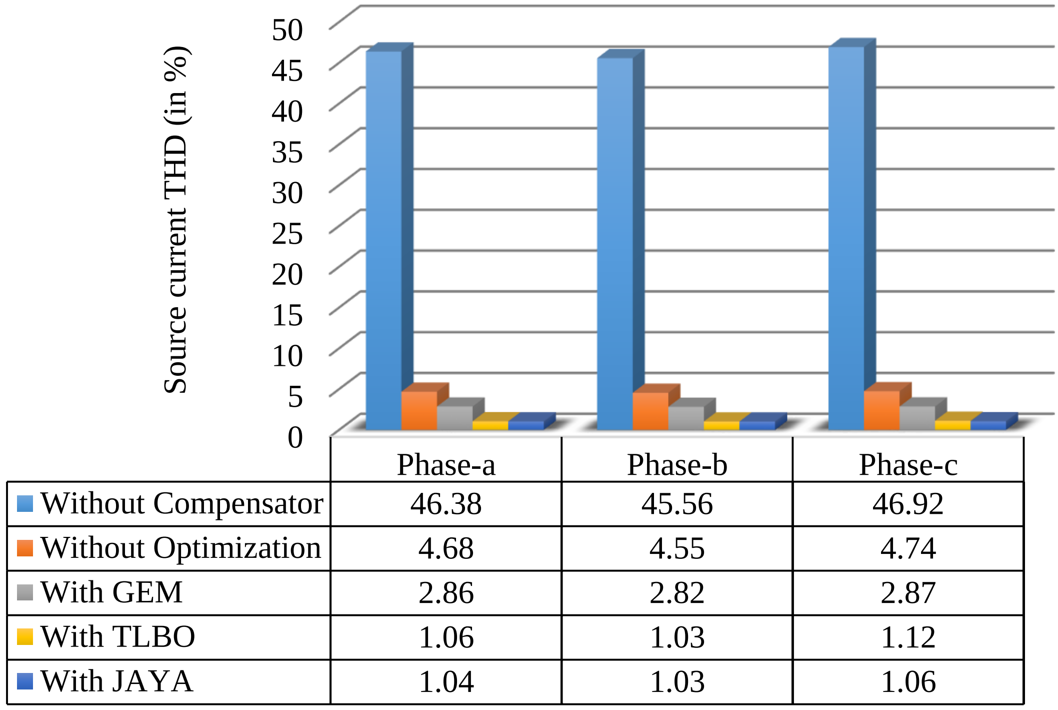

	Phase-a	Phase-b	Phase-c
🟦 Without Compensator	46.38	45.56	46.92
🟧 Without Optimization	4.68	4.55	4.74
⬜ With GEM	2.86	2.82	2.87
🟨 With TLBO	1.06	1.03	1.12
🟦 With JAYA	1.04	1.03	1.06

Fig. 4.16 Bar graph showing the percentage of total harmonic distortion for source current

4.5.1.5 Response during unbalance load and with different loads

In this case, the linear unbalanced load and nonlinear load (i.e. diode bridge rectifier with inductive-ohmic load) is considered for simulation. The system is simulated with both the load till 0.2 seconds and at 0.21 second, the unbalanced load is turned off. The model is operated with only nonlinear load for 20 cycles. Then the linear unbalanced load is connected to the system and bridge rectifier load is taken out at 0.4 second. After 20 cycle of operation with linear load, again the rectifier load is switched on and the system is simulated with both the loads. The load currents during these load switching are shown in Fig. 4.17, Fig. 4.19 and Fig. 4.21 respectively. For all optimized system, the source currents after compensation during load change are shown in Fig. 4.18, Fig. 4.20 and Fig. 4.22 respectively. From the responses, it is depicted that though GEM optimized system is being able to diminish the load unbalancing but the settling time required after load switching is more as compared to TLBO and JAYA optimized PV-DSTATCOM. The analytical comparison of proposed JAYA based PV-DSTACOM with GEM and TLBO optimized system is presented in a nutshell in Table 4.3.

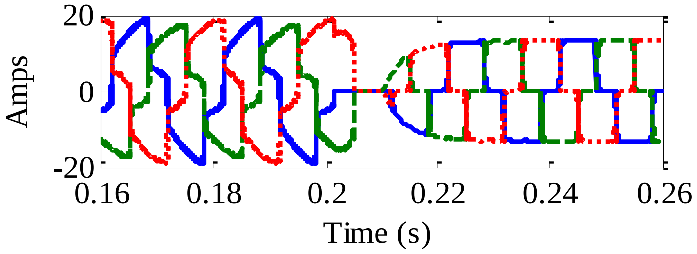

Fig. 4.17 Load Current during load change (Nonlinear unbalance load to nonlinear load)

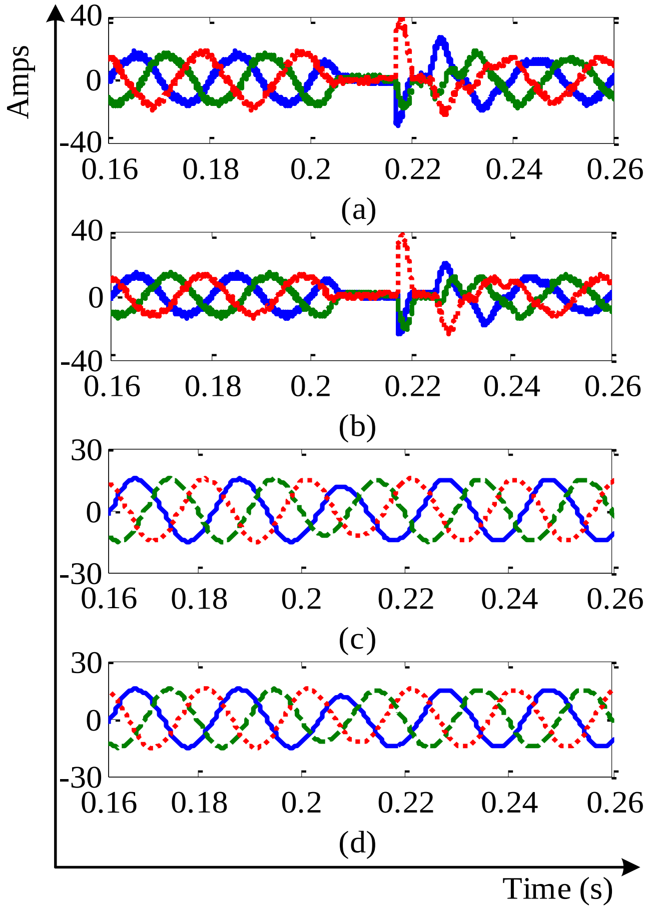

Fig. 4.18 Source current after compensation (nonlinear unbalance to nonlinear) (a) without optimization. With (b) GEM. (c) TLBO. (d) JAYA.

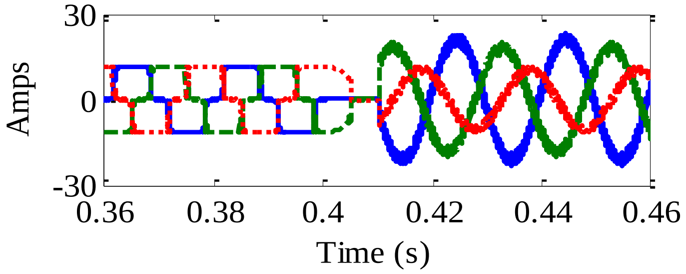

Fig. 4.19 Load current during load change (Nonlinear load to linear unbalance load)

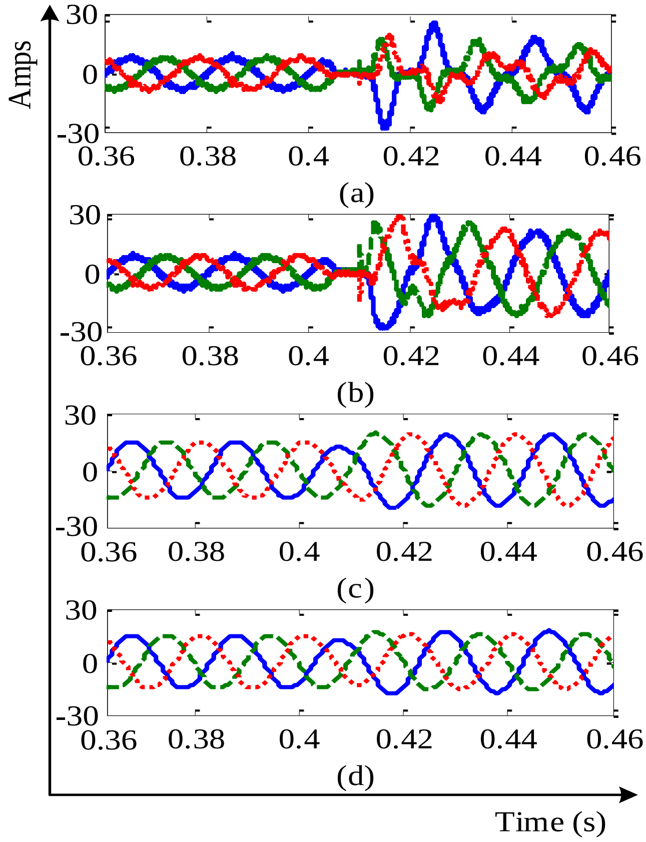

Fig. 4.20 Source current after compensation (nonlinear to linear unbalance) (a) without optimization. With (b) GEM. (c) TLBO. (d) JAYA.

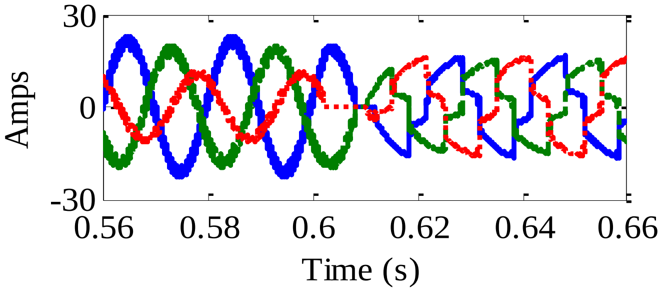

Fig. 4.21 Load current during load change (Linear to linear unbalanced and nonlinear load)

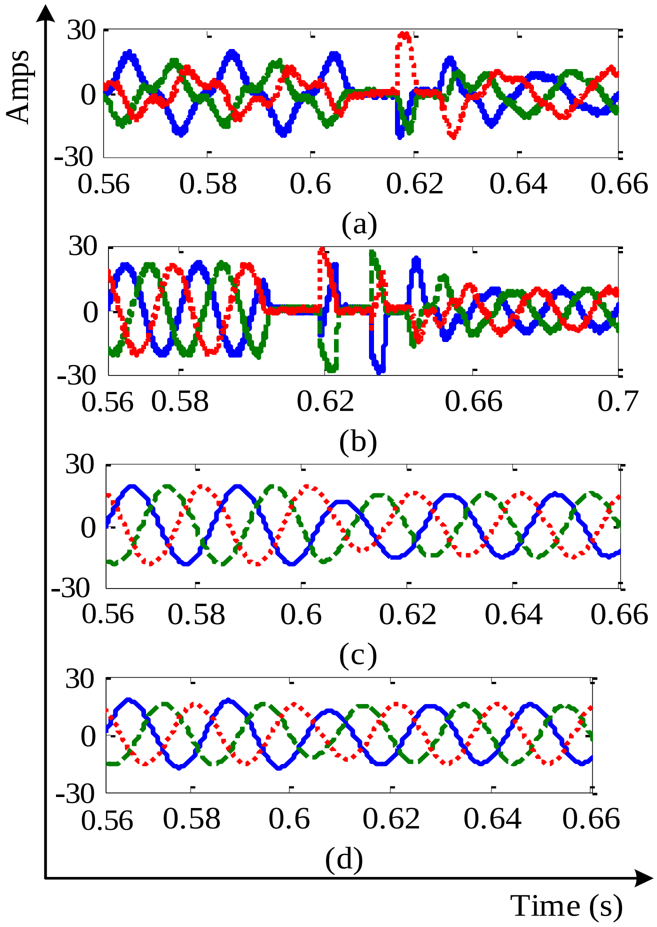

Fig. 4.22 Source current after compensation (linear to linear unbalanced and nonlinear) (a) without optimization. With (b) GEM. (c) TLBO. (d) JAYA.

Table 4.3 Performance analysis of GEM, TLBO and JAYA based PV-DSTATCOM

Type	GEM	TLBO	JAYA
Dependency on algorithm-specific control parameter	High	Not dependent	Not dependent
THD (in %) under steady state	2.41	1.06	1.04
Switching harmonics	High	Low	Low
Convergence to optimum solution	Slow	Fast	Very Fast
Settling time after switch on (in cycles)	1	2.5	0
Reference tracking with controlled rectifier load	Good	Accurate	Accurate
Reference tracking when load unbalancing occurs	Good	Better	Accurate
Implementation complexity	High	Medium	Low
Dynamic response	Poor	Good	Good

4.5.2 Experimental Results

The experimental setup is developed for validating the effectiveness of the proposed JAYA based PV-DSTATCOM. For the interfacing between controller and hardware model, dSPACE 1103 is used. Using ADC and DAC channels of dSAPCE the PWM switching signals are given to SEMIKRON inverter. As the magnitudes of output PWM pulses from dSPACE are 5 volts, the required 15 volts PWM pulses for inverter are given through CD4504 drivers. The CD4504 drivers amplify the magnitude of pulses to required 15 volts. Hall Effect sensors (LA 55-P, LV-25-P) are used to sense the currents and voltages required by the controller and given as input to the controller through ADC channels. Protection circuits are used to avoid any damages or malfunctioning of developed model due to over-voltage or over-current.The developed model is operated at a reduced voltage level of 110 volts rms per phase. The three phase bridge rectifier draws load current of 10 amperes from the source. Switching frequency of 10 KHz is selected and the other parameters are chosen same as simulation parameters.

The source voltage and highly harmonics contaminated load current is shown in Fig. 4.23 and Fig. 4.24. From Fig. 4.25, it is observed that, without optimization though the source current is sinusoidal after compensation, it has high switching harmonics. Fig. 4.26 ratifies that the switching harmonics of source current further reduces with GEM optimized PI gains and filter parameters, as compared to non-optimized system after compensation. From Fig. 4.27 and Fig. 4.28, it has been spotted that, with TLBO and JAYA the source current contains minimum amount of switching frequency component. But with TLBO optimized system, the compensated source current has some notches, since with TLBO working procedure, the parameters reach to optimum value by improving the mean result of the learners (i.e. deign variables). Through this process, though the objective function gets optimized, sometimes the design variables may not achieve their optimum value. But with JAYA optimization, the notches are removed from the source current after compensation.

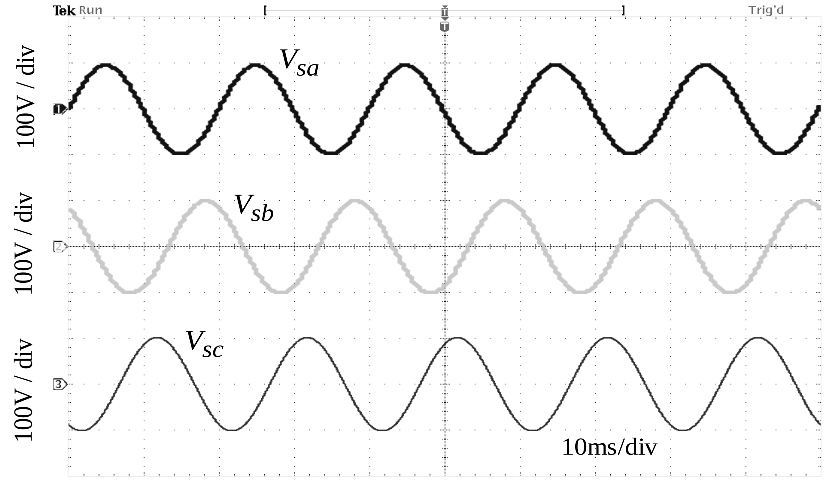

Fig. 4.23 Experimental result for ideal source voltage

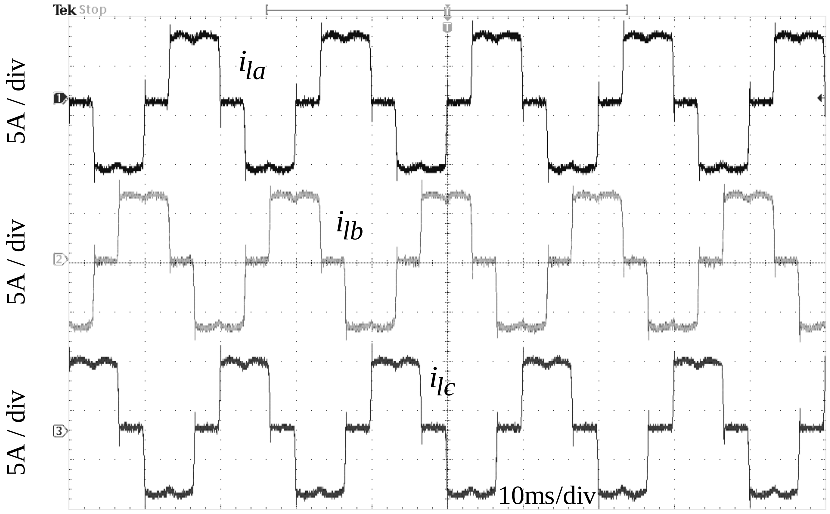

Fig. 4.24 Experimental result for nonlinear load current before compensation

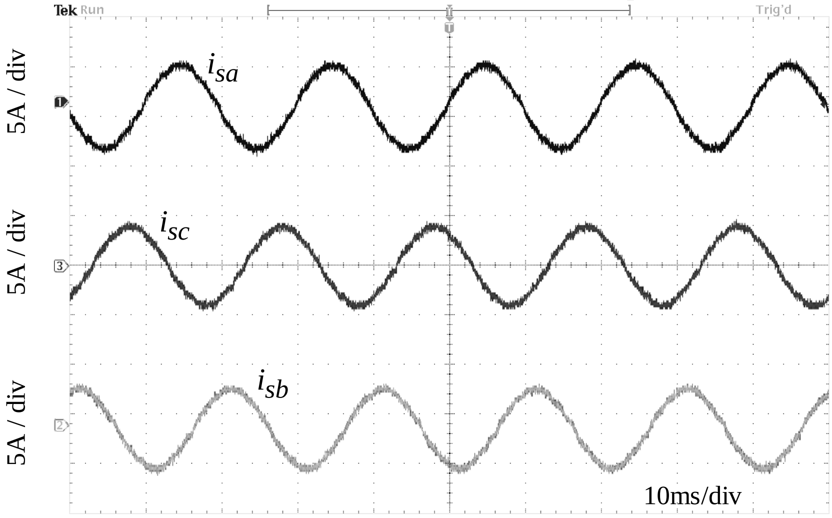

Fig. 4.25 Experimental result for source current after compensation without optimization

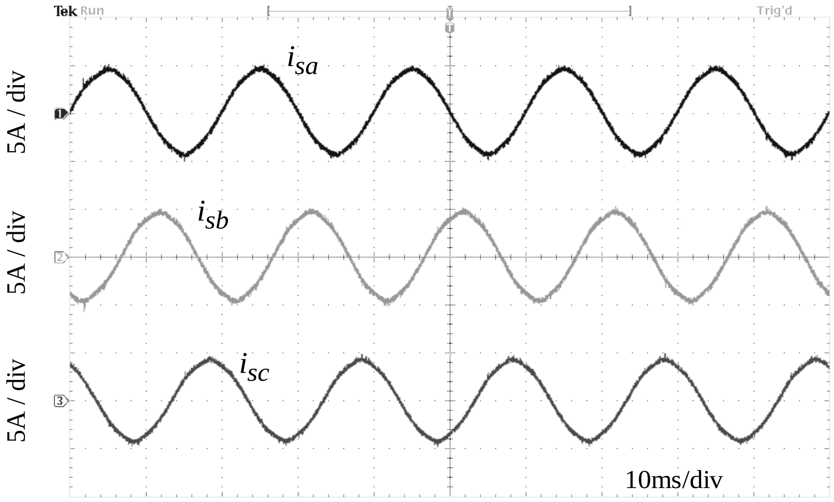

Fig. 4.26 Experimental result for source current after compensation with GEM optimization

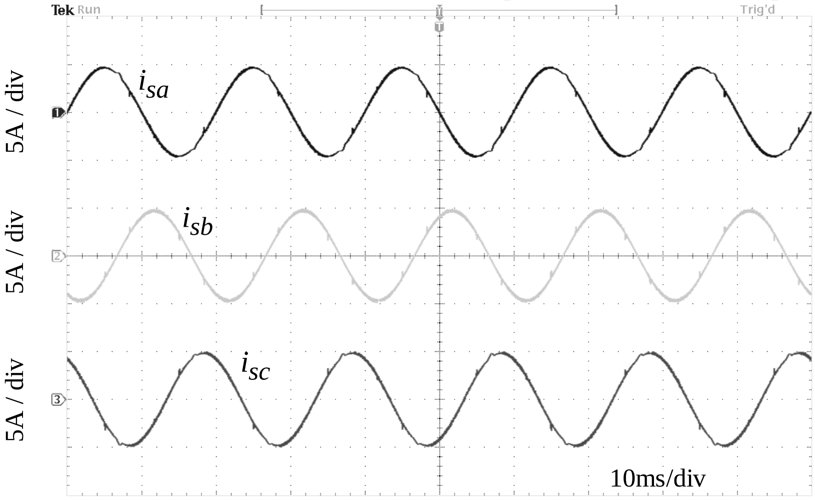

Fig. 4.27 Experimental result for source current after compensation with TLBO optimization

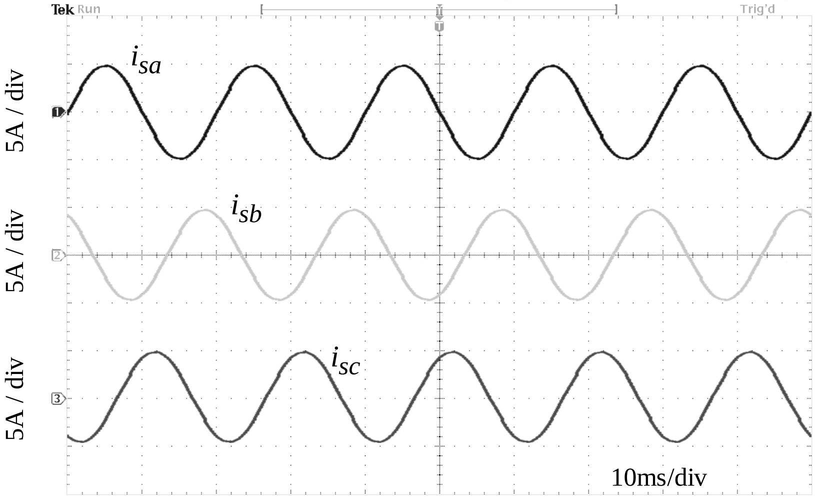

Fig. 4.28 Experimental result for source current after compensation with JAYA optimization

However, there are difficulties of getting system parameters updated through optimization algorithms in the practical environment, as the need of local system changes over time but these problems can be reduced either by considering all nonlinear and saturation limits of the controllers or by developing adaptive optimization algorithms.

4.6 Chapter Summary

The chapter proposes the implementation of an algorithm specific control parameter independent optimization tool “JAYA” to solve the current harmonics problem. To clarify the superiority of JAYA algorithm over other optimization algorithms, another two different type of optimization tools GEM (dependent on algorithm specific control parameter), TLBO (independent of algorithm specific parameter) are applied to LCLC-type PV-DSTATCOM. Optimization algorithms are utilized here to find out optimized values of filter parameters and PI controller gains for improved total harmonic distortion.

From the obtained results it is observed that, algorithm specific control parameter independent optimization tools (i.e. TLBO and JAYA) performs better in each and every possible way than the algorithm specific control parameter dependent optimization tool. The maximum overshoot is exceptionally small for both TLBO and JAYA optimization-based PV-DSTATCOM during load transient than GEM. Moreover, the proposed JAYA optimized LCLC-type PV-DSTATCOM tracks the reference and compensates the harmonics more efficiently even if the load is completely changed, followed by TLBO and GEM optimized PV-DSTATCOM. This fact has been supported by both analytical and experimental results. FFT analysis indicate the THD obtained with JAYA to be the lowest, though TLBO and GEM also yield lesser THDs compared to the conventional one. From the study it is found that though both TLBO and JAYA optimization tools performance is independent of algorithm specific control parameters, JAYA is much simpler to implement. Hence, JAYA algorithm has an edge over the TLBO, especially in context to the convergence behaviour of the algorithm very near to the optima.

5 Chapter 5

Sliding mode Control of LCLC-type PV-DSTATCOM

- Develop an average model of LCLC-type PV-DSTATCOM for better understanding of compensator dynamics.
- Apply sliding mode controller to current control scheme for enhanced tracking performance under ideal as well as adverse operating conditions.
- To simulate the proposed system in MATLAB/Simulink for different supply voltages and load conditions.
- To analyze the effectiveness of the SMC based PV-DSTATCOM in real time domain through experimentation.

The performance of the LCLC-type PV-DSTATCOM mainly depends on the accuracy of reference current extraction by the current controller. If there is any change in supply voltage conditions or in system parameters then the linear current controllers are not being able to generate the reference current accurately. So when switching signal are synthesized from the error generated by comparing the reference source current and actual source current, the PV-DSTATCOM do not compensate that effectively as they should do. In Chapter 4, an optimized PV-DSTATCOM is developed but still the controller used is a linear controller. Also to implement the optimization techniques online in real time is a difficult process. As discussed above the linear controllers are sensitive to any change in operating conditions or system parameter [91] [92]. So in this Chapter a nonlinear controller named as Sliding Mode Controller (SMC) has been applied to the current control scheme of PV-DSTATCOM for enhancing the compensating ability under non-ideal operating conditions. The main strength of sliding mode control is its robustness. Because the control can be as simple as a switching between two states (e.g., "on"/"off" or "forward"/"reverse"), it need not be precise and will not be sensitive to parameter variations that enter into the control channel [93]. Additionally, because the control law is not a continuous function, the sliding mode can be reached in finite time. Due to low sensitivity to plant parameter variations and disturbances, the SMC based systems eliminates the necessity of exact modeling.

In this Chapter an average nonlinear modeling of LCLC-type PV-DSTATCOM is derived by considering the PV system and solar inverter. A dc voltage droop regulator is used to control the power flow from solar system and to maintain dc link voltage. To make the system robust, switching pulses for inverter is generated using sliding mode controller. To validate the efficacy of the implemented sliding mode controller for the power quality improvement, the performance of the proposed system is observed with both linear and non-linear controller and compared by taking total harmonic distortion as performance index. At the end, the simulation results are validated by experimentation.

5.1 Average modeling of LCLC-type PV-DSTATCOM

The topology of LCLC-type PV-DSTATCOM is shown in Fig. 3.11. The equivalent single phase circuit diagram of the proposed system can be represented as shown in Fig. 5.1.

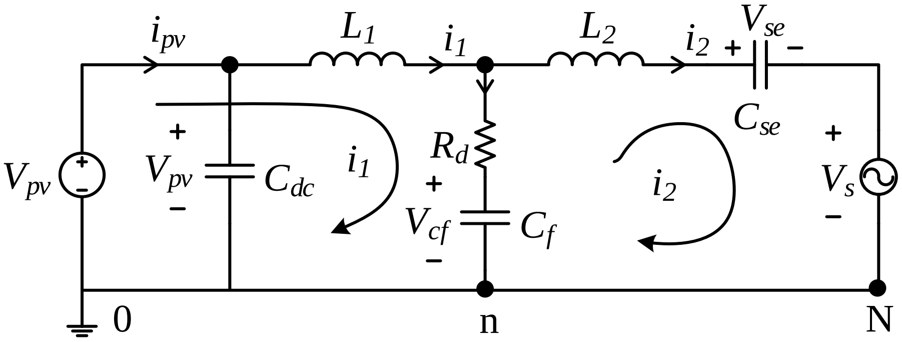

Fig. 5.1 Single phase circuit diagram of LCLC-type PV-DSTATCOM

Here i_{1d}, i_{1q}, i_{2d} and i_{2q} denote d-q axis VSI currents and filter currents respectively, V_{cfd} and V_{cfq} are the d-q axis voltage across shunt capacitor, V_{sed} and V_{seq} are the voltages across the series capacitor, D_d and D_q stands for d-q axis duty ratio functions.

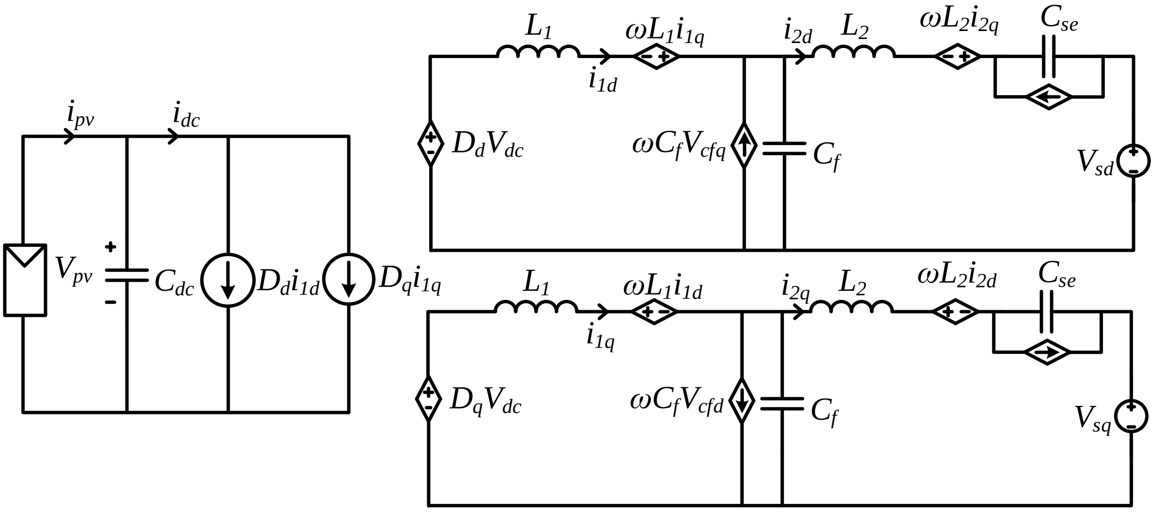

Fig. 5.2 Average model of LCLC-type PV-DSTATCOM under synchronous reference frame

5.2 Controller design

Without an efficient and perfect controller, a well-designed system performance will end as a disaster. So choosing an appropriate controller is much more important issue than the other aspects of designing problems. In this part, the synthesis of sliding mode control for photovoltaic fed hybrid DSTATCOM along with the reference current generation and dc link voltage control is carried out. For the simplicity of implementing the controlling theory, the system can be represented as shown in the following equations.

$$\dot{x} = f(x) + G(x)u$$
$$y = H(x)$$

where the system state vector, control vector and system output vectors are $x = [i_{1d}, i_{1q}, i_{2d}, i_{2q}, V_{cfd}, V_{cfq}, V_{sed}, V_{seq}, V_{pv}]$, $u = \left[D_d, D_q\right]^T$, $y = [i_{2d}, i_{2q}]$ respectively. The functions can be represented as

$$f(x) = \begin{bmatrix} -\frac{R_d}{L_1} i_{1d} + \frac{R_d}{L_1} i_{2d} - \frac{V_{cfd}}{L_1} + \omega i_{1q} \\ -\frac{R_d}{L_1} i_{1q} + \frac{R_d}{L_1} i_{2q} - \frac{V_{cfq}}{L_1} - \omega i_{1d} \\ \frac{R_d}{L_2} i_{1d} - \frac{R_d}{L_2} i_{2d} - \frac{V_{sed}}{L_2} - \frac{V_{sd}}{L_2} + \frac{V_{cfd}}{L_2} + \omega i_{2q} \\ \frac{R_d}{L_2} i_{1q} - \frac{R_d}{L_2} i_{2q} - \frac{V_{seq}}{L_2} - \frac{V_{sq}}{L_2} + \frac{V_{cfq}}{L_2} - \omega i_{2d} \\ \omega V_{cfq} + \frac{1}{C_f}[i_{1d} - i_{2d}] \\ -\omega V_{cfd} + \frac{1}{C_f}\left[i_{1q} - i_{2q}\right] \\ \omega V_{seq} + \frac{1}{C_{se}} i_{2d} \\ -\omega V_{sed} + \frac{1}{C_{se}} i_{2q} \\ \frac{1}{C_{dc}} i_{pv} \end{bmatrix} G(x) = \begin{bmatrix} \frac{V_{pv}}{L_1} & 0 \\ 0 & \frac{V_{pv}}{L_1} \\ 0 & 0 \\ 0 & 0 \\ 0 & 0 \\ 0 & 0 \\ 0 & 0 \\ 0 & 0 \\ \frac{i_{id}}{C_{dc}} & \frac{i_{1q}}{C_{dc}} \end{bmatrix} H(x) = \begin{bmatrix} i_{2d} \\ i_{2q} \end{bmatrix}$$

5.2.1 Design of sliding mode controller

Due to the robustness, fastness and stability under load or parameter variations, the sliding mode controller is widely used in power converters. Under parameter variation or load change, the steady state error of a system may deviate from zero value. So to improve the robustness of the system towards these changing conditions, a controller is designed to track the reference current successfully. For improved operation of LCLC-type PV-DSTATCOM a sliding surface is designed as follows:

$$S = \begin{bmatrix} S_d \\ S_q \end{bmatrix} = \begin{bmatrix} (i_{2d}^* - i_{2d}) + \gamma_1 \int_0^t (i_{2d}^* - i_{2d}) d\tau \\ \left(i_{2q}^* - i_{2q}\right) + \gamma_2 \int_0^t \left(i_{2q}^* - i_{2q}\right) d\tau \end{bmatrix} \tag{5.1}$$

where γ_1 and γ_2 are positive constants. Once the sliding surface is chosen the control law should be derived. The system to remain in the sliding surface, the law to be satisfied is

$$\dot{S} = 0$$

Taking above expression into consideration, Eq. (5.1) can be written as

$$\dot{i}_{2d} = \dot{i}_{2d}^* + (K_1 + \gamma_1)(i_{2d}^* - i_{2d}) + K_2 sign(S_d) \tag{5.2}$$

$$\dot{i}_{2q} = \dot{i}_{2q}^* + (K_3 + \gamma_2)\left(i_{2q}^* - i_{2q}\right) + K_4 sign(S_q) \tag{5.3}$$

Again

$$(\dot{i}_2)_{d,q} = (\dot{i}_1)_{d,q} - C_f \frac{d}{dt}(V_{cf})_{d,q} \tag{5.4}$$

Substituting Eq. **Error! Reference source not found.** and Eq. **Error! Reference source not found.** into Eq. (5.4) and comparing it with (5.2) and (5.3), the non-linear control law can be derived as

$$\begin{aligned} D_d = \Big[& \dot{i}^*_{2d} + (K_1 + \gamma_1)(i^*_{2d} - i_{2d}) + K_2 sign(S_d) + \frac{R_d}{L_1} i_{1d} - \frac{R_d}{L_1} i_{2d} \\ & + \frac{V_{cfd}}{L_1} - \omega i_{1q} + C_f \frac{d}{dt} V_{cfd} \Big] \frac{L_1}{V_{pv}} \end{aligned} \tag{5.5}$$

$$\begin{aligned} D_q = \Big[& \dot{i}^*_{2q} + (K_3 + \gamma_2)(i^*_{2q} - i_{2q}) + K_2 sign(S_q) + \frac{R_d}{L_1} i_{1q} - \frac{R_d}{L_1} i_{2q} \\ & + \frac{V_{cfq}}{L_1} + \omega i_{1d} + C_f \frac{d}{dt} V_{cfq} \Big] \frac{L_1}{V_{pv}} \end{aligned} \tag{5.6}$$

5.2.2 Droop Controller

For a perfect balance of real power flow between the grid, photovoltaic system and nonlinear load the dc link voltage should be maintained constantly at its reference value. Previously, to maintain the dc link voltage at its required magnitude a PI controller was used. But the performance of PI controller mainly depends upon it controller gains (K_p, K_i) which are very difficult to tune for a universal purpose. So here a droop controller is implemented for maintaining the dc link voltage at the required value. Basic concept of a droop controller can be understood from Fig. 5.3.

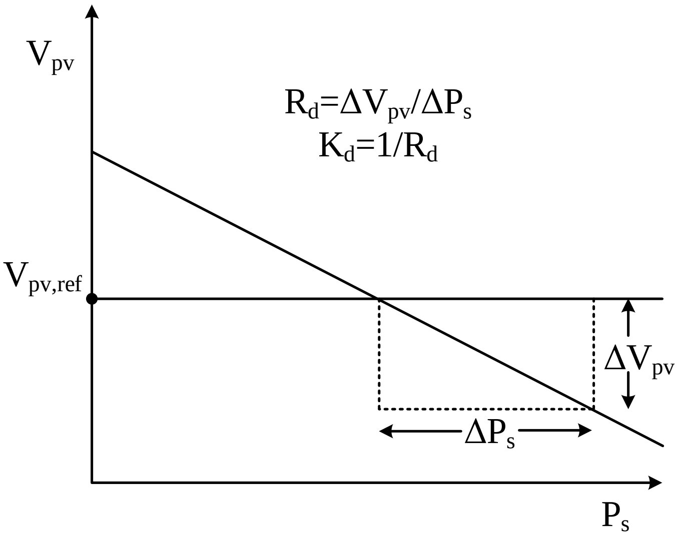

Fig. 5.3 Basic concept of a droop controller

To obtain the current injected to dc bus, the dc bus voltage error is passed through a droop controller. The power injected to dc bus can be determined by following expression:

$$P_s = K_d V_{pv}\left(V_{pv,ref} - V_{fpv}\right)$$

where $i = K_d\left(V_{pv,ref} - V_{fpv}\right)$

The operation of dc voltage regulator is explained in flowchart shown in Fig. 5.4. For satisfactory operation of the voltage regulator, the dc reference voltage is split into two limits, the upper limit $\left(V_{pvrefu}\right)$ and lower limit$\left(V_{pvrefl}\right)$. If the dc link voltage is higher than the upper limit, then the power is negative. So the converter reduces the power injected to the load from PV system. Lower dc link voltage compared to the lower limit defines the requirement of power by the load. So the power is injected from the photovoltaic system to maintain the dc link voltage at its reference value.

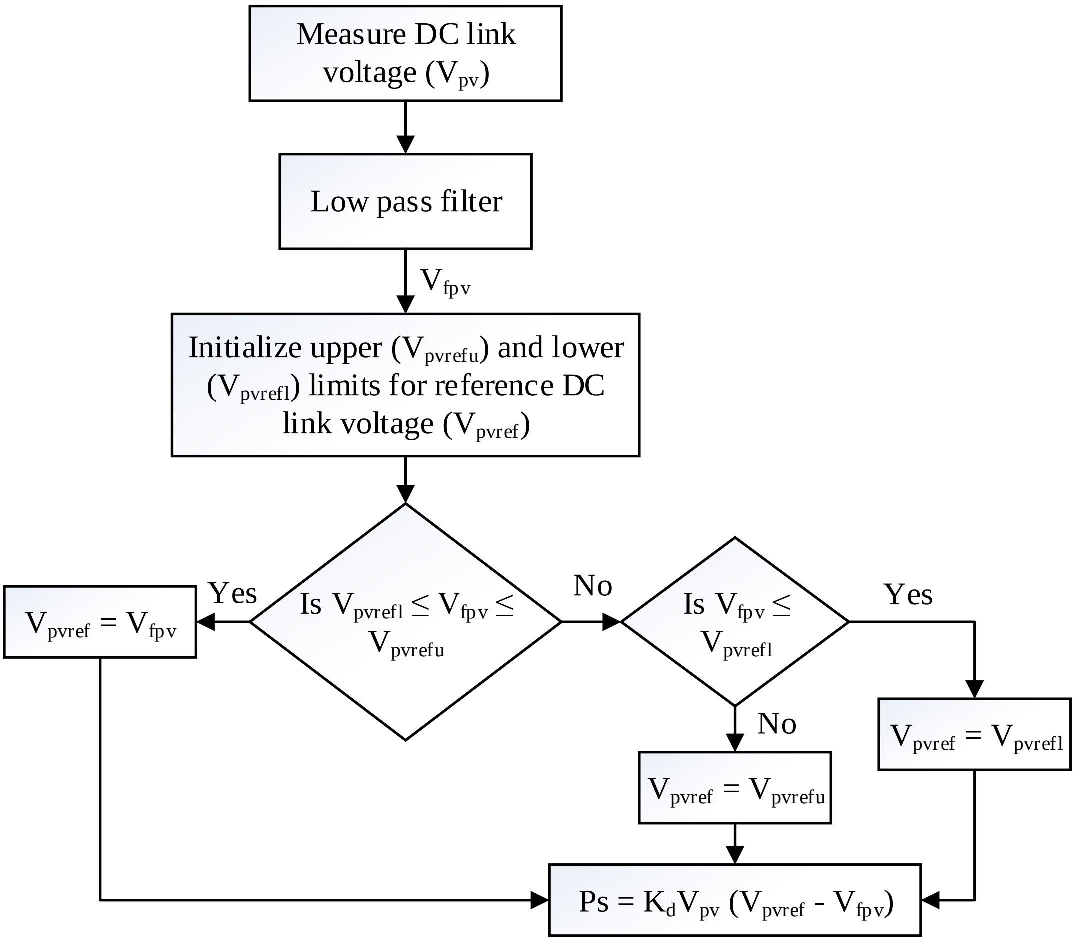

Fig. 5.4 Flowchart of dc voltage regulator

5.2.3 Reference current generation

Under this section the generation of reference current using IcosΦ is discussed. The reference currents are generated in abc platform as discussed in Section 2.3.1.3. Then the reference source currents are transformed to dq domain with the transformation matrix expressed below:

$$\begin{bmatrix} i_{sd}^* \\ i_{sq}^* \\ i_{s0}^* \end{bmatrix} = \frac{2}{3}\begin{bmatrix} \cos(\omega t) & \cos\left(\omega t - \frac{2\pi}{3}\right) & \cos\left(\omega t + \frac{2\pi}{3}\right) \\ -\sin(\omega t) & -\sin\left(\omega t - \frac{2\pi}{3}\right) & -\sin\left(\omega t + \frac{2\pi}{3}\right) \\ \frac{1}{2} & \frac{1}{2} & \frac{1}{2} \end{bmatrix}\begin{bmatrix} i_{sa}^* \\ i_{sb}^* \\ i_{sc}^* \end{bmatrix}$$

The reference filter current can be calculated as follows:

$$i_{2d}^* = i_{ld} - i_{sd}^*$$

$$i_{2q}^* = i_{lq} - i_{sq}^*$$

Now the reference filter currents are given as the input to the sliding mode controller and the switching signal are synthesized as shown in Fig. 5.5.

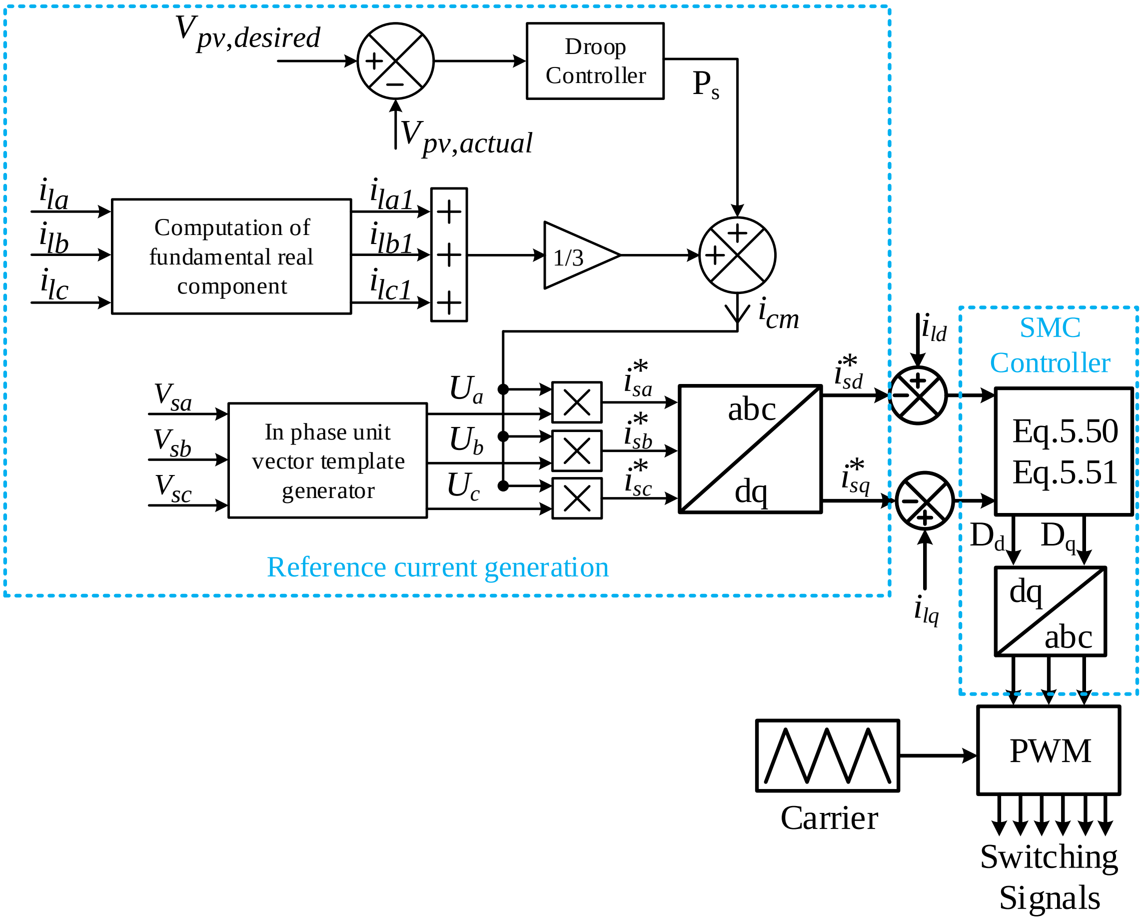

Fig. 5.5 Overall control structure of SMC controlled LCLC-type PV-DSTATCOM

5.3 Results and Discussions

5.3.1 Simulation Results

To evaluate the performance of the proposed LCLC-type photovoltaic fed DSTATCOM with sliding mode controller, the system is simulated under MATLAB/Simulink environment. A three-phase diode bridge rectifier with ohmic and inductive load is used as non-linear load for simulation. Along with non-linear load, different magnitudes of impedances are connected to each phase to make the load unbalanced. The system is simulated under two supply conditions to ratify the robustness of the system. The total harmonic distortion (THD) is taken as the evaluating parameter to appraise the harmonic elimination performance of the controller. For the distinct visualization of harmonic orders before and after compensation, spectrum analysis is carried out.

5.3.1.1 Steady-state performance of the system with SMC controller under ideal source

In this case, the system is simulated under pure sinusoidal source and with SMC controller based reference current controller. From Fig. 5.6, we can realize that the three phase load currents are highly distorted and non-sinusoidal due to the nonlinear load. After the compensation, the source current becomes pure sinusoidal and free of distortions. As compared to linear controllers the SMC controller based reference current controller performs better in terms of THD values. The THD of the source current reduces from 49.80% to 0.86% after compensation, which is well under the requirement of IEEE 519 standard (5%). A comparison of SMC based LCLC-type PV-DSTATCOM with others is given in Table 5.1.

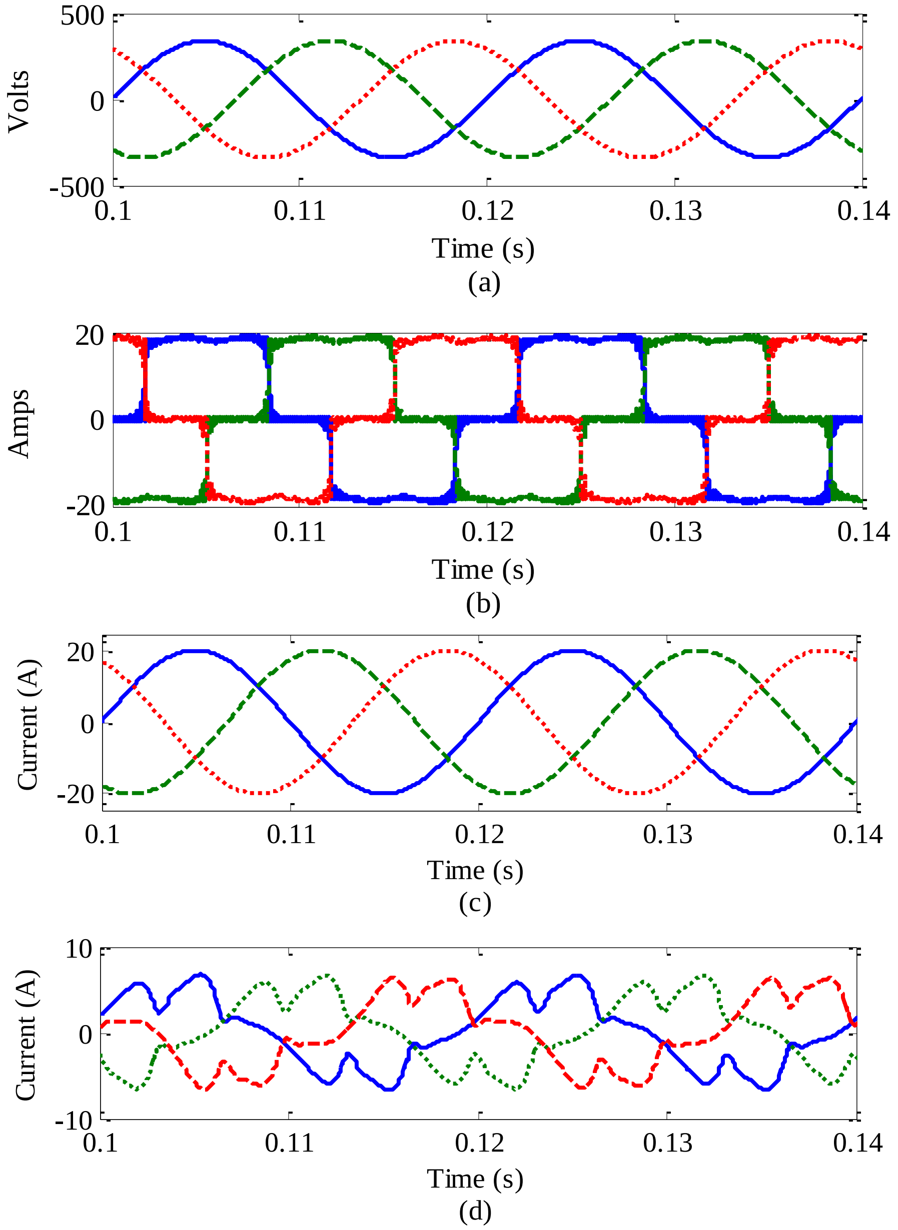

Fig. 5.6 Steady state performance with sliding mode controller (a) ideal mains voltage (b) load current before compensation (c) source current after compensation (d) filter current.

Table 5.1 Performance comparison of SMC based LCLC-type PV-DSTATCOM with other linear controllers

PV-DSTATCOM	THD (in %) before compensation	THD (in %) before compensation
L-type with IcosΦ algorithm	35.23	3.10
LCL-type with IcosΦ algorithm	33.95	2.14

LCLC-type with IcosΦ algorithm	49.80	6.27
LCLC-type with JAYA optimization	49.80	1.04
LCLC-type with SMC controller	49.80	0.86

5.3.1.2 Steady-state performance of the system with SMC under distorted source

The performance of the system is evaluated under distorted mains voltage with sliding mode controller. From Fig. 5.7 it is evident that though source voltage and load current are distorted before compensation, after compensation source current is distortion free and in phase with the source voltage. That implies to the power factor improvement and reactive power compensation of source current even under distorted supply voltage conditions. The total harmonic distortion of source current after compensation reduces from 52.03% to 1.02%, satisfying the IEEE 519 standard requirement.

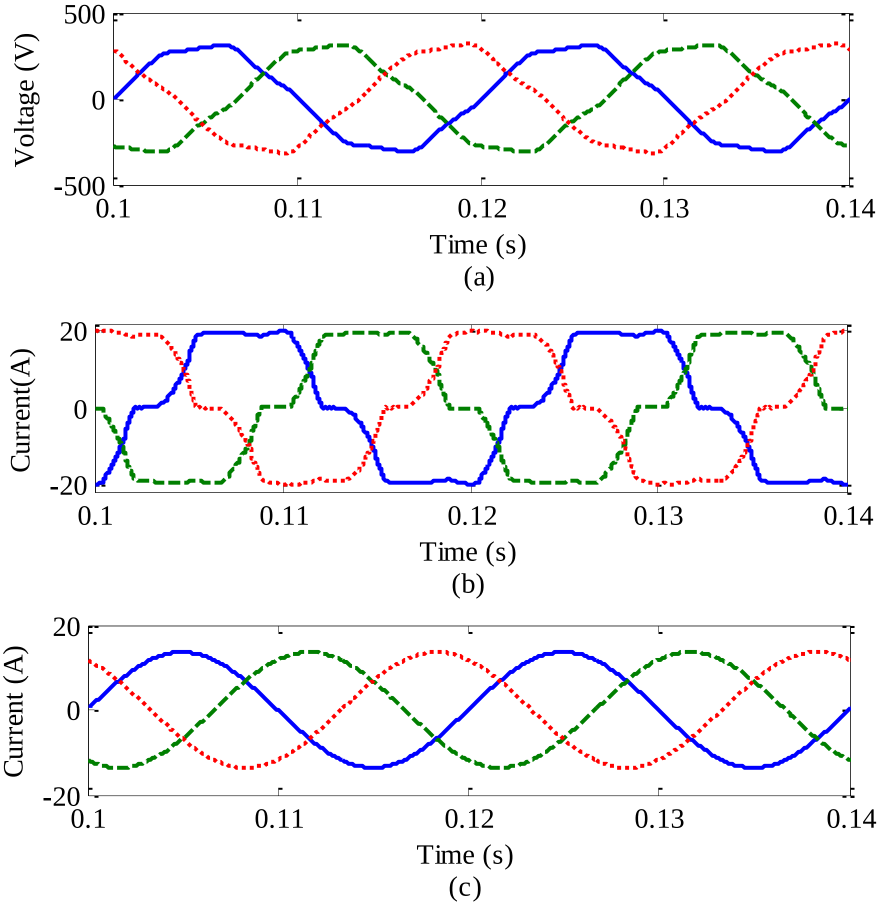

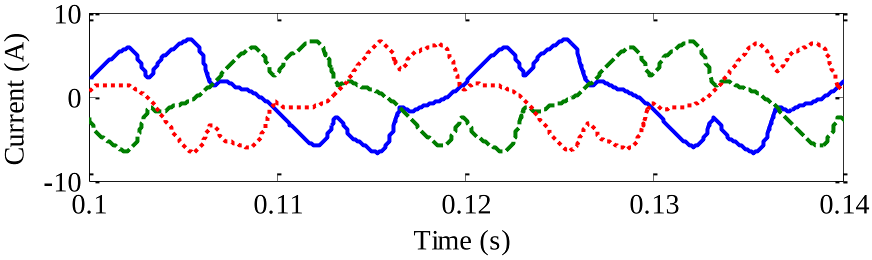

(d)

Fig. 5.7 Steady state performance with sliding mode controller (a) distorted mains voltage (b) load current before compensation (c) source current after compensation (d) filter current

5.3.1.3 Transient performance with SMC under ideal source

To validate the performance of proposed system under transient conditions with sliding mode control based controller, change in the type of load is considered. Three phase rectifier with an unbalanced load, three phase rectifier without unbalanced load and linear unbalanced loads are considered for load variation. Initially, the proposed system is operated with three phase rectifier with inductive-ohmic load and linear unbalanced load. During this period the value of dc side inductance and resistance is taken as 200mH and 50ohm whereas the linear unbalanced load consist of resistances and inductances whose values are 30ohm & 0.199mH, 40ohm & 0.249mH, 50ohm & 0.159mH for phase a, phase b and phase c respectably. At 0.2 seconds, the linear unbalanced load is disconnected and the system is operated for 10 cycles only with the same non-linear rectifier load. After 10 cycles the non-linear load is disconnected and a linear unbalanced is connected having the resistances values as 5.2ohm, 5.4ohm, and 5.6ohm for phase a, phase b and phase c respectably Again after 0.2 seconds the linear unbalanced load is disconnected and the non-linear load with unbalanced linear load is connected.

The efficacy of the proposed system with SMC controller during transient operation can be verified from Fig. 5.8 and Fig. 5.9. The proposed system is being able to track its reference and perform satisfactorily even during the transient period. Whenever there is a change in load, the controller is being able to drag the system to its steady state within 1 to 2 cycles after every alteration.

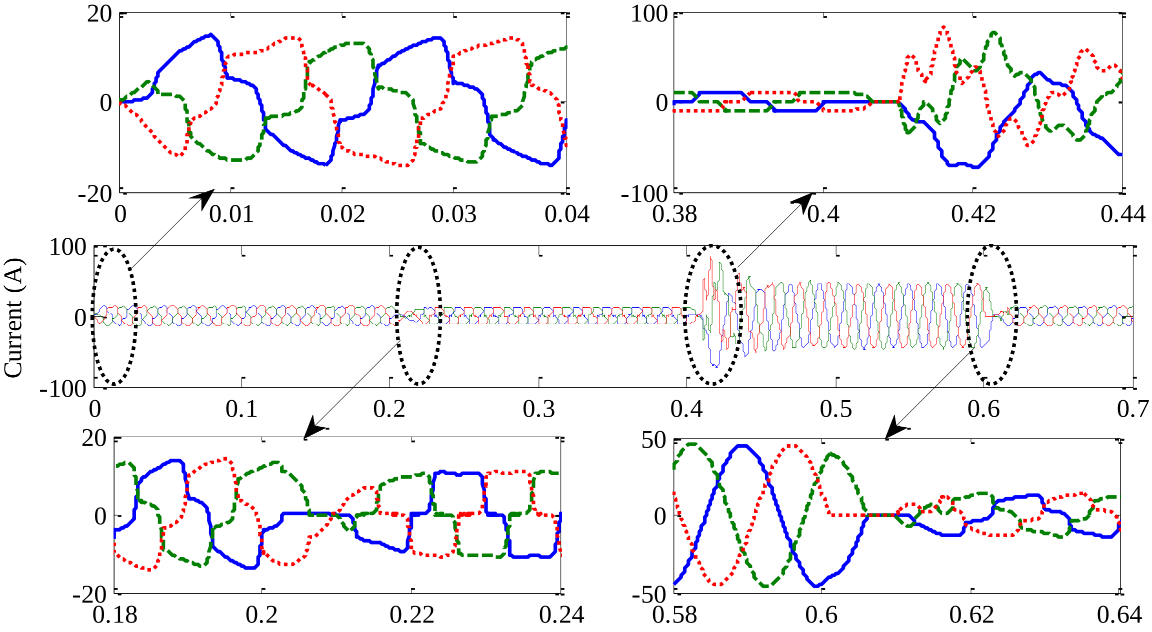

Fig. 5.8 Zoomed view load current before compensation during transient condition

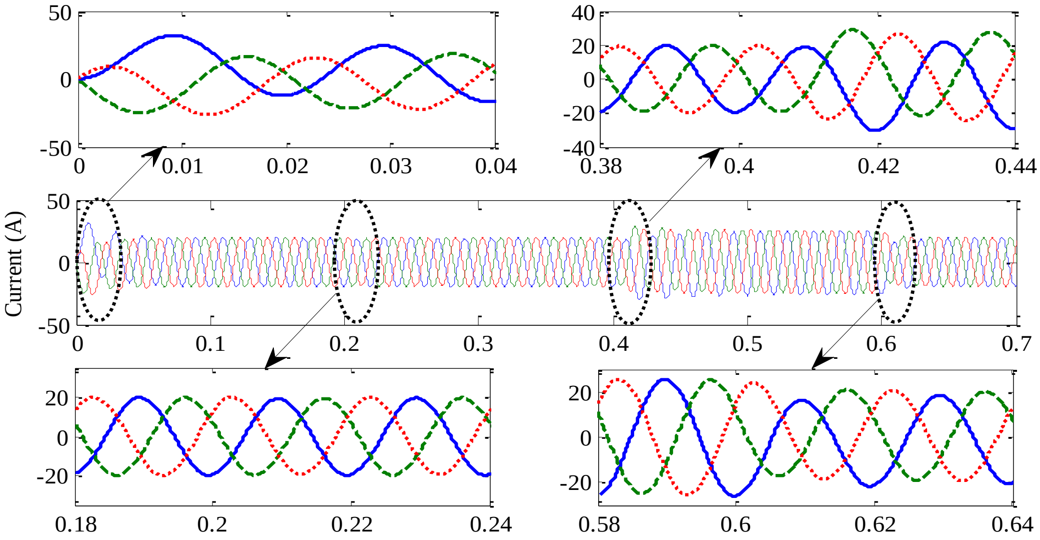

Fig. 5.9 Zoomed view source current after compensation during transient condition

5.3.2 Experimentation Results

The power control circuit for SMC based LCLC-type PV-DSTATCOM is shown in Fig. 5.5. The details of developed experimental setup is already discussed in Section 3.3 of Chapter 3. Here the LCLC-type PV-DSTATCOM is realized with sliding mode controller under dSPACE 1103 platform. Hall Effect sensors (LA 55-P, LV-25-P) are used to sense the currents and voltages required by the controller and given as input to the controller through ADC channels. The signals are then processed in the host computer and with the help of DAC channels of dSPACE, the PWM switching signals are given to SEMIKRON inverter. The source voltages (V_{sa}, V_{sb}, V_{sc}), load currents before compensation (i_{la}, i_{lb}, i_{lc}), source currents after compensation (i_{sa}, i_{sb}, i_{sc}) and filter currents (i_{fa}, i_{fb}, i_{fc}) are sensed and observed through DSO.

5.3.2.1 Steady state performance under ideal supply voltage condition

Under this section the proposed system is operated in real time under ideal supply voltage condition. The three phase bridge rectifier with ohmic-inductive load is taken as the nonlinear load. The ideal source voltage and nonlinear source current before compensation contaminated heavily with harmonics are observed through DSO as shown in Fig. 5.10 and Fig. 5.11. With SMC controller after compensation the source current is sinusoidal and in phase with source voltage which implies the ability of controller to compensate reactive power. From Fig. 5.12, it is found that after compensation the harmonics present in the source current are reduced and the THD is 1.12%. The filter current and spectral analysis of source current before and after are shown in Fig. 5.13 and Fig. 5.14 respectively.

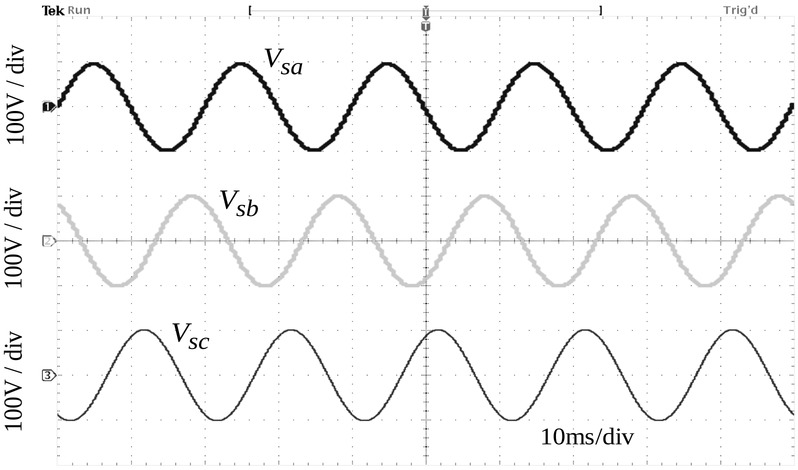

Fig. 5.10 Real time result for ideal source voltage

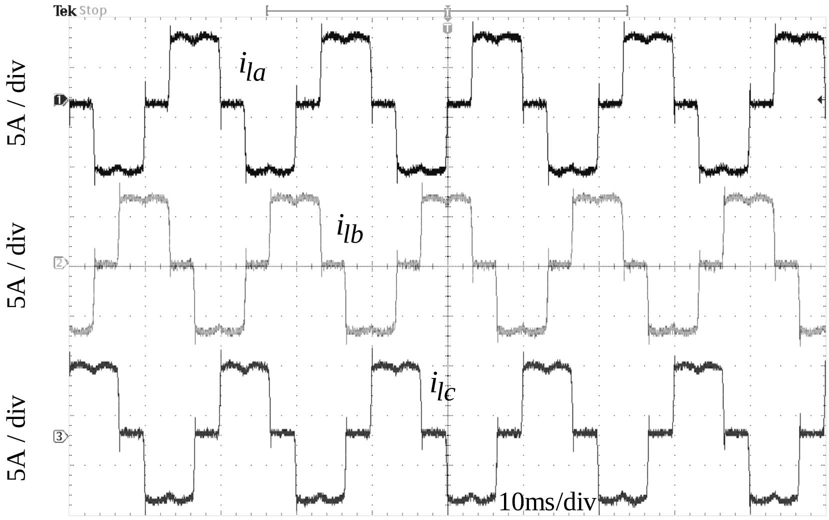

Fig. 5.11 Real time result for source current before compensation

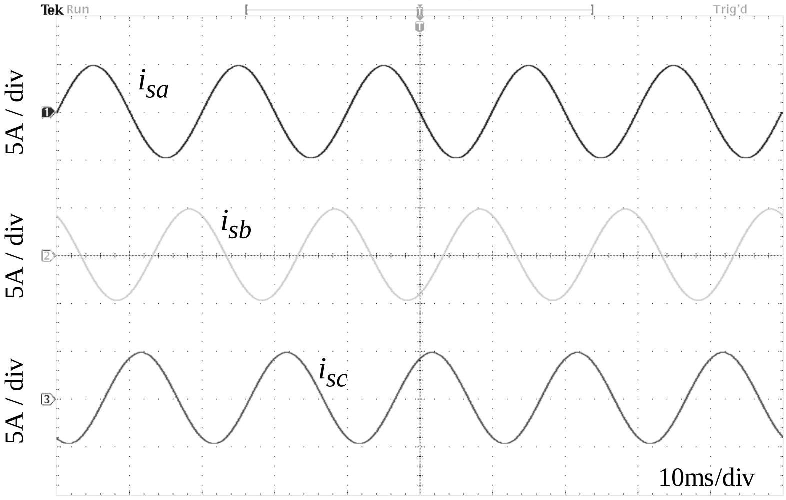

Fig. 5.12 Real time result for source current after compensation

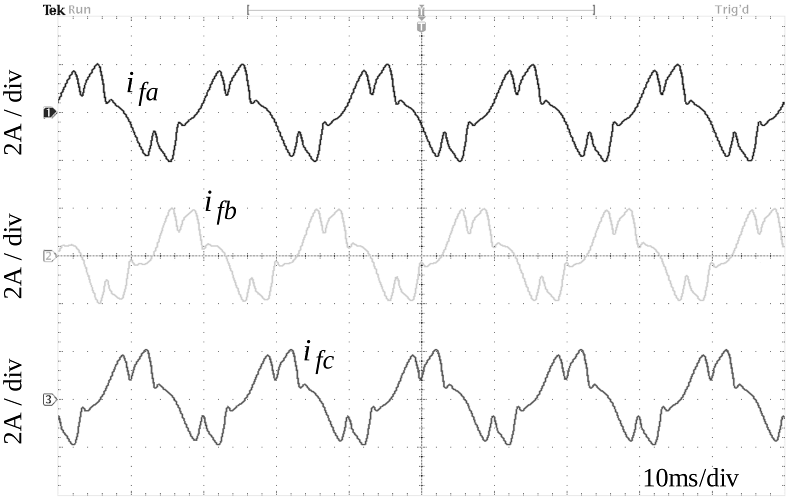

Fig. 5.13 Real time result for filter current

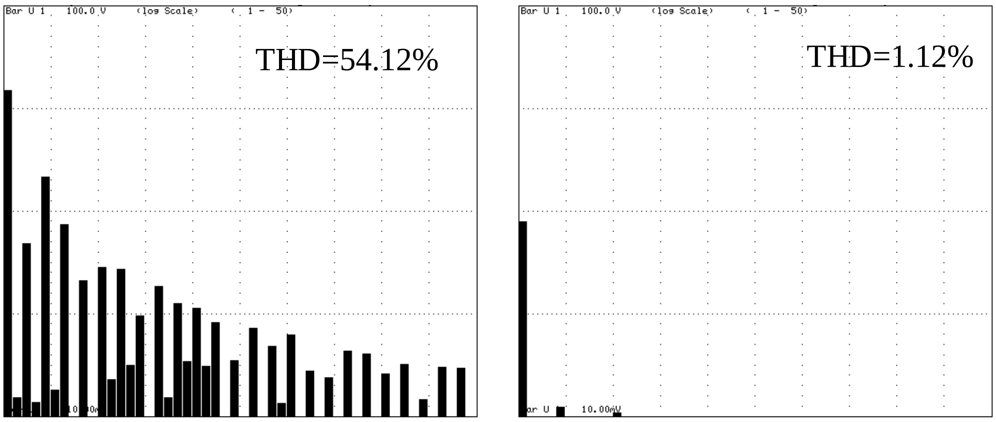

(a) (b)

Fig. 5.14 Spectral analysis for source current (a) before compensation (b) after compensation

5.3.2.2 Steady state performance under distorted supply voltage condition

In this case the proposed system is operated with SMC controller under distorted supply voltage condition. The source voltage is kept at 100V and shown in Fig. 5.15. The source current is heavily distorted and contaminated with harmonics before compensation and after the compensation it becomes sinusoidal, distortion free and in phase with source voltage. The source current before and after compensation is shown in Fig. 5.16 and Fig. 5.17 respectively. The THD of source current observed to be reduced from 53.14% to 1.24% with SMC controller as shown in Fig. 5.18.

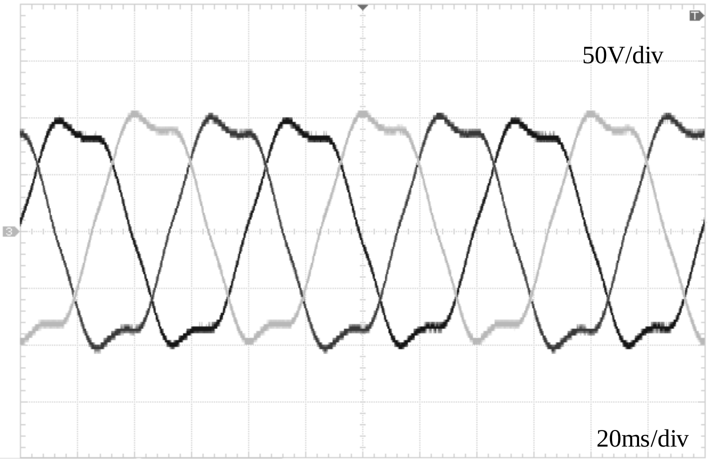

Fig. 5.15 Experimental results for distorted source voltage

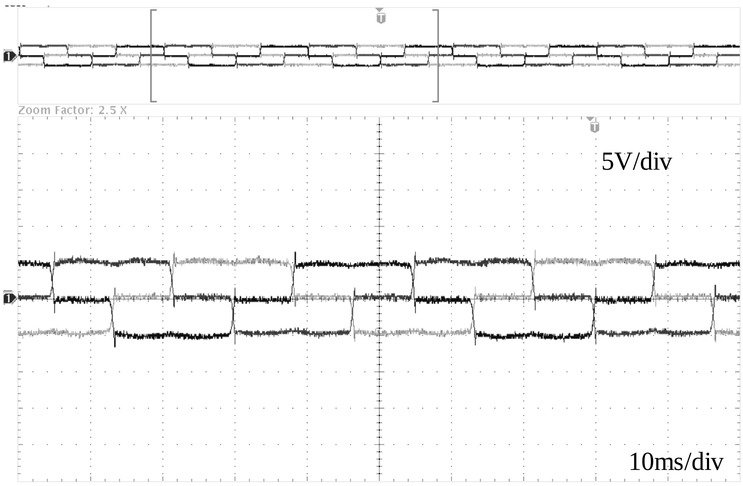

Fig. 5.16 Experimental result for source current before compensation

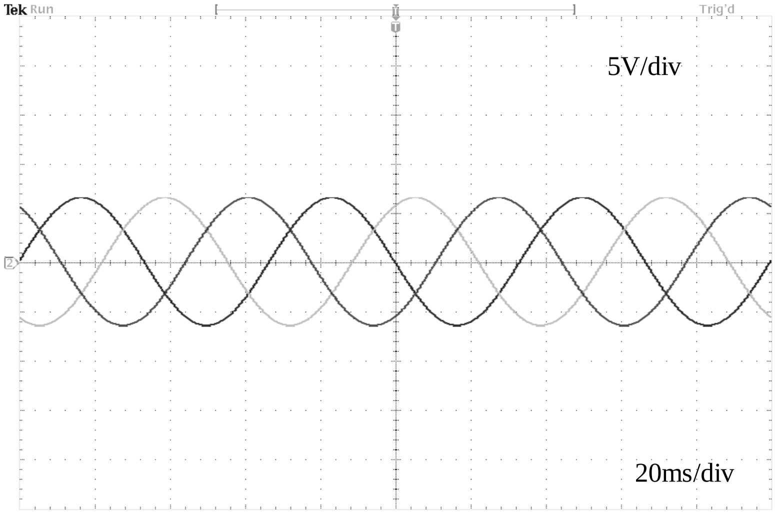

Fig. 5.17 Experimental result for source current after compensation

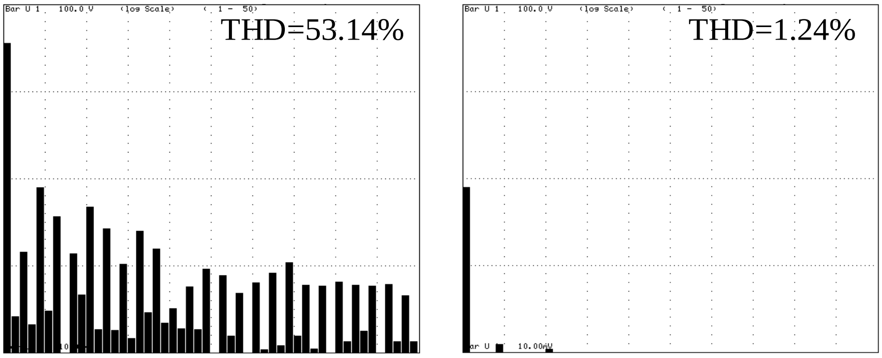

(a) (b)

Fig. 5.18 Spectral analysis of source current under distorted supply condition (a) before compensation (b) after compensation

5.4 Chapter Summary

The chapter proposes the implementation of a nonlinear controller named as sliding mode controller for the current controller. Also an average model of the LCLC-type PV-DSTATCOM is derived and presented considering the photovoltaic system and series capacitor. The SMC based current controller loop effectively handles any disturbance in the system whether it is in supply side or in the load side. To clarify the superiority of SMC control the system is simulated under ideal as well as distorted supply voltage conditions both in MATLAB/Simulink and hardware prototype. From the obtained result it is concluded that as compared to all other linear controller discussed in the dissertation the SMC based reference generation technique tracks the reference more accurately under all adverse conditions.

6 Chapter 6

Conclusions and Suggestion for Future Work

In this chapter the overall conclusions and the suggestions for some future scope of research work is proposed.

6.1 Overall Conclusions

The main objectives of the research work is to compensate current harmonics generated due to the presence of nonlinear loads in the solar energy integrated distribution system. The research studies presented in this thesis starts with an introduction to causes of power quality issues and harmonics clearly specifying its description, causes and consequences. The role and drawbacks of passive power filters in harmonics elimination is discussed. To avoid the inevitable drawbacks of passive filters, we moved towards the use of Distributed static compensators (DSTATCOMs). The importance of renewable energy and advantages of solar energy is discussed briefly. To increase the efficiency of grid integrated solar energy system and to reduce losses, a photovoltaic fed DSTATCOM (PV-DSTATCOM) is proposed. The PV-DSTATCOM compensate harmonics and inject active power to grid in the day time simultaneously. But in night time or during unavailability of solar irradiation it only compensate harmonics and reactive power.

This dissertation presents an extensive review on different topologies of PV-DSTATCOM with emphasis on their merits and demerits, and evaluate with respect to their benefits, drawbacks and appliances. A new topology is proposed to reduce the voltage across dc-link. Also special attention has been given to the control strategies and optimization of filter parameters and PI gains to enhance the compensating performance of PV-DSTATCOM.

In Chapter 2, performance of an L-type PV-DSTATCOM with IRP, MIRP and IcosΦ control schemes is evaluated by comparing the THDs in compensated source currents under ideal supply, non-ideal supply and sudden load change conditions. From the obtained simulation results it is found that, IcosΦ control scheme performs better than the IRP and MIRP theory. Also IcosΦ algorithm is simple to implement and free from the requirement of PLL for synchronization. DC-link voltage regulation with the help of PI controller to minimize the power losses occurring inside PV-DSTATCOM is studied. But there is high voltage drop across the L-type passive ac interface filter due to its high inductance value. So to maintain the power flow from PV source to grid a high voltage across the dc link need to be maintained. That enforces the need of high rating solar inverter. High value of passive filter and dc link voltage makes the system lossy, costly and heavy.

Hence a LCL-type PV-DSTATCOM is proposed in Chapter 3 to reduce the rating of passive filters. The system performance is evaluated in simulation with IcosΦ control scheme. From the obtained results it is observed that LCL-type PV-DSTATCOM performs better than the L-type PV-DSTATCOM in terms of harmonic compensation as the THD of source current reduces from 3.10% to 2.14% after compensation. With LCL-type passive ac interface filter the value and cost of the passive filters are reduced still the voltage across the dc-link is maintained at a higher value. Latter in this Chapter, a LCLC-type PV-DSTATCOM is proposed keeping the advantage of LCL-type passive interface filter advantages intact. The new proposed topology overcomes the disadvantage of LCL-type passive filter by compensating harmonics with a much reduced (680V to 165V) value of dc-link voltage. Though the LCLC-type PV-DSTATCOM compensates harmonics with reduced dc-link voltage but the THD of source current after compensation increased due to mismatching of passive filter values.

To find the correct value of passive filters and gains of PI controllers, it is needed to derive the exact modeling of the system considering all the nonlinearities. This a complex and time consuming process. So different optimization techniques are applied to PV-DSTATCOM for finding the optimize value for passive filters and PI controller gains. But those optimization tools are dependent upon the algorithm-specific control parameters. So if these parameters are not chosen correctly then there is a possibility of converging to local optima or the optimization tool may take more time to reach the global optimum value. Hence in Chapter 4 an optimization tool named as JAYA is proposed for PV_DSTATCOM whose performance is independent of algorithm-specific control parameters. The superiority of the JAYA optimized PV-DSTATCOM is verified over GEM and TLBO optimization based PV-DSTATCOM through both simulation and experimentation. With JAYA optimized PV-DSTATCOM

All the current controller presented in Chapter 2, Chapter 3 and Chapter 4 are linear controller. But the power network used are complex and nonlinear in nature. So when operating conditions changed or system parameter varies then the linear controllers do not track the reference current so effectively. Therefore in Chapter 5, a nonlinear controller named as sliding mode control is implemented to current controller of PV-DSTATCOM. As a result of which, the current controller is able to track the reference current under non ideal operating conditions. From the obtained simulation and experimental results, it is found that the THDs of the source current after compensation are reduced to 0.86% from 1.04%. Hence SMC based PV-DSTATCOM is more suitable for harmonic as well as reactive power compensation.

6.2 Contribution of the Thesis

The contribution of the thesis are as follows.

- In Chapter 2, a comparison between IRPT, MIRPT and IcosΦ control schemes has been proposed for observing the load compensation capability of L-type PV-DSTATCOM under non-ideal supply, sudden load change and unbalanced loading conditions.
- A new LCLC-type topology is proposed in Chapter 3 for PV-DSTATCOM with which it operates with a low dc-link voltage (exactly 165V). Due to lower voltage across dc-link, the rating of the solar inverter decreases which reduces the cost of the PV-DSTATCOM. Also the load compensating capability of LCLC-type PV-DSTATCOM is compared with LCL-type PV-DSTATCOM.
- An optimization technique called as JAYA is proposed for PV-DSTATCOM in Chapter 4. The JAYA optimization is independent of algorithm-specific control parameters. Therefore it converges faster to global optimum as compared to other optimization tools like GEM and TLBO and load compensation capability of PV-DSTATCOM has been improved with JAYA optimized parameters. These advantages are observed from the results obtained through both simulation and experimentation.
- In Chapter 5, the sliding mode control is applied to current controller of the PV-DSTATCOM to make the compensation performance robust towards any system parameter variations. The system efficacy is verified through both in simulation and experimentation.

6.3 Suggestion for the Future Work

- This dissertation focuses upon PV-DSTATCOM system, which attempts to solve PQ problems such as current harmonics and reactive power through different topologies and control strategies. As the modern distribution system demands a better quality of voltage being supplied and current drawn, integration of both PV-DSTATCOM and PV-DVR, i.e. PV-UPQC has great scope in actual practical implementation. Hence, an immediate extension of the thesis work is to apply above control strategies for PV-UPQC.
- An immediate extension to the work is to study the PV-DSTATCOM under different dynamics of photovoltaic system and integrate other micro sources such as wind energy systems, fuel cells etc. to develop dc distribution grid.
- Different advanced nonlinear controllers and adaptive controllers can be applied to current controller or to inverter switching techniques so that the power quality can still be improved.

References

[1] Y. Hamakawa, "Recent advances in solar photovoltaic technology and its new role for environmental issue," *Renewable energy,* vol. 5, no. 1, pp. 34-43, 1994.

[2] Y. Hamakawa, "New energy option for 21st century—recent progress in solar photovoltaic energy," *Oyobutsuri,* vol. 69, no. 8, p. 993–998, 2000.

[3] B. Ho, S. Chung and S. Hui, "An integrated inverter with maximum power tracking for grid-connected PV systems," *IEEE Transactions on Power Electronics,* vol. 20, no. 4, pp. 953-962, 2005.

[4] H. Koizumi, T. Mizuno, T. Kaito, Y. Noda, N. Goshima, M. Kawasaki, K. Nagasaka and K. Kurokawa, "A Novel Microcontroller for Grid-Connected Photovoltaic Systems," *IEEE Transactions on Industrial Electronics,* vol. 53, no. 6, pp. 1889-1897, 2006.

[5] E. Roman, R. Alonso, P. Ibanez, S. Elorduizapatarietxe and D. Goitia, "Intelligent PV Module for Grid-Connected PV Systems," *IEEE Transactions on Industrial Electronics,* vol. 53, no. 4, pp. 1066-1073, 2006.

[6] B. C. Babu et. al., "Analysis of mathematical modeling of PV module with MPPT algorithm," in *IEEE 15th International Conference on Environment and Electrical Engineering (EEEIC),* 2015.

[7] P. Janik et. al., "Analysis and modeling of a photovoltaic system using directional irradiances and optimization techniques," in *IEEE 16th International Conference on Environment and Electrical Engineering (EEEIC),* 2016.

[8] . L. Shuhui , A. H. Timothy, L. Dawen and H. Fei , "Integrating photovoltaic and power converter characteristics for energy extraction study of solar PV systems," *Renewable Energy ,* vol. 36 , pp. 3238-3245, 2011.

[9] D. Das, "A fuzzy multiobjective approach for network reconfiguration of distribution systems," *IEEE Transactions on Power Delivery,* vol. 21, no. 1, pp. 202 - 209, 2006.

[10] D. Das, "Optimal placement of capacitors in radial distribution system using a Fuzzy-GA method," *Int. Journal of Electrical Power & Energy Systems,* vol. 30, no. 6-7, p. 361–367, 2008.

[11] D. Das, "Reconfiguration of distribution system using fuzzy multi-objective approach," *Int. Journal of Electrical Power & Energy Systems,* vol. 28, no. 5, p. 331–338, 2006.

[12] A. Tah and D. Das, "An Enhanced Droop Control Method for Accurate Load Sharing and Voltage Improvement of Isolated and Interconnected DC Microgrids," *IEEE Transactions on Sustainable Energy,* vol. 7, no. 3, pp. 1194 - 1204, 2016.

[13] V. Srinivasarao, S. P. Singh and G. S. Raju, "Active and Reactive power rescheduling for congestion management using descent gradient method," in *Fifteenth National Power Systems Conference (NPSC),* IIT Bombay, 2008.

[14] T. K. Swain, S. P. Singh and G. S. Raju, "Optimal VAR Control for Voltage Stability Enhancement in Power Systems," in *Proc. International Conference on Computer Applications in Electrical Engineering - Recent Advances (CERA 97),* 1997.

[15] A. Ghosh and G. Ledwich, Power Quality Enhancement Using Custom Power Devices, Kluwer Academic Publishers, 2002.

[16] *IEEE Standard for Interconnecting Distributed Resources with Electric Power Systems, IEEE Std. 15471,* 2005.

[17] "IEEE Recommended Practice and Requirements for Harmonic Control in Electric Power Systems," *IEEE Standard 519-2014,* pp. 1-29, 2014.

[18] T. M. Blooming and D. J. Carnovale, "Harmonic convergence," *IEEE Industry Applications Magazine,* vol. 13, no. 1, pp. 21-27, January/February 2007.

[19] ""IEC 1000-3-2," Electromagnetic compatibility Part 3: Limits - Section 2: Limits for harmonic current emissions (equipment input current < 16A per phase)," 1995.

[20] ""IEC 1000-3-4," Electromagnetic compatibility Part 3: Limits - Section 4: Limits for harmonic current emissions (equipment input current > 16A per phase)," 1995.

[21] A. K. Reddy and S. P. Singh, "Congestion mitigation using UPFC," *IET Generation, Transmission & Distribution* , vol. 10, no. 10, p. 2433 – 2442, 2016.

[22] A. Banerji, S. K. Biswas and B. Singh, "DSTATCOM Control Algorithms: A Review," *International Journal of Power Electronics and Drive Systems,* vol. 2, no. 3, pp. 285-296, 2012.

[23] S. Saha, B. Majumdar and S. K. Biswas, "Improved active power factor correction circuit using a fully soft-switched boost converter," *IET power electronics,* vol. 4, no. 7, pp. 835-841, 2011.

[24] P. Chakraborty et. al., "Enhancement of voltage stability of autonomous wind power generation system using DSTATCOM," in *IEEE International Conference on Power Electronics, Drives and Energy Systems (PEDES),* 16/12/2014.

[25] A. Banerji, S. K. Biswas and B. Singh, "DSTATCOM Application for Mitigation of Voltage Sag Caused by Dynamic Loads in Autonomous Systems," *International Journal of Power Electronics and Drive Systems*, vol. 2, no. 2, pp. 232-240, 2012.

[26] J. Michalik, J. Molnar and Z. Peroutka, "Single-phase active current-source rectifier operated with power factor and Distortion Power Factor control," in *IEEE 9th International Conference on Power Electronics and Drive Systems (PEDS)*, 2011.

[27] J. Molnar, J. Michalik and Z. Peroutka, "Single Phase Current-Source Active Rectifier: design, simulation and practical problems," in *IEEE International Symposium on Industrial Electronics*, 2007.

[28] B. Singh, P. Jayaprakash, D. P. Kothari, A. Chandra and K. A. Haddad, "Comprehensive Study of DSTATCOM Configurations," *IEEE Trans. on Industrial Informatics*, vol. 10, no. 2, pp. 854-870, May 2014.

[29] F. Wu, B. Sun, J. Duan and K. Zhao, "Online Variable Topology-Type Photovoltaic Grid-Connected Inverter," *IEEE Transactions on Industrial Electronics*, vol. 62, no. 8, pp. 4814-4822, 2015.

[30] F. Wu, L. Zhang and Q. Wu, "Simple unipolar maximum switching frequency limited hysteresis current control for grid-connected inverter," *IET Power Electronics*, vol. 7, no. 4, pp. 933 - 945, 2014.

[31] W. Stronger, F. Wu and S. Li, "Grid Inverters LCL filter new active damping control," *Electric Power Automation Equipment*, vol. 31, no. 5, pp. 75-79, 2011.

[32] X. Bao, F. Zhuo, Y. Tian and P. Tan, "Smplified feedback linearization control of three-phase photovoltaic inverter with an LCL filter," *IEEE Transaction on Power Electronics* , vol. 28, no. 2, pp. 1560-1567, 2013.

[33] L. Chen , A. Amirahmadi, Q. Zhang, N. Kutkut and I. Bataresh, "Design and implementation of three phase two-stage grid-connected module integrated converter," *IEEE Transaction on Power Electronics*, vol. 29, no. 8, pp. 3881-3892, 2014.

[34] C.-S. Chen, C.-H. Lin, W.-L. Hsieh, C.-T. Hsu and T.-T. Ku, "Enhancement of PV penetration with DSTATCOM in taipower distribution system," *IEEE Transaction on Power Systems*, vol. 28, no. 2, pp. 1560-1567, 2013.

[35] C. Photong, C. Klumpner and P. Wheeler, "Evaluation of single-stage power converter topologies for grid-connected photovoltaics," in *in Proc. Int. Conf. Ind. Technol.*, 2010.

[36] H. R. Seo et. al., "Harmonics and reactive power compensation method by grid-connected photovoltaic generation system," in *in Proc. Int. Conf. Elect. Machines Syst.*, 2009.

[37] M. A. S. Masoum, H. Dehbonei and E. F. Fuchs, "Theoretical and experimental analyses of photovoltaic systems with voltage and current-based maximum power-point tracking," *IEEE Trans. Energy Convers.*, vol. 17, no. 4, pp. 514-522, 2002.

[38] H. S. Kim et. al., "Analysis of bi-directional PWM converter for application of residential solar air conditioning system," in *in Proc. Photovoltaic Specialists Conf.*, 1994.

[39] A. Gaviano, K. Weber and C. Dirmeier, "Challenges and Integration of PV and Wind Energy Facilities from a Smart Grid Point of View," in *PV Asia Pacific Conference*, Munich, Germany, 2012.

[40] A. Lohner, T. Meyer and A. Nagel, "A new panels-integratable inverter concept for grid-connected photovoltaic systems," in *IEEE Int. Symp. Ind. Electron.*, Warsaw, Poland, 1996.

[41] N. g. Sung, J. d. Lee, B. t. Kim and Minwon, "Novel Concept of a PV Power Generation System adding the Function of Shunt Active Filter," in *Transmission and Distribution Conference and Exhibition*, 2002.

[42] M. I. Marei, E. F. El-Saadany and M. Magdy, "A Novel Control Algorithm for the DG Interface to Mitigate Power Quality Problems," *IEEE Transactions on Power Delivery*, vol. 19, no. 3, pp. 1384-1392, 2004.

[43] H. Calleja and H. Jimenez, "Performance of a grid connected PV system used as active filter," *Energy Conversion and Management*, vol. 45, pp. 2417-2428, 2004.

[44] S. Mekhilef and N. Rahim, "Implementation of Grid-Connected Photovoltaic System with Power Factor Control and Islanding Detection," in *35th Annual IEEE Power ElecrronicsSpecialists Conference*, Aachpn, Germany, 2004.

[45] T.-F. Wu et.al., "A Single-Phase Inverter System for PV Power Injection and Active Power Filtering With Nonlinear Inductor Consideration," *IEEE Transactions on Industry Applications*, vol. 41, no. 4, pp. 1075-1083, 2005.

[46] W. Libo et. al., "Modified MPPT strategy applied in single-stage grid-connected photovoltaic system," in *8th Int. Conf. Electr. Mach. Syst. Conf.*, 2005.

[47] L. Wu, Z. Zhao and J. Liu, "A Single-Stage Three-Phase Grid-Connected Photovoltaic System With Modified MPPT Method and Reactive Power Compensation," *IEEE Transactions on Energy Conversion*, vol. 22, no. 4, pp. 881-886, 2007.

[48] H. Patel and V. Agarwal, "PV Based Distributed Generation with Compensation Feature Under Unbalanced and Non-linear Load Conditions for a 3-phase, 4-Wire System," in *IEEE International Conference on Industrial Technology*, 2006.

[49] T. F. Wu et. al., "PV Power Injection and Active Power Filtering With Amplitude-Clamping and Amplitude-Scaling Algorithms," *IEEE Transactions on Industry Applications,* vol. 43, no. 3, pp. 731-741, 2007.

[50] R. R. Sawant and M. C. Chandorkar, "A Multi-functional Four-leg Grid Connected Compensator," in *Power Conversion Conference,* Nagoya, 2007.

[51] L. Yu Kang, T. P. Lee and K. H. Wu, "Grid-Connected Photovoltaic System With Power Factor Correction," *IEEE Transactions on Industrial Electronics,* vol. 55, no. 5, pp. 2224-2227, 2008.

[52] Martins, M. F. Schonardie and C. Denizar , "Three-Phase Grid-Connected Photovoltaic System With Active And Reactive Power Control Using dq0 Transformation," in *Power Electronics Specialists Conference*, 2008.

[53] H. Patel and V. Agarwal, "Investigation into the performance of photovoltaic-based active filter configurations and their control schemes under uniform and non-uniform radiation conditions," *IET Renew. Power Gener.,* vol. 4, no. 1, pp. 12-22, 2010.

[54] P. Flores et. al., "Static Var Compensator and Active Power Filter With Power Injection Capability, Using 27-Level Inverters and Photovoltaic Cells," *IEEE Transactions on Industrial Electronics,* vol. 56, no. 1, pp. 130-138, 2009.

[55] M. B. B. Sharifian, Y. Mohamadrezapour, M. Hosseinpour and S. Torabzade, "Single-stage grid connected photovoltaic system with reactive power control and adaptive predictive current controller," *Journal of Applied Sciences,* vol. 9, no. 8, pp. 1503-1509, 2009.

[56] L. Hassaine, E. Olias, J. Quintero and M. Haddadi, "Digital power factor control and reactive power regulation for grid-connected photovoltaic inverter," *Renewable Energy,* vol. 34, pp. 315-321, 2009.

[57] F. L. Albuquerque et. al., "Photovoltaic solar system connected to the electric power grid operating as active power generator and reactive power compensator," *Solar Energy,* vol. 84, pp. 1310-1317, 2010.

[58] Z. A. Ghani, M. Hannan and A. Mohamed, "Renewable energy inverter developement using dSPACE DS1104 controller board," in *IEEE International Conference on Power and Energy (PECon2010),* Kuala Lumpur Malaysia, 2010.

[59] G. Tsengenes and G. Adamidis, "Investigation of the behavior of a three phase grid connected photovoltaic system to control active and reactive power," *Electric Power Systems Research,* vol. 81, pp. 177-184, 2011.

[60] P. P. Dash and K. Mehrdad , "Dynamic Modeling and Performance Analysis of a Grid-Connected Current-Source Inverter-Based Photovoltaic System," *IEEE Transactions on Sustainable Energy,* vol. 2, no. 4, pp. 443-450, 2011.

[61] Y. A. R. I. Mohamed, "Mitigation of dynamic, unbalanced, and harmonic voltage disturbances using grid-connected inverters with LCL filter," *IEEE Transactions on Industrial Electronics,* vol. 58, no. 9, pp. 3914-3924, 2011.

[62] Z. A. Ghani, M. Hannan and A. Mohamed, "Investigation of three-phase grid connected inverter for photovoltaic application," *Przeglad Elektrotechniczny (Electrical Review),* pp. 8-13, 2012.

[63] V. Kamatchi Kannan and N. Rengarajan, "Photovoltaic based distribution static compensator for power quality improvement," *Electrical Power and Energy Systems,* vol. 42, pp. 685-692, 2012.

[64] X. Wang et. al., "Modeling and Control of Dual-Stage High-Power Multifunctional PV System in d–q–o Coordinate," *IEEE Transactions on Industrial Electronics,* vol. 60, no. 4, pp. 1556-1570, 2013.

[65] R. Noroozian and G. B. Gharehpetian, "An investigation on combined operationof active power filter with photovoltaic arrays," *Electrical Power and Energy Systems,* vol. 46, pp. 392-399, 2013.

[66] M. S. Munir and Y. W. Li, "Residential distribution system harmonic compensation using PV interfacing inverter," *IEEE Transactions on Smart Grid,* vol. 4, no. 2, pp. 816-827, 2013.

[67] M. I. Hamid, A. Jusoh and M. Anwari, "Photovoltaic plant with reduced output current harmonics using generation-side active power conditioner," *IET Renew. Power Gener.,* vol. 8, no. 7, pp. 817-826, 2014.

[68] V. Kamatchi Kannan and N. Rengarajan, "Investigating the performance of photovoltaic based DSTATCOM using Icos algorithm," *Electrical Power and Energy Systems*, vol. 54, pp. 376-386, 2014.

[69] B. Singh, C. Jain and S. Goel, "ILST Control Algorithm of Single-Stage Dual Purpose Grid Connected Solar PV System," *IEEE Transactions on Power Electronics,* vol. 29, no. 10, pp. 5347-5357, 2014.

[70] B. Singh and S. R. Arya , "Adaptive Theory-Based Improved Linear Sinusoidal Tracer Control Algorithm for DSTATCOM," *IEEE Transactions on Power Electronics,* vol. 28, no. 8, pp. 3768-3778, 2013.

[71] P. Kumar, N. Kumar and A. K. Akella, "A simulation based case study for control of DSTATCOM," *ISA Transactions*, vol. 53, pp. 767-775, 2014.

[72] H. Akagi, Y. Kanazawa and A. Nabae, "Instantaneous reactive power compensators comprising switching devices without energy storage components," *IEEE Trans. Ind. Appl.,* vol. 20, pp. 625-630, 1984.

[73] M. Kale and E. Ozdemir, "Harmonic and reactive power compensation with shunt active power filter under non-ideal mains voltage," *Electric Power System Research,* vol. 77, pp. 363-370, 2005.

[74] "Electromagnetic Compatibility (EMC)-Part 3: Limits for Harmonic Current Emissions (Equipment Input Current>16 A per phase)," IEC 61000-3-4 Document, 1998.

[75] R. Z. Xu, L. Xia, J. Zhang and J. Ding, "Design and research on the LCL filter in three-phase PV grid-connected inverters," *Int. J. Comput. Elect. Eng.,* vol. 5, no. 3, pp. 322-325, Jun. 2013.

[76] E. Twining and D. Holmes, "Grid current regulation of a three-phase voltage source inverter with an LCL input filter," in *IEEE PESC’02*, 2002.

[77] C. Kumar and M. K. Mishra, "An improved hybrid DSTATCOM topology to compensate reactive and nonlinear loads," *IEEE Transaction on Industrial Electronics,* vol. 61, no. 12, pp. 6517-6527, 2014.

[78] "LEM Datasheet: LV 25-P, LEM, Japan, 1996".

[79] "LEM Datasheet: LA 55-P, LEM, Japan, 1996".

[80] M. El-Habrouk and M. K. Darwish, "A New Control Technique for Active Power Filters Using a Combined Genetic Algorithm/Conventional Analysis," *IEEE Transaction on Industrial Electronics,* vol. 49, no. 1, pp. 58-66, 2002.

[81] S. Mishra and C. N. Bhende, "Bacterial Foraging Technique-Based Optimized Active Power Filter for Load Compensation," *IEEE Transaction on Power Delivery,* vol. 22, no. 1, pp. 457-465, 2007.

[82] N. He, D. Xu and L. Huang, "The Application of Particle Swarm Optimization to Passive and Hybrid Active Power Filter Design," *IEEE Transaction on Industrial Electronics*, vol. 56, no. 8, pp. 2841-2851, 2009.

[83] H. Wang, X.-p. Meng, L. Zhao and T.-m. Zhao, "Controlling Study of D-STATCOM Based on Hybrid Genetic Optimization PID Algorithm," in *24th Chinese Control and Decision Conference,* 2012.

[84] M. Farhoodnea, A. Mohamed, H. Shareef and H. Zayan, "Optimum D-STATCOM Placement Using Firefly Algorithm for Power Quality Enhancement," in *IEEE 7th International Power Engineering and Optimization Conference*, Langkawi, Malaysia, 2013.

[85] P. Kopulwar et. al., "Particle Swarm Optimization Based Distribution Static Compensator for Load Compensation," in *IEEE Int. Conf. on Advanced Communication Control and Computing Technologies*, 2014.

[86] A. Ahrari and A. A. Atai, "Grenade Explosion Method—A novel tool for optimization of multimodal functions," *Applied Soft Computing,* vol. 10, pp. 1132-1140, 2010.

[87] R. V. Rao and V. Patel, "An improved teaching-learning-based optimization algorithm for solving unconstrained optimization problems," *Scientia Iranica,* vol. 20, no. 3, p. 710–720, 2013.

[88] R. Rao, V. Savsani and D. Vakharia, "Teaching–learning-based optimization: A novel method for constrained mechanical design optimization problems," *Computer-Aided Design,* vol. 43, no. 3, p. 303–315, 2011.

[89] R. Rao, V. Savsani and D. Vakharia, "Teaching–Learning-Based Optimization: An optimization method for continuous non-linear large scale problems," *Information Sciences,* vol. 183, no. 1, p. 1–15, 2012.

[90] R. V. Rao, "Jaya: A simple and new optimization algorithm for solving constrained and unconstrained optimization problems," *International Journal of Industrial Engineering Computations,* vol. 7, no. 1, pp. 19-34, 2016.

[91] C. Meza, D. Biel, D. Jeltsema and J. M. A. Scherpe, "Lyapunov-based control scheme for single-phase grid-connected PV central inverters," *IEEE Trans. Control Syst. Technol.,* vol. 20, no. 2, pp. 520-529, Mar. 2012.

[92] W. Lu, C. Li and C. Xu, "Sliding mode control of shunt hybrid active power filter based on the inverse system method," *Electrical Power and Energy Systems,* vol. 57, pp. 39-48, 2014.

[93] A. Ghamri, M. T. Benchouia and A. Golea, "Sliding mode control based three phase shunt active power filter: Simulation and Experimentation," *Electric Power Components and Systems,* vol. 40, no. 4, pp. 383-398, 2012.